



Titre: Synthesis and Characterization of Palladium-Cobalt Alloy for New
Title: Medical Micro-Devices

Auteur: Lina Kafrouni
Author:

Date: 2016

Type: Mémoire ou thèse / Dissertation or Thesis

Référence: Kafrouni, L. (2016). Synthesis and Characterization of Palladium-Cobalt Alloy for
Citation: New Medical Micro-Devices [Thèse de doctorat, École Polytechnique de Montréal].
PolyPublie. <https://publications.polymtl.ca/2091/>

 **Document en libre accès dans PolyPublie**
Open Access document in PolyPublie

URL de PolyPublie: <https://publications.polymtl.ca/2091/>
PolyPublie URL:

**Directeurs de
recherche:** Oumarou Savadogo
Advisors:

Programme: Génie biomédical
Program:

UNIVERSITÉ DE MONTRÉAL

SYNTHESIS AND CHARACTERIZATION OF PALLADIUM-COBALT ALLOY FOR NEW
MEDICAL MICRO-DEVICES

LINA KAFROUNI

INSTITUT DE GÉNIE BIOMÉDICAL
ÉCOLE POLYTECHNIQUE DE MONTRÉAL

THÈSE PRÉSENTÉE EN VUE DE L'OBTENTION
DU DIPLÔME DE PHILOSOPHIAE DOCTOR
(GÉNIE BIOMÉDICAL)

MARS 2016

UNIVERSITÉ DE MONTRÉAL

ÉCOLE POLYTECHNIQUE DE MONTRÉAL

Cette thèse intitulée:

SYNTHESIS AND CHARACTERIZATION OF PALLADIUM-COBALT ALLOY FOR NEW
MEDICAL MICRO-DEVICES

présentée par : KAFROUNI Lina

en vue de l'obtention du diplôme de : Philosophiae Doctor

a été dûment acceptée par le jury d'examen constitué de :

M. YAHIA L'Hocine, Ph. D, président

M. SAVADOGO Oumarou, D. d'état, membre et directeur de recherche

M. MÉNARD David, Ph. D., membre

M. ASSELIN Éric, Ph. D., membre

DEDICATION

This thesis is dedicated to my family.

ACKNOWLEDGEMENTS

This thesis not only represents my efforts, but also the energies of some others who have assisted me on my journey by providing their support, understanding and time. There are numerous people who have influenced me and my work and deserve recognition.

First and foremost I would like to express my deepest appreciation to my thesis supervisor, Professor Oumarou Savadogo, for the opportunity he gave me to be part of his research group, and mostly his confidence in my work. During the most difficult times, he gave me the moral support and the freedom I needed to move on. I always remember him saying: ‘Perfection simply doesn’t exist in science as in life’. Thank you for giving valuable guidance and insightful suggestions throughout the project’s duration.

Special thanks to Professor Yahia L’Hocine for his inspiring attitude and spirit of adventure and excitement for novel scientific undertakings. Thanks also for his comments and inputs, and for sharing his expertise in biocompatibility and nanotoxicity.

Thanks to Professor David Ménard for the use of his laboratory facilities and for taking the time to evaluate this thesis.

I am very grateful to my friend and mentor Professor Rosa Rego, for her constant encouragement and her personal guidance for successful completion of this research work.

I have no words to express my gratitude to my friend Mrs. Carole Massicotte, who I interacted with every day in the lab. She helped me a lot morally and technically without any hesitation during my doctoral research.

I owe special thanks to Dr. Josianne Lefebvre, Dr. Christian Lacroix and Dr. Taraneh Djavanbakht for their help, sympathy and precious advices during my experimental work.

I am personally thankful to all technicians and employees of the CM2. The training and guidance that I gained from them are much appreciated.

Many thanks go to my colleagues at École Polytechnique: Ali Seifitokaldani, Isabelle Fotsing, Maryam Haddad, Ricardo Galindo, Kentaro Oishi, Sandra Dórea, Eric Nguwuo Petuenju and Bintou Ouedraogo.

I would like to express my endless thankfulness to my husband for his encouragement and love, as well as my parents and my sisters who have always supported me to achieve my goals, even in the distance.

Lastly, I wish to acknowledge the financial support from the Fonds de recherche du Québec- Nature et Technologies (FQRNT), Fondation Universitaire Pierre Arbour and Australian Endeavour Fellowship.

RÉSUMÉ

Selon les statistiques canadiennes sur le cancer, on estime que 196 900 Canadiens développeront un cancer et que 78 000 en mourront en 2015. Étant donné que les cellules tumorales sont plus sensibles que les cellules saines à une augmentation de température, cette propriété peut être utilisée *in vivo* pour détruire les cellules cancéreuses par l'élévation de la température du corps, également connu sous le nom d'hyperthermie. L'hyperthermie magnétique est une technique prometteuse pour le traitement ciblé du cancer à l'aide des nanoparticules magnétiques, et ayant donc moins d'effets secondaires que la chimiothérapie et la radiothérapie.

Malgré que l'hyperthermie magnétique a été utilisée depuis des milliers d'années pour le traitement du cancer, le défi de destruction des cellules cancéreuses reste très difficile. Pour cette raison, les oncologues utilisent souvent le traitement par hyperthermie magnétique en combinaison avec la radiothérapie et/ou la chimiothérapie. Cette approche thérapeutique combinée a pour but de sensibiliser les cellules cancéreuses résistantes à la radiothérapie et/ou la chimiothérapie.

Pour utiliser l'hyperthermie magnétique toute seule dans le traitement du cancer, des difficultés au niveau de la modification de surface des particules magnétiques, pour une absorption sélective par les cellules cancéreuses, et au niveau de la stabilité et des propriétés magnétiques, pour une capacité de chauffage élevée ($> 1000 \text{ W/g}$), doivent être surmontées. L'objectif ultime de cette thèse est de synthétiser un excellent candidat pour une hyperthermie magnétique puissante.

En raison des progrès rapides effectués dans le domaine des nanotechnologies, un procédé de synthèse de nanoparticules ayant une capacité de contrôle rigoureux de: la structure et la morphologie, la taille, la forme et la cristallinité, est nécessaire. L'électrodéposition est un procédé polyvalent pour la synthèse des NPs métalliques directement et sélectivement sur des substrats conducteurs par simple réglage du courant ou de la tension appliquée. En outre, la taille des particules et la forme sont facilement contrôlables, et les études ont montré que l'électrodéposition est d'une grande utilité dans la fabrication d'alliages palladium-cobalt (PdCo) nanocristallins.

L'objectif principal de ce projet est de synthétiser des NPs d'alliage PdCo par électrodéposition sur une électrode de graphite. Les objectifs secondaires sont d'optimiser les paramètres suivants: la composition, la taille, la forme et la surface des NPs d'alliage PdCo afin d'améliorer leur stabilité, production de chaleur et nanotoxicité pour répondre aux besoins cliniques.

Pour synthétiser des NPs d'alliage PdCo monodispersées, nous avons développé une nouvelle méthode de synthèse impliquant une électrodéposition séquentielle de NPs PdCo, sur du graphite modifié par des atomes de Pd, suivi par un revêtement à l'aide de monomères de 1-dodécane-thiol (DDT). Les paramètres d'électrodéposition tels que les grains d'activation, la composition du bain électrolytique, le potentiel appliquée, et le temps de dépôt ont été étudiés. La microscopie électronique à balayage (MEB) a montré que le revêtement des NPs de PdCo avec du DDT pendant 19 heures augmente la concentration et la stabilité des nanoparticules de PdCo déposées. Les images MEB et la spectroscopie de rayons X à dispersion d'énergie ont montré que lorsque le potentiel appliqué passe de -1.0V à -1.3V: la morphologie des NPs PdCo change et évolue d'une forme de plaquette vers une forme sphérique et une agglomération de sphères, et la teneur en Co augmente pour atteindre un maximum de 35,65 %. Selon la diffraction des rayons X, la présence de glycine dans la solution du bain électrolytique améliore la structure cristalline des films de PdCo déposés.

Dans une deuxième étape, la résistance à la corrosion des nanoparticules Pd₆₅Co₃₅, synthétisées précédemment pour l'hyperthermie magnétique, a été évaluée. En plus, on a étudié l'influence du traitement thermique à 200°C, 300°C et 400°C et de la passivation de la surface avec des monomères de DDT sur la résistance à la corrosion des NPs de PdCo. Pour atteindre cet objectif, on a effectué des tests de polarisation potentiodynamiques dans une solution de Ringer's à 37°C suivie par l'analyse de la surface et du surnageant, pour comparer la stabilité des échantillons traités avec celle du control. D'après les tests de polarisation, les NPs de PdCo traitées par la chaleur possèdent les plus faibles densités de courant de corrosion i_{corr} environ 0.022114 $\mu\text{A}/\text{cm}^2$ pour 400°C, 0.027084 $\mu\text{A}/\text{cm}^2$ pour 200°C et 0.065828 $\mu\text{A}/\text{cm}^2$ pour 300°C. Par contre, l'échantillon traité avec des monomères de DDT et le control présentent des densités de courant de corrosion les plus élevées, environ 0.87202 $\mu\text{A}/\text{cm}^2$ et 0.23874 $\mu\text{A}/\text{cm}^2$ respectivement. Selon la SAA, le traitement thermique et la passivation avec de l'alcanethiole diminuent significativement la libération d'ions Pd et Co dans le surnageant après le test de polarisation dans l'ordre 200°C > 400°C > 300°C > DDT > control. En effet, les analyses XPS montrent que la corrosion des échantillons de PdCo varie selon la composition chimique à la surface, qui s'est révélée dépendante du type de traitement. De plus, après 7 jours d'immersion dans une solution de Ringer's à 37°C les échantillons traités et le control montrent une excellente résistance à la corrosion ([Pd] < 0.01 ppm; [Co] < 0.01 ppm). D'après cette étude, on peut conclure que nos nanoparticules de PdCo peuvent

être utilisées comme nanodispositif médical, si ils sont traitées avec de la chaleur ou avec des monomères d'alcanethiole pour prévenir le relargage des ions Pd and Co dans l'environnement biologique et éviter ainsi une nanotoxicité ultérieure.

Dans une troisième étape, des mesures de la boucle d'hystérésis et du point de Curie ont été effectuées sur deux échantillons de NPs de PdCo. Les résultats des mesures de la boucle d'hystérésis semblent très prometteurs. Ils ont montré un comportement ferromagnétique, et de bonnes aimantations à saturation (152.78 memu/g et 233.54 memu/g) par rapport à la masse très faible des NPs. D'autre part, les mesures du point de Curie ont confirmé l'utilité du traitement thermique après l'électrodéposition pour améliorer la microstructure de l'alliage.

Pour conclure, dans ce projet une nouvelle méthode de synthèse de NPs de Pd₆₅Co₃₅ sphériques, à l'échelle de 30-50 nm, a été réalisée par une électrodéposition séquentielle sur du graphite modifié par des atomes de Pd. De plus, le traitement des NPs de Pd₆₅Co₃₅ avec la chaleur ou à l'aide des monomères d'alcanethiol à diminuer la libération d'ions Pd et Co, pour atteindre [Pd] = 0.01 ppm ; [Co] = 0.013 ppm, dans la solution de Ringer après le test de polarisation. Cependant, les tests magnétiques ont montré que les NPs de PdCo non traités présentent un comportement ferromagnétique, en raison de la présence d'agglomération de particules, et un faible moment magnétique maximal (environ de 0.6 memu) comme résultat de la faible masse de particules déposées. Par conséquent, de nouvelles stratégies pour l'amélioration de la masse de NPs de PdCo déposée sur le substrat en graphite, essentielle pour une aimantation et une efficacité de chauffage élevées, doivent être mises en place. En outre, les techniques de sonication et de filtration doivent être optimisées afin d'étudier la biocompatibilité et superparamagnétisme de ces NPs.

ABSTRACT

According to Canadian Cancer Statistics, it is estimated that 196,900 Canadians will develop cancer and 78,000 will die of cancer in 2015. Given that tumor cells are more sensitive to a temperature increase than healthy ones, this property can be used in vivo to destroy the cancerous cells by elevation of body temperature, otherwise known as hyperthermia. Magnetic hyperthermia is a promising technique for cancer treatment because of ease in targeting the cancerous cells using magnetic nanoparticles (MNPs) and hence having fewer side effects than chemotherapy and radiotherapy.

Despite the use of magnetic hyperthermia to treat cancer for thousands of years, the challenge of only heating malignant cells remains daunting. Thus, oncologists often use the heat treatment in combination with radiotherapy or chemotherapy or both. The combined approach results in eliminating many cancer cells in addition to making the resistant cancer cells more vulnerable to other treatments.

To use stand-alone magnetic hyperthermia therapy, difficulties in surface modification of magnetic particles for selective uptake by cancerous cells and stability as well as magnetic properties for high heating capacity ($> 1000 \text{ W/g}$) must be overcome. The ultimate objective of this thesis is to synthesize an excellent candidate for a powerful magnetic hyperthermia.

Due to rapid advances in nanotechnology, a synthesis method of nanoparticles (NPs) with the ability to rigorously control the structure and morphology, such as size, shape and crystallinity, is needed. Electrodeposition is a versatile method for the synthesis of metal NPs directly and selectively onto conductive substrates, simply by regulating applied current or voltage. Furthermore, the particles size and the shape are easily controllable. Besides, studies have shown that the electrodeposition technique is of great utility in the fabrication of nanocrystalline palladium-cobalt (PdCo) alloys.

The primary goal of this project is to synthesize monodispersed PdCo alloy NPs by electrodeposition, on graphite electrode. The secondary goals are to optimize the following parameters: composition, size, shape and surface of the PdCo alloy NPs in order to enhance its stability, heat generation and nanotoxicity facing their use for clinical applications.

To synthesize monodispersed PdCo alloy NPs, we first developed a new synthetic method involving a sequential electrodeposition of PdCo nanoparticles, onto Pd-modified graphite, followed by 1-dodecanethiol (DDT) coating. The electrodeposition parameters such as activation seeds, electrolytic bath composition, applied potential, and time of deposition were investigated. The scanning electron microscopy (SEM) results showed that coating PdCo NPs with DDT for 19 hours will increase the concentration and the stability of the deposited PdCo nanoparticles. The SEM images and the energy dispersive x-ray spectroscopy (EDS) patterns showed that when the applied potential decreases from -1.0V to -1.3V: the morphology of PdCo nanoparticles changes from platelet to spherical and agglomeration-of-spheres, and the Co content increases to reach a maximum of 35.65 %. According to the x-ray diffraction (XRD) patterns, the presence of glycine in the electrolytic bath solution enhances the crystalline structure of the deposited PdCo films.

In a second step, the corrosion resistance of previously synthesized Pd₆₅Co₃₅ nanoparticles (NPs) for magnetic hyperthermia was evaluated. Furthermore, the influence of heat treatment at 200°C, 300°C and 400°C and surface passivation with DDT monomers on the corrosion resistance of PdCo NPs was investigated. We compared the corrosion behaviour of the treated samples with the control using potentiodynamic polarization assay in Ringer's solution, followed by surface and corrosion electrolyte analysis. During polarization test, PdCo NPs treated with heat displayed the lowest corrosion current density i_{corr} of 0.022114 $\mu\text{A}/\text{cm}^2$ for 400°C, 0.027084 $\mu\text{A}/\text{cm}^2$ for 200°C and 0.065828 $\mu\text{A}/\text{cm}^2$ for 300°C. On the contrary, the sample treated with DDT monomers and the control exhibited the highest corrosion density of i_{corr} of 0.87202 $\mu\text{A}/\text{cm}^2$ and 0.23874 $\mu\text{A}/\text{cm}^2$ respectively. According to AAS, the heat and alkanethiol treatments significantly decrease the release of Pd and Co ions in the supernatant after the polarization assay in the order 200°C > 400°C > 300°C > DDT > Untreated. XPS analysis showed that the corrosion of treated/untreated PdCo samples varies upon the chemical composition at the surface, which revealed to be treatment-dependent. Moreover, after 7 days of immersion in 37°C Ringer's solution both treated and untreated samples exhibited an excellent corrosion resistance ([Pd] < 0.01 ppm; [Co] < 0.01 ppm). This study concluded that PdCo NPs could be use as medical nanodevice if they were treated with heat or alkanethiol monomers to prevent high Pd and Co ions release in biological environment and subsequent nanotoxicity.

In a third step, the hysteresis loop and Curie point measurements were done over two samples of PdCo NPs. The results of the hysteresis loop measurements are very promising. They showed a

ferromagnetic behavior, and good saturation magnetizations (152.78 memu/g and 233.54 memu/g) compared to the very low mass of NPs. Besides, Curie point measurements confirmed the usefulness of the heating treatment after electrodeposition to enhance the microstructure of the alloy.

To conclude, in this project a new synthesis method of spherical Pd₆₅Co₃₅ NPs, in the range of 30-50 nm, was achieved by a sequential electrodeposition onto Pd-modified graphite. Moreover, the heat treated and alkanethiol treated Pd₆₅Co₃₅ NPs samples exhibited a low release of Pd and Co ions, which may reach [Pd] = 0.01 ppm; [Co] = 0.013 ppm, in the Ringer's solution after the polarization assay. However, magnetic tests showed that untreated PdCo NPs exhibit ferromagnetic behaviour, due to the presence of agglomerated particles, and low maximum magnetic moment (about 0.6 memu) as result of low deposited mass of particles. Therefore, new strategies to improve the deposited mass of PdCo NPs onto graphite substrate, essential for high magnetizations and heating efficiencies, must be developed. In addition, sonication and filtration techniques must be optimized in order to study the biocompatibility and superparamagnetic properties of PdCo NPs.

TABLE OF CONTENTS

DEDICATION	III
ACKNOWLEDGEMENTS	IV
RÉSUMÉ.....	VI
ABSTRACT	IX
TABLE OF CONTENTS	XII
LIST OF TABLES	XIV
LIST OF FIGURES.....	XV
LIST OF SYMBOLS AND ABBREVIATIONS.....	XVIII
CHAPTER 1 INTRODUCTION	1
CHAPTER 2 LITERATURE REVIEW	7
2.1 ARTICLE 1: RECENT PROGRESS ON MAGNETIC NANOPARTICLES FOR MAGNETIC HYPERTHERMIA	7
2.1.1 Introduction	7
2.1.2 Basics of magnetism in magnetic hyperthermia	8
2.1.3 Biomaterials for magnetic hyperthermia.....	17
2.1.4 Nanotoxicity of biomaterials	22
2.1.5 Conclusions	28
Acknowledgments	28
CHAPTER 3 OBJECTIVES AND METHODOLOGY	29
CHAPTER 4 SUMMARY OF THE WORKS.....	36
4.1 ARTICLE 2: ELECTRODEPOSITION OF PdCo NANOPARTICLES ONTO Pd-MODIFIED GRAPHITE ELECTRODE FOR FUTURE MEDICAL NANODEVICES	36
4.1.1 Introduction	37
4.1.2 Materials and methods	38
4.1.3 Results and discussion.....	42

4.1.4 Conclusion.....	52
Acknowledgments	52
4.2 ARTICLE 3: CORROSION BEHAVIOR OF PALLADIUM-COBALT NANOPARTICLES FOR THE DESIGN OF NEW HYPERTHERMIA IMPLANTS	53
4.2.1 Introduction	54
4.2.2 Materials and methods	57
4.2.3 Results and discussion.....	60
4.2.4 Conclusions	77
Acknowledgments	78
CHAPTER 5 GENERAL DISCUSSION	79
CHAPTER 6 CONCLUSION AND RECOMMENDATIONS.....	93
6.1 CONCLUSION	93
6.2 RECOMMENDATIONS	95
BIBLIOGRAPHY	97

LIST OF TABLES

Table 2-1 Magnetic parameters at room temperature [51].....	11
Table 2-2 Maximum radius for superparamagnetic NPs of different compositions [54,55].	14
Table 2-3 Magnetizations of a variety of types of MNPs of varying sizes.	14
Table 4-1 Energy dispersive x-ray spectroscopy (EDS) results of electrodeposited PdCo at different electrodeposition parameters before and after addition of Glycine.	46
Table 4-2 Corrosion parameters for the PdCo samples extracted from Tafel curves.	62
Table 4-3 Corrosion supernatants analysis by atomic absorption spectroscopy.	63
Table 4-4 Static contact angle measurements before the corrosion assay on the PdCo samples...64	
Table 4-5 Surface average roughness (Rq) of the 4 samples, obtained from AFM images before and after the polarization test.	68
Table 4-6 Chemical composition of the elements for PdCo samples surface before (B.P.) and after polarization (A.P.).	73
Table 4-7 Identification and quantification of the binding energies of Pd3d5/2, O1s and Co2p3/2, involved in chemical species at the surface of the various PdCo samples, from high energy resolution.	74
Table 4-8 Atomic composition of the chemical elements observed in the survey spectra of the untreated PdCo alloy before and after sputtering.	75
Table 4-9 Quantity of metal ions released during 166 hours.	77

LIST OF FIGURES

Figure 2-1 Typical hysteresis loop of ferromagnetic materials [49].	10
Figure 2-2 Relative stability of multi-domain and single-domain [50].	11
Figure 2-3 The magnetic response characteristic of a superparamagnetic material [49].	12
Figure 2-4 Schematic of anisotropy energy barrier for magnetization reversal [52].	13
Figure 2-5 Illustration of the covalent interaction between Fe 3d and Pd 4d orbitals [92].	21
Figure 2-6 Pourbaix diagram showing iron and palladium species and water stability region [116].	25
Figure 2-7 Growth curves for a) the pure metals composing the Pd-Co alloys, b) the Pd ₃₄ Co ₅₇ alloys [117].	26
Figure 2-8 Phase diagram of PdCo system obtained from FactSage software [131].	28
Figure 3-1: Schematic of three electrodes electrochemical cell [147].	31
Figure 4-1 Illustration of the three treatments (T1, T2, and T3) for coating PdCo nanoparticles by self-assembled monolayers of DDT.	41
Figure 4-2 Cyclic Voltammograms (10 th cycle) curves of clean and Pd-modified graphite registered in the electrolytes with different composition of both palladium (II) and cobalt (II) ions. (Scan rate: 50 mV/s).	43
Figure 4-3 XRD patterns of electrodeposited PdCo films at different electrodeposition parameters, after addition of glycine.	45
Figure 4-4 SEM images of electrodeposited PdCo films before (a) and after (b) the addition of glycine to the bath solution. (Magnification of 3K x)	47
Figure 4-5 SEM images of electrodeposited PdCo NPs at: -1.0 V (a); -1.1 V (b); -1.2 V (c) and -1.3 V (d). (magnification of 100k x)	49
Figure 4-6 SEM images of electrodeposited PdCo at different time of deposition: 5 minutes (a); 2 minutes (b); and 1 minute (c). (magnification of 100k x)	50

Figure 4-7 SEM images and the corresponding size distribution histograms of two sequential electrodeposition of PdCo with and without treatment with 1-dodecanthiol (DDT): without treatment (a); treatment 1 (b); treatment 2 (c); and treatment 3 (d). (magnification of 100K x).	51
Figure 4-8 Phase diagram of PdCo system obtained from FactSage software [171].	55
Figure 4-9 Pourbaix diagram showing palladium and cobalt species and water stability region.	56
Figure 4-10 Open circuit potential (vs ESCE) as function of time for the 5 differently treated PdCo NPs samples, immersed in 37 °C Ringer's solution.	61
Figure 4-11 Polarization curves of PdCo NPs samples in Ringer's solution.	62
Figure 4-12 Contact angles of a) graphite, PdCo NPs b) untreated, c) DDT treated and d) treated with heat at 200 °C and e) at 300 °C.	64
Figure 4-13 SEM micrographs of PdCo NPs before (left) and after (right) polarization assay. (A): untreated, (B): treated with DDT, (C): heated at 200 °C, (D): heated at 300 °C, and (E): heated at 400 °C.	66
Figure 4-14 AFM images of PdCo NPs before and after polarization assay, left and right respectively. (A): untreated, (B): treated with DDT, (C): heated at 200 °C, and (D): heated at 300 °C.	67
Figure 4-15.a XPS survey spectra before (upper) and after (lower) polarization of untreated PdCo samples.	70
Figure 4 15.b XPS survey spectra before (upper) and after (lower) polarization of PdCo samples protected with DDT.	72
Figure 4 15.c XPS survey spectra before (upper) and after (lower) polarization of PdCo samples heated at 200 °C.	73
Figure 4 15.d XPS survey spectra before (upper) and after (lower) polarization of PdCo samples heated at 300 °C.	74
Figure 4-16 High resolution XPS of Pd 3d _{5/2} and Co 2p _{3/2} before (upper) and after sputtering (lower).	77

Figure 5-1 Longitudinal M–H hysteresis loop for Pd–14 % Co (A) and Pd–12 % Co (B) alloys, obtained by two sequential electrodepositions at -1.2 V, during 1 minute each and followed by DDT protection (19 h).....	82
Figure 5-2 SEM images of electrodeposited Pd–14 % Co (A) and Pd–12 % Co (B) alloys obtained by two sequential electrodepositions at -1.2 V, during 1 minute each and followed by DDT protection (19 h). (magnification of 20k x).....	83
Figure 5-3 Curie point as a function of the atomic percentage of cobalt [186].	84
Figure 5-4 Magnetic moment as a function of temperature for sample B (Pd–12 % Co), obtained by two sequential electrodepositions at -1.2 V, during 1 minute each and followed by DDT protection (19 h).	85
Figure 5-5 Magnetic moment as a function of temperature for Pd–30 % Co (left), deposited at -1.2 V for 45 s, and for graphite (right).	85
Figure 5-6 Magnetic moment as a function of temperature for sample B and sample Pd–30 % Co after subtraction of the graphite magnetic moments.	87
Figure 5-7 SEM images of (a) PdCo sample before sonication, (b) PdCo sample after sonication for 30 minutes at room temperature and (c) 36 μ L solution of PdCo on graphite.	88
Figure 5-8 SEM images of (a) PdCo sample after sonication for 7 hours and 30 minutes at room temperature and (b) 36 μ L solution of PdCo on brass.	89
Figure 5-9 SEM images of (a) PdCo sample after sonication for 7 hours and 30 minutes at room temperature and more 6 hours at 55 °C, and (b) 36 μ L solution of PdCo on brass.	90

LIST OF SYMBOLS AND ABBREVIATIONS

AAS	Atomic absorption spectroscopy
AMF	Alternating magnetic field
CE	Counter electrode
CVs	Cyclic voltammograms
DDT	1-dodecanethiol
EDS	Energy dispersive x-ray spectroscopy
FCC	Face centered cubic
H _c	Coercive field
HER	Hydrogen evolution reaction
IONPs	Iron oxide nanoparticles
LD ₅₀	Median lethal dose
MNPs	Magnetic nanoparticles
Mr	Magnetic remanence
MRI	Magnetic resonance imaging
Ms	Saturation magnetization
NPs	Nanoparticles
OCP	Open circuit potential
PEG	Polyethylene glycol
PSA	Prostate specific antigen
RE	Reference electrode
ROS	Reactive oxygen species
SAMs	Self assembled monolayers
SAR	Specific absorption rate

SCA	Static contact angle
SCE	Saturated calomel electrode
SDS	Sodium dodecyl sulfate
SEM	Scanning electron microscopy
SLP	Specific loss of power
SPMIONPs	Superparamagnetic iron oxide nanoparticles
SPMNP	Superparamagnetic nanoparticles
WE	Working electrode
XRD	X-ray diffraction

CHAPTER 1 INTRODUCTION

The term of nanotechnology is attributed to Nobel Laureate in physics Richard Feynman when he proposed miniaturizing computing devices toward their physical limits, during a speech in December 1959 at an annual meeting of the American Physical Society (at Caltech) [1].

Nanotechnology refers to a field whose theme is the understanding and control of matter at dimensions of roughly 1–100 nanometers. Nanoparticles (NPs) are one of the most important ingredients in nanotechnology. NPs are the simplest form of structures, having one or more dimensions of the order of 100 nanometres or less. Due to their very small size, NPs display an immense surface area per unit volume. The resulting unique chemical and/or physical properties can differ quite extensively from the properties of the corresponding bulk material [2].

It has been recognized that, ‘In a relatively short interval for an emerging technology, nanotechnology has made a significant economic impact in numerous sectors including semiconductor manufacturing, catalysts, medicine, agriculture, and energy production’ [3]. According to the National Science Foundation, the value of products incorporating nanotechnology as the key component reached about \$200 billion in value worldwide in 2008, and an estimation for a product value of \$1 trillion by 2015 [4].

The concept of nanoscale particles is not new. NPs occur naturally in biologic systems, such as protein (dimensions in the range of 1.0-20 nm), or formed in combustion process. Today, nanotechnology brings the capability to control production and make engineered particles of very specific sizes and shapes, based on its properties at the atomic scale [5].

The progress forward in nanotechnology requires collaboration among interdisciplinary area of research in science, medicine and engineering. Research and development in nanotechnology is changing how bioscientific research is conducted and how medicine is practiced. Nanotechnology is expected to revolutionize the practice of medicine [6].

Nanomedicine is the medical application of nanotechnology. It seeks to deliver a valuable set of research tools and clinical devices [7]. Over the past decade, several NPs-based therapeutic and diagnostic agents have been developed for the treatment and detection of cancer, infectious

diseases, and allergens [8]. The greatest impact of nanomedicine is expected to be in cancer therapy [9].

Due to their size-tunable light emission (or magnetic properties) when used in conjunction with X-ray radiation (or magnetic resonance imaging), NPs can produce a high contrast image. Another nanoproperties are: i) the high surface area to volume ratio, which allows many functional group to be attached in order to seek out and bind to certain tumor cells, and ii) the small size, which endows them to penetrate through leaky angiogenic vessels to finally accumulate at tumor sites, due to lack of an effective lymphatic drainage system [7].

Since the late 1960s, the interest in using magnetic hyperthermia therapy in medicine has increased. In oncology, magnetic hyperthermia is meant to target unhealthy cells and keep the healthy cells unharmed. Given that healthy cells have organized and systematic blood flow in their surrounding vascular network, they can easily cool down and dissipate excessive heat. However, cancer cells have often far less developed vascular network and therefore overheat [10].

Magnetic Hyperthermia can be achieved by heating tumors or tissues to temperatures between 40°C and 45°C via MNPs in alternating magnetic field (AMF) [11], either to:

- i) *Sensitise tumor to conventional treatments* [12]. Studies show that moderate hyperthermia below 42°C increases tumor blood flow, which leads to higher supply of oxygen and nutritious supplements to the tumor. The resultant increase in blood flow assists in efficient delivery of drugs and chemotherapeutic agents to the tumor, and increased oxygen supply favors radiotherapy effects. In fact, in physiological conditions the blood flow is tightly regulated by vasodilatation factors that stimulate endothelial cells to release nitric oxide, which then causes relaxation of the vascular smooth muscle and subsequent increased blood flow [13]. On the other hand, moderate hyperthermia showed to increase the amount of the overall tumor nitric oxide production [14] and thus increase the tumor oxygenation.
- ii) *Perform tumor-targeted drug delivery* [10]. Recently, there has been considerable attention on developing drug release systems through hyperthermia using thermosensitive magnetic gels, such as Poly (N-isopropylacrylamide). The thermosensitive Poly (N-isopropylacrylamide) hydrogels were found to exhibit volume

changes of over 800% when immersed in distilled water or seawater solutions at temperatures ranging from 5 °C to 50 °C [10]. In addition, these hydrogels are swollen at temperatures below 34 °C but collapse at 34 °C and above [15]. Therefore, by introducing magnetic particles within thermo sensitive hydrogel; as the magnetic particles get heated, they will raise the temperature of the hydrogel inducing the collapse transition. Hence, drug molecules dissolved in the hydrogel will be released during this collapse transition, creating a novel combined drug release and hyperthermia system.

- iii) *Induce tumor regression.* The study performed by Loo et al. [16] showed that at temperatures *above* 42 °C tumor blood flow decreases, due to changes in viscosity of blood cell membrane, leading to hypoxia, acidosis, and cell energy deprivation. In general, the tumor blood flow decreases as the tumors grow larger due to progressive deterioration of vascular beds and rapid growth of tumor cell population relative to vascular beds [17]. Consequently, the heat dissipation by blood flow in tumors is slow and thus their temperatures of tumor rise during heating. As a result, vasculature in tumor is significantly damaged upon heating [17].
- iv) *Boost immune system* [18]. Pre-clinical studies suggest that, similar to fever, hyperthermia is associated with immunological reactions and can stimulate and activate host immune systems against malignant cells. Whole body hyperthermia in animals has been shown to reduce pathology and increase natural killer cell activity [19], since natural killer cells are thought to play an important role in the first line of defense against infectious and malignant disease [20].

Superparamagnetic NPs are suitable candidates for magnetic hyperthermia. Due to thermal fluctuations in sufficiently small size, they have no remanent magnetization at room temperature [21]. This minimizes the possibility of aggregation, which could have harmful effects, and favors biological absorption and eventually the excretion of particles by the body.

Metals such as iron, cobalt and nickel (and their alloys) are useful MNPs for magnetic hyperthermia, because they are able to create heat once placed in an external AMF. Various compositions such as Cu-Ni [22], Gd-substituted Mn-Zn ferrite [23], CoFe_2O_4 [24], and Mn-Zn ferrite have also been used for the purpose of hyperthermia.

Among different chemical compositions of MNPs, the most studied superparamagnetic nanoparticles for hyperthermia are those of iron oxide, Magnetite (Fe_3O_4) and Maghemite ($\gamma\text{-Fe}_2\text{O}_3$). That is due to its proven biocompatibility, very low toxicity and biodegradability [25]. Iron cobalt has shown higher magnetization than iron oxide [26]. However, due to unknown toxicity issues of this magnetic compound further investigation is required before it can reach human clinical trials.

To use stand-alone magnetic hyperthermia therapy, difficulties in surface modification of magnetic particles for selective uptake by cancerous cells and stability as well as magnetic properties for high heating capacity ($> 1000 \text{ W/g}$) must be overcome [27].

According to Rosensweig, the heating efficiency in a uniform magnetic field only depends upon the saturation magnetization (M_s), Néel relaxation time and the volume fraction of the superparamagnetic particles [28]. However, the preparation of metallic NPs with high M_s ($>100 \text{ emu/g}$) remains challenging due to: i) the chemical synthesis of the nanoparticles, which is often associated with a poorly crystalline structure and the presence of oxides [29], or ii) the oxidation of nanoparticles and the release of metallic ions [30]. This explains why the heating efficiency of the common MNPs is low ($<1000 \text{ W/g}$).

In general, an annealing step followed by a polymer (or silica) coating is required to improve their M_s by avoiding the oxidation of the metal [31]. However, the existence of a magnetically dead layer on the surface of particles can lead to a decrease of the M_s with respect to the core value [32].

On the other hand, modern implant design is directed on making use of the immune response to improve implant integration while avoiding its perpetuation leading to chronic inflammation and foreign body reactions, and thus loss of the intended function [33]. The adsorbed protein layer on biomaterial surface usually provides binding sites for protein-specific receptors (integrins, specific pattern recognition receptors) on polymorphonuclear neutrophils, monocytes and macrophages. Thus, depending on the surface chemistry of the nanoparticles proteins adhering may either initiate and foster inflammation or assist healing.

To conclude, there is an unmet technical challenge to design new MNPs which possess not only high thermal efficiency as heating elements and stability in physiological medium but are also immunomodulator to escape the immune system. To successfully overcome the issues mentioned

above, the relationship between the magnetic and the physicochemical properties as well as the interaction between the NPs's surface and biological medium must be investigated.

Due to rapid advances in nanotechnology, a synthesis method of NPs with the ability to rigorously control the structure and morphology, such as size, shape and crystallinity, is needed. Electrodeposition is a versatile method for the synthesis of metal nanoparticles directly and selectively onto conductive substrates, simply by regulating applied current or voltage [34]. Furthermore, the particles size and the shape are easily controllable. Besides, studies have shown that the electrodeposition technique is of great utility in the fabrication of nanocrystalline PdCo alloys [35].

The ultimate objective of this project is to synthesize new candidate for a stand-alone magnetic hyperthermia. The primary goal is to synthesize monodispersed PdCo alloy NPs by electrodeposition, on graphite electrode, and optimize the following parameters: composition, size, shape and surface. The secondary goals are to study the corrosion resistance and the magnetic performance in order to evaluate the stability, heat generation and nanotoxicity of our PdCo NPs facing their use for clinical applications. Moreover, complementary magnetic tests (such as hysteresis loop and Curie point measurements) and ultrasonic bath were done over PdCo NPs samples to investigate their magnetic behavior and the feasibility of separating these NPs from the graphite electrode, respectively.

PdCo is chosen based on: i) the excellent corrosion resistance of palladium [36], unlike iron which is the most corrosion vulnerable metal and ii) the great magnetic properties of cobalt, CoFe achieved an extremely high heating performance of 1300–1600 W/g [37]. The significance of our project is to develop a PdCo based MNPs with better magnetic properties than iron oxide due to less corrosion-related problems, and uselessness of coating material. Moreover, the values of the saturation magnetization (M_s) for PdCo alloys of 5 mm diameter and 0.1 mm thickness disk were given by Bagguley et al. [38] and are very promising. The values of M_s decreased with the cobalt content from a value near 89.96 emu/g for the 74.7 at. % Co to reach 40.60 emu/g for the 23.0 at. % of Co.

In addition, Pd-based material has a powerful oxygen reduction properties compared to iron, which can be used to decrease the Reactive Oxygen Species¹ (ROS) level and thus enhance the biocompatibility of NPs.

The ROS (such as superoxide, hydrogen peroxide, hydroxyl radical, hydroxyl ion, and nitric oxide) are free radicals derived from sequential reduction of atomic oxygen, which have two unpaired electrons in its outer electron shell, through the addition or loss of electrons. Metals such as iron are capable of redox cycling in which a single electron may be accepted (e.g. Fe(III)) or donated (e.g. Fe(II)) by the metal, according to Fenton reactions [39]. Thus, the presence of such metals in biological systems catalyzes the production of ROS and can significantly increase the level of oxidative stress.

The ROS is the most commonly considered factor in the NP toxicity studies because NPs have high surface-to-volume ratio that make interaction with surrounding elements and electron attack more likely [40]. Moreover, NPs can induce ROS both outside and inside cells, disrupting organelles such as mitochondria, lysosomes, and nuclei and trigger cell signaling pathways, leading to cell death through necrosis or apoptosis [41].

Furthermore, there is a lack of research on PdCo alloys for biomedical application, which makes this project unique. In general, PdCo is most studied as magnetic film for magnetic recording media and catalyst for fuel cell application.

¹ Known also as oxidative stress, ROS (such as oxygen ions and peroxides) are chemically reactive molecules containing oxygen. They are formed as a natural byproduct of the normal metabolism of oxygen.

CHAPTER 2 LITERATURE REVIEW

2.1 Article 1: Recent progress on magnetic nanoparticles for magnetic hyperthermia

Lina Kafrouni^{1,2} and Oumarou Savadogo^{1,2 *}

¹ Department of Chemical Engineering, Polytechnique Montréal, C.P. 6079, Succursale Centre-ville, Montréal, Québec, H3C 3A7, Canada.

² Laboratory of New Materials for Energy and Electrochemistry systems (LaNoMat).

* Phone: +1-514-340-4725; fax: +1-514-340-4468; e-mail: osavadogo@polymtl.ca

Submitted to Progress in Biomaterials, on February 23rd, 2016. (PIBM-D-16-00005)

Abstract- Recent advances in nanomaterials science contributed to develop new micro- and nano-devices as potential diagnostic and therapeutic tools in the field of oncology. The synthesis of superparamagnetic nanoparticles (SPMNPs) has been intensively studied, and the use of these particles in magnetic hyperthermia therapy has demonstrated successes in treatment of cancer. However, some physical limitations (such as the saturation magnetization ‘Ms’ is inversely proportional to the particle size) have been found to impact the heating efficiency required to kill cancer cells. Moreover, the bio-safety of NPs remains largely unexplored. The primary goals of this review are to summarize the recent progress in the development of magnetic nanoparticles (MNPs) for hyperthermia, and discuss the limitations and advances in the synthesis of these particles. Based on this knowledge, new perspectives on development of new biocompatible and biofunctional nanomaterials for magnetic hyperthermia are discussed.

Keywords— Magnetic nanoparticles, synthesis, magnetic hyperthermia, cancer.

2.1.1 Introduction

According to the national cancer institute, cancer is currently the second leading cause of death in the United States, exceeded only by heart disease as the number one killer. A total of 1,620 Americans are expected to die of cancer per day in 2015.

Significant progress has been made so far in nanotechnology for the diagnosis and treatment of cancer. A variety of magnetic nanomaterials has been developed to achieve improved efficacy in

cancer therapy as well as reduced side effects compared to conventional therapies. The interest in MNPs is due to their unique magnetic properties, they exhibit diagnostic tool, drug carrier and heat generator for therapy in magnetic resonance imaging (MRI), so-called ‘theranostic’ and their small sizes, which allow the particles to reach most biological tissues. Currently, iron oxide nanoparticles (IONPs) are the most explored MNPs for magnetic hyperthermia, because of their lack of toxicity and their known pathways of metabolism [42].

The generation of heat by the exposition of MNPs to a non-invasive alternating magnetic field (AMF) can be used to destroy tumor tissue, given that heat promotes cell apoptosis through irreversible physiological changes [43]. This approach is known as magnetic hyperthermia.

Apoptosis is generally induced through extrinsic and intrinsic pathways. The extrinsic pathway is mediated through cell surface death receptors and the intrinsic pathway is mediated through the mitochondria [44]. In the extrinsic pathway, the tumor necrosis factor receptor-associated death domain protein binds to and activates apoptosis initiator caspases-8 and caspases-10 [45]. Whereas in the intrinsic pathway, DNA damage with subsequent translocation of Bax protein to the mitochondria results in dissipation of mitochondrial transmembrane potential with release of cytochrome-c and thus induce apoptosis through activation of apoptosis initiator caspase-9 [46].

The basics of the magnetic properties required in MNPs for magnetic hyperthermia applications will be discussed later in details.

The synthesis methods of MNPs have an impressive impact on the magnetic and morphological properties of the final product [47]. Therefore, a synthesis method with the ability to rigorously control the composition, size and shape, is needed. This paper presents a short review on the current methods for synthesis of MNPs for nanomedicine, and discusses important findings reported earlier.

2.1.2 Basics of magnetism in magnetic hyperthermia

An understanding of the relationship between physicochemical properties (for example: structure, particle size) and magnetic properties is essential in order to design new magnetic materials for magnetic hyperthermia applications. Therefore, a review on the basic concepts in nano-magnetism will be discussed shortly.

2.1.2.1 Soft and hard magnets

When a ferromagnetic material, such as Iron, nickel and cobalt, is placed in a magnetic field of strength 'H', the atoms acquire an induced magnetic moment 'm' randomly oriented. The magnetic moments pointed in the same direction per volume of atoms are called magnetization 'M'. The magnetic induction 'B' is given by Maxwell's equation (Equation 1) [48].

$$B = \mu_0(H + M) \quad (\text{Equation 1})$$

Where μ_0 is the permeability in vacuum, and has an exact value of $4\pi \cdot 10^{-7} \text{ V.s/A.m}$.

The small regions of magnetization are called magnetic domains, and the boundaries between domains are called domain walls. In the absence of an external magnetic field, ferromagnetic material does not show any magnetization due to the random orientation of the magnetizations in magnetic domains (Point a, figure 2-1). However, when an external magnetic field is applied magnetic moments become aligned to the direction of the magnetic field, so domain walls disappear and the magnetization becomes saturated, so-called saturation magnetization (M_s) (figure 2-1).

Once the applied magnetic field is removed, ferromagnetic materials keep some memory of the applied field (Point b, figure 2-1), called remanence (M_r). A coercive force must be applied to reduce the remanent magnetization to zero and close the loop.

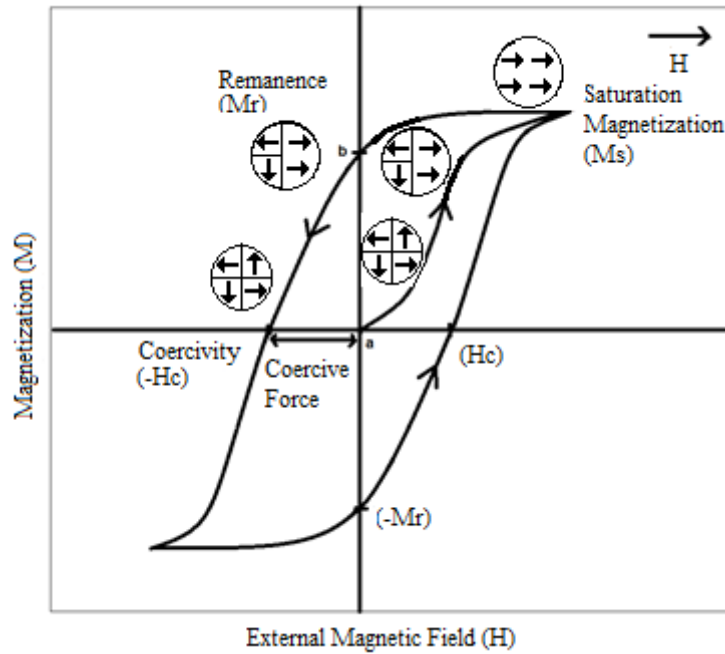


Figure 2-1 Typical hysteresis loop of ferromagnetic materials [49].

Ferromagnetic materials can be categorized into soft and hard magnets [49]. Soft magnets have a low coercivity (H_c), so they can be demagnetized at low magnetic field. However, hard magnets exhibit a high H_c and thus they are difficult to demagnetize.

2.1.2.2 Multi-domain to single domain

The magnetostatic (dipole-dipole) energy is inversely proportional to the volume of the particle (r^3), and the domain-wall energy is proportional to the area of the wall (r^2) (Figure 2-2) [50].

By looking at the balance between the magnetostatic energy and the domain wall energy, it is energetically unfavorable to form domain walls below a critical radius, because the domain-wall energy is very low, and a single-domain is formed as result of high magnetostatic energy.

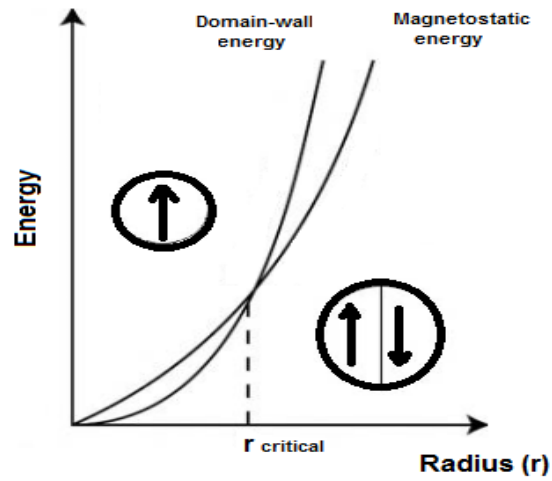


Figure 2-2 Relative stability of multi-domain and single-domain [50].

For a sphere containing two semi-sphere domains of opposite magnetization with axial magnetic anisotropy, the critical single-domain radius is given by equation 2 [51].

$$r_{critical} = \frac{36\sqrt{AK_1}}{\mu_0 M_s^2} \quad (\text{Equation 2})$$

Where A is the exchange stiffness and K_1 is first uniaxial anisotropy constant.

The critical radius values corresponding to ferromagnetic elements Fe, Co and Ni are calculated according to equation 2 and are presented in table 2-1.

Table 2-1 Magnetic parameters at room temperature [51].

Ferromagnetic particles	Fe	Co	Ni
A (pJ/m)	8.3	10.3	3.4
K_1 (MJ/m ³)	0.05	0.53	-0.005
$\mu_0 M_s$ (T)	2.15	1.76	0.61
r_c (nm)	6	34	16

2.1.2.3 Superparamagnetism

It has been found that with a further decrease in particle size below the critical radius, the coercivity H_c decreases significantly to reach zero. When the coercivity becomes zero, the particles magnetize in the presence of an external magnetic field and revert to a non-magnetic state when the external magnetic field is removed (Figure 2-3) [49].

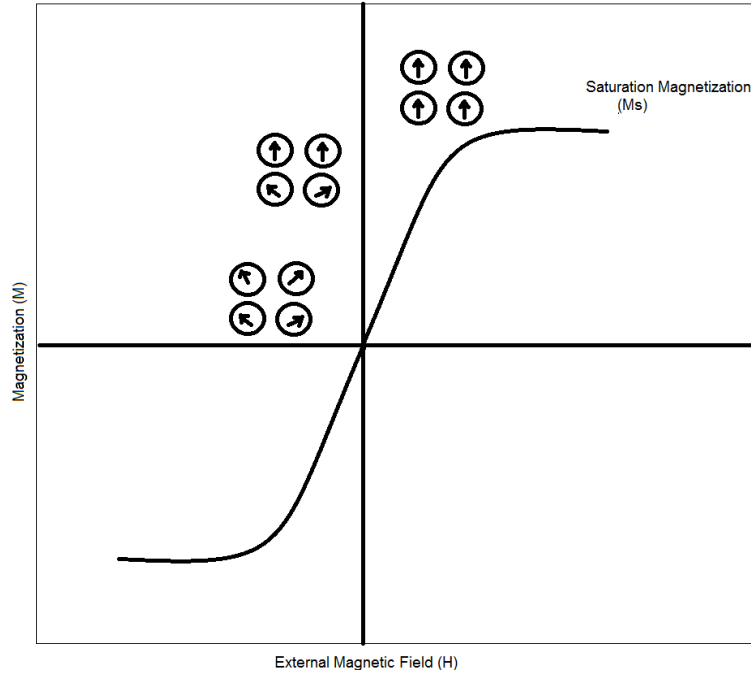


Figure 2-3 The magnetic response characteristic of a superparamagnetic material [49].

This behavior can be explained by the fact that a small magnetic particle less than critical size prefers to be uniformly magnetized along one of its easy axes ($\theta = 0, \theta = \pi$), and the energy required to rotate the magnetization away from the easy direction is called magnetic anisotropy energy. In a simple model for a non-interacting single-domain spherical particle with uniaxial anisotropy in zero magnetic field, the magnetic anisotropy energy ' E_A ' is given by an expression of equation 3 [52].

$$E_A = K.V.\sin^2\theta \quad (\text{Equation 3})$$

Where K is the anisotropy constant, V is the volume of the particle and θ is the angle between the particle magnetization and the easy magnetization axis of the particle.

According to equation 3, the magnetic anisotropy energy decreases when the volume of the particle becomes smaller. Furthermore, the anisotropy energy becomes comparable to or even lower than the thermal energy ($E_{thermal}=k_B.T$, where k_B is Boltzmann constant) [53]. As a result, the energy barrier for magnetization reversal can be overcome thermally (Figure 2-4). This phenomenon is called ‘superparamagnetism’.

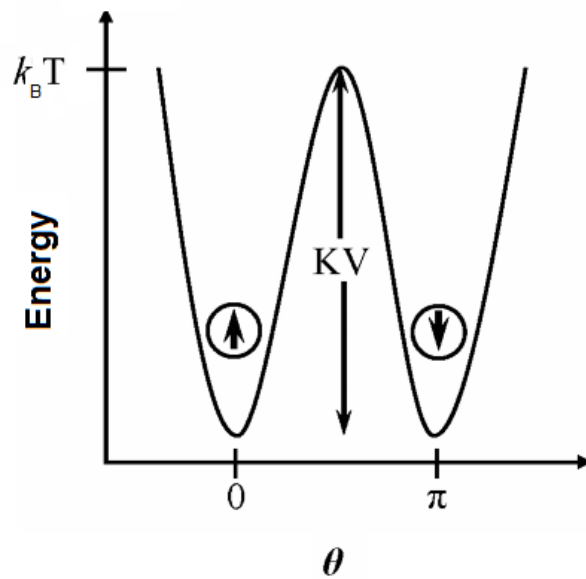


Figure 2-4 Schematic of anisotropy energy barrier for magnetization reversal [52].

Due to the fact that these particles are magnetically controlled by an external magnetic field and maintain a colloidal stability upon removal of the external magnetic field, superparamagnetic particles have a unique advantage for biomedical applications.

For spherical magnetic particles, the transition from single-domain to superparamagnetic ‘ r_0 ’ depends upon the size and/or geometry of the particles and can be determined by the following equation [54]:

$$r_0 = \left(\frac{6 \cdot k_B \cdot T_B}{K} \right)^{1/3} \quad (\text{Equation 4})$$

Where T_B is the blocking temperature.

Table 2-2 provides calculated values of the transition radius ‘ r_0 ’, according to equation 4, for the main magnetic nanomaterials [54,55].

Table 2-2 Maximum radius for superparamagnetic NPs of different compositions [54,55].

Superparamagnetic NPs	Co	CoPt	CoFe ₂ O ₄	FeCo	Fe ₃ O ₄	Fe ₂ O ₃	FePt	Ni
r_0 (nm)	5	1	5	10	12.5	15	1.5	15

Although particle moves toward superparamagnetism when the size of the particle decreases below the transition point and becomes suitable for biomedical application, the saturation magnetization ‘Ms’ reduces. The magnitude of Ms is inversely proportional to the ratio of disordered spin layer at the surface to the radius of the particle, which significantly increases when the size of the nanoparticle becomes too small. The relationship between Ms, the size and the disordered spin layer is described by equation (5) [56]:

$$M_s = M_{s_b} \left[\frac{(r-d)}{r} \right]^3 \quad (\text{Equation 5})$$

Where d is the thickness of the particle’s surface exhibiting disordered spins, and M_{s_b} is the bulk Ms. Recent studies on the effect of the size of MNPs upon its saturation magnetization are summarized in table 2-3. According to the studies listed in table 2-3, the Ms increases with the size of the MNPs due to the reduction of the spin disorder effect.

Table 2-3 Magnetizations of a variety of types of MNPs of varying sizes.

MNPs	Size (nm)	Ms (emu/g)	Ref
CoFe ₂ O ₄	4.2	30.6	[57]
	4.8	46.0	
	18.6	48.8	
Fe ₃ O ₄	4.9	60.4	[58]
	6.3	64.8	
Ni	24	25.3	[58]
	50	32.3	

Recent study done by Guardia et al. have demonstrated that the surface coating of iron oxide (Fe_3O_4) NPs with oleic acid increases their measured Ms to reach the bulk value, by reducing the level of surface spin disorder [59].

2.1.2.4 Heat generation

Heating tumor cells with SPMNPs by magnetic hyperthermia is based on Néel and Brownian relaxations. In the presence of an external alternating magnetic field, the magnetic moment rotates and the nanoparticle itself rotates then relax back to their original magnetic field orientation. The rotation of the magnetic moment (Néel mode) and the friction arising from particle oscillations (Brownian mode) lead to a phase lag between applied magnetic field and the direction of the magnetic moments. As result, the heat is released.

The efficiency of heating is measured in terms of the specific absorption rate (SAR), or specific loss of power (SLP), which is defined in equation 6. For biomedical applications, the value of SAR is crucial because the higher the specific absorption rate, the lower the injected dose to the patient.

$$\text{SAR or SLP (W/g)} = C \frac{\Delta T}{\Delta t} \quad (\text{Equation 6})$$

Where C is the specific heat capacity of water, and $\Delta T/\Delta t$ is the rate of change of temperature versus time.

According to Rosensweig [60], there is a strong relationship between the SAR of SPMNPs and its magnetic relaxation ‘ τ ’ (Equation 7).

$$\text{SAR} = 4.1868\pi \mu_0^2 \frac{\phi M_s^2 V}{1000kT} H_0^2 \nu \frac{2\pi\nu\tau}{1+(2\pi\nu\tau)^2} \quad (\text{Equation 7})$$

Where ϕ is the volume fraction of the SPMNPs, $V = \frac{4\pi r^3}{3}$ is the magnetic volume for a particle of radius r, H_0 is the magnetic field intensity, ν is the frequency of the oscillating magnetic field and τ is the relaxation time.

Also, equation 7 shows that the SAR strongly depends on the M_s and the volume fraction of the SPMNPs. Not only high M_s values are required for thermal energy dissipation in the tumor cells, but also to give more control on the magnetophoretic velocity of the MNPs ‘ V_{mag} ’ in the blood using external magnetic field [61] (Equation 8).

$$V_{mag} = \frac{M_s V_{microdevice} \nabla B}{6\pi R_{microdevice} \mu} \quad (\text{Equation 8})$$

Where $V_{microdevice}$ is the volume of microdevice (m^3), ∇B is the magnetic gradient applied (T/m), $R_{microdevice}$ is the microdevice radius (m) and μ is the blood viscosity (Pa.s).

Theoretically, a critical diameter d_c is defined as the diameter for which Néel relaxation time ' τ_N ' (equation 9) is equal to Brownian relaxation time ' τ_B ' [62] (equation 10). For small particles with a diameter $< d_c$, Néel relaxation is predominant. However, the heating is primarily due to Brownian rotation in larger particles with a diameter $> d_c$. The dominating contribution will be by the faster relaxation time.

$$\tau_N = \tau_0 e^{\frac{K.V}{k_B.T}} \quad (\text{Equation 9})$$

$$\tau_B = \frac{3\eta V_B}{k_B.T} \quad (\text{Equation 10})$$

Where $\tau_0 \approx 10^{-9}$ - 10^{-12} s is the relaxation time of non-interacting MNPs, η is the viscosity of the surrounding liquid and V_B is the hydrodynamic volume of the particle.

The frequency ν_N for maximal heating via Neel relaxation is given by equation 11, and the frequency ν_B for maximal heating via Brown rotation is given by equation 12 [63].

$$2\pi\nu_N\tau_N = 1 \quad (\text{Equation 11})$$

$$2\pi\nu_B\tau_B = 1 \quad (\text{Equation 12})$$

When the diameter of the particle is close to d_c , $\tau_N \approx \tau_B$ and an effective relaxation time ' τ_{eff} ' is defined in equation 13. The frequency for maximal heating ' ν_{eff} ' is then given by equation 14 [64].

$$\tau_{eff} = \frac{\tau_N\tau_B}{(\tau_N + \tau_B)} \quad (\text{Equation 13})$$

$$2\pi\nu_{eff}\tau_{eff} = 1 \quad (\text{Equation 14})$$

Recent research optimized the heating efficiency by tuning the MNPs size in order to match the total relaxation time ($\tau_{total} = \tau_N + \tau_B$) to the applied frequency ($\nu = \frac{1}{2\pi\tau_{total}}$) [65].

The strong dependence of the SAR on multiple magnetic properties such as saturation magnetization and relaxation time, physical parameters like size, shape and composition can be

tailored to enhance the heat dissipation and thus lower the injected dose of SPMNPs in the tumor site.

2.1.3 Biomaterials for magnetic hyperthermia

In order to develop excellent candidates for magnetic hyperthermia, it is very important to review the recent advances and limitations in the development of MNPs for magnetic hyperthermia applications.

Superparamagnetic iron oxide nanoparticles (SPMIONPs) are the most used MNPs for biomedical applications, especially magnetic hyperthermia. They received considerable attention due to their biocompatibility compared to other magnetic materials such as cobalt and nickel [66]. The high biocompatibility of IONPs is due to well controlled cell homeostasis by uptake, excretion and storage [67]. Moreover, they do not cause oxidative stress even at high doses [68]. However, nickel and cobalt are susceptible to oxidation and toxic, even though they exhibit a high magnetic moment, because they are not essential elements to the body like iron and thus accumulate in the body and cause illness.

IONPs become superparamagnetic at room temperature when their radius is below about 15 nm [55], and aggregation is a common phenomenon among SPMIONPs [69]. Therefore, bare SPMIONPs are coated against aggregation by either non-magnetic or magnetic shell [70]. Usually the type of coatings has an impact on the heating efficiency of the core through modifying the surface properties. Details on the types of shells used to protect IONPs and their effect over magnetic properties will be discussed.

Among iron oxides, magnetite (Fe_3O_4) and maghemite ($\gamma\text{-Fe}_2\text{O}_3$) are very popular candidates and have unique magnetic properties suitable for biomedical applications.

Iron metal (Fe) has a higher magnetization than magnetite and maghemite. However, Fe is highly susceptible to oxidation, which limits its use for biomedical applications. Qiang et al. synthesize oxidative stable Fe-core MNPs coated with iron oxide and having an increasing Ms from about 80 emu/g (at the cluster size of 3 nm) to 200 emu/g (at the size of 100 nm) [71].

In general, MNPs are coated with a selected material to enhance their colloidal stability and biocompatibility or to offer them the capacity to functionalize the surface, like in the case of a

coating of silica (SiO_2) [72]. Furthermore, coating can be used to modify MNPs surface in order to increase their M_s and consequently increase the SAR.

Studies show that coating MNPs with non-magnetic material, for example Fe_3O_4 coated with SiO_2 [73], will reduce M_s (from 72 emu/g to 37 emu/g) and hence SAR (from 1.5 ± 0.1 W/g to 1.08 ± 0.04 W/g) as compared to uncoated MNPs. The decrease in M_s was attributed to the enhanced surface spin effects, and thus not all the IONPs mass contribute to M_s . Furthermore, the effective anisotropy constant ' K_{eff} ' increases due to the strain and surface spin disorders created by SiO_2 coating, and the blocking temperature T_B experience similar variations since T_B is defined as the product of the K_{eff} and the volume of the nanoparticles ' V ' (Equation 15) [74].

$$T_B = \frac{K_{\text{eff}} \cdot V}{25 \cdot k_B} \quad (\text{Equation 15})$$

Surface spin effect (or surface spin disorder) is the result of the surface electrons engagement in the bond with the coating material, which no longer participate in the magnetic super-exchange bonds between metal cations (example: Fe-O-Fe), and thus reduce the coordination between surface spins [75].

Fe_3O_4 NPs coated with SiO_2 and functionalized with propylamine groups showed higher magnetization saturation ($M_s \approx 42$ emu/g) than uncoated Fe_3O_4 ($M_s \approx 27$ emu/g), where both were synthesized by thermal decomposition in oleic acid [76]. It seems that the surface of Fe_3O_4 is magnetically more active in Fe_3O_4 NPs coated with silica-propylamine than that of uncoated Fe_3O_4 covered with oleic acid.

On the contrary, Fe_3O_4 NPs coated with silica-propylamine showed slightly lower magnetization saturation ($M_s \approx 58$ emu/g) than uncoated Fe_3O_4 ($M_s \approx 60$ emu/g) [77], where Fe_3O_4 NPs were obtained by co-precipitation in aqueous medium. The contradictory results of these two studies suggest that the synthesis and coating methods can be tailored to enhance the magnetic properties of the MNPs.

Capping Co-MNPs with metallic shell (such as Cu or Au) provides us a high tuning opportunity over the magnetic properties (for example, enhance surface anisotropy and higher blocking temperature), due to the bonding of the d-orbital electrons of the core to the conduction band orbitals of the capping layer [78]. This suggests that the surface anisotropy is mainly determined

by the electronic states of the core-shell metals and therefore it could be tuned by choosing materials with appropriate electronic band structures.

For hyperthermia applications, an SLP of 1000 W/g is necessary at 100 kHz and 20 mT (human-compatible conditions). By taking advantage of the exchange coupling between a magnetically hard core (CoFe_2O_4) and soft shell (MnFe_2O_4), MNPs exhibiting a significant enhancement in SLP have been developed [79]. Various combinations of core-shell nanoparticles tuned M_s of the single-component MNPs to achieve high SLP while maintaining the superparamagnetism. For example $\text{Zn}_{0.4}\text{Co}_{0.6}\text{Fe}_2\text{O}_4$ core and $\text{Zn}_{0.4}\text{Mn}_{0.6}\text{Fe}_2\text{O}_4$ shell MNPs have an SLP of 3866 W/g and thus exhibit 1.7 times higher SLP than that for CoFe_2O_4 (core) MnFe_2O_4 (shell) MNPs (2274.12 W/g) (NP size= 12 nm, at 500 kHz and 37.3 kA/m) and 34 times larger than that for commercial Feridex Fe_3O_4 NPs (210 W/g) (NP size= 10-12 nm, at 880 kHz and 7.2 kA/m).

Spherical MnFe_2O_4 SPMNPs show lower SLP of 411 W/g ($r=15$ nm) when compared to that of MnFe_2O_4 (core) CoFe_2O_4 (shell) ($r=12$ nm) where SLP is about 3034 W/g (at 500 kHz and 37.3 kA/m) [80]. Clearly, core-shell design has the advantage in achieving large SLP while keeping the superparamagnetism of the nanoparticle. In the same work, cubes of CoFe_2O_4 coated with $\text{Zn}_{0.4}\text{Fe}_{2.6}\text{O}_4$ (NP size= 60 nm) showed a 4-fold increase in coercivity as compared to the core alone (NP size= 50 nm). This increase is consequently followed by a dramatically higher SAR for the shell-core MNPs (10 600 W/g) when compared to that of MNPs composed of just the core (4060 W/g) (at 500 kHz and 37.4 kA/m).

Many efforts have been dedicated toward understanding the relationship between the shape of MNPs and their magnetic properties. Several studies showed that the M_s is proportional to the volume of the particle (V) with the same crystalline composition but different shape [81,82], due to the decrease of the surface-to-volume ratio and consequently surface spin disorder. For example, considering MNPs having the same unit size (d) (where 'd' corresponds to the side length for nanocubes, the width for nanorods and the diameter for nanospheres), the V of nanocube is higher than the V of nanorod, and the V of nanosphere is lower than the V of nanorod. Therefore, the same order of M_s is expected (M_s of nanocube $>$ M_s of nanorod $>$ M_s of nanosphere).

A study on the effect of the shape of Fe_3O_4 NPs over its saturation magnetization is done by Zhen et al. [83]. The authors observed a higher M_s for the cubic shape ($M_s=40$ emu/g) compared to the

spherical shape ($M_s = 31$ emu/g), where the volume of the cube is slightly higher than that of the sphere ($V_{cube} > V_{sphere}$). They attributed the lower magnetization of spherical Fe_3O_4 NPs to their crystalline defect structure or greater degree of oxidation and non-magnetic iron oxide (Fe_2O_3) content.

According to Noh et al. [80], the cubic shape of $Zn_{0.4}Fe_{2.6}O_4$ has a higher M_s (165 emu/g) value than the spherical shape (145 emu/g) with the same volume. In fact, the surface of the cube shape has a smaller surface anisotropy since its topology comprises low energy facets. As result, disordered magnetic spins in cubic NPs (4 %) are lower than in spherical NPs (8 %).

However, in a study done by Montferrand et al. on Fe_3O_4 NPs [84] M_s for the cubic shape (40 emu/g) is lower than the spherical shape (80 emu/g) of the same size. Unexpected M_s could be related to size polydispersity and polymorphism detected in TEM images.

Magnetic properties are also defined by the atomic state of the elements, especially the number of unpaired valence electrons. For example, Fe(III) have five unpaired electrons and thus a moment of $5 \times 1.73 = 8.65$ Bohr magnetons. Moreover, the distribution of ions in the structure is another parameter responsible for the determination of the moment. For example, in an inverse spinel structure of ferrites, the magnetic moments of the cations in the octahedral sites are aligned parallel to the magnetic field, and the ones in the tetrahedral sites are antiparallel, leading to a decrease in the net moment [85].

Hence, doping MNPs with cations is of great interest in nanomedicine because it tailors the physical and magnetic properties, without affecting its crystal structure, due to the nature of the cation and its relative distribution in the tetrahedral and octahedral sites [86].

Lee et al. [85] compared the crystal structure of four spinel ferrites (MFe_2O_4): $MnFe_2O_4$ (110 emu/g), $FeFe_2O_4$ (101 emu/g), $CoFe_2O_4$ (99 emu/g), and $NiFe_2O_4$ MNPs (85 emu/g). $MnFe_2O_4$ had a mixed spinel structure, where Mn^{2+} and Fe^{3+} occupied both octahedral and tetrahedral sites, and an inverse spinel structure where Mn^{2+} and Fe^{3+} occupied octahedral sites and only Fe^{3+} occupied the tetrahedral sites.

The inclusion of Ni^{2+} in the ferrite spinel structure ($Ni_xFe_{3-x}O_4$ with $x = 0, 0.04, 0.06$ and 0.11) has no substantial change in the value of M_s , where Ni^{2+} occupy Fe^{2+} octahedral sites [87]. Gabal

et al. examined the Zn^{2+} doped nickel ferrite ($\text{Ni}_{1-x}\text{Zn}_x\text{Fe}_2\text{O}_4$; $0 < x < 1$) and noticed that the M_s increases by increasing Zn doping levels up to 0.5 [88]. This behavior can be explained by the fact that magnetite (Fe_3O_4), with a spinel structure, has Fe^{3+} ions occupying tetrahedral (inverse) sites and Fe^{2+} with Fe^{3+} ions residing in the octahedral sites. During cation exchange Fe^{2+} in octahedral site is replaced by Ni^{2+} and NiFe_2O_4 is formed. Since the tetrahedral and octahedral sites are antiferromagnetically coupled, the net moment of Ni ferrite equals the moment of octahedral site ($\text{Ni}^{2+}, \text{Fe}^{3+}$) minus the moment of tetrahedral (Fe^{3+}). The inclusion of non-magnetic Zn^{2+} in NiFe_2O_4 substitutes Ni^{2+} then occupies a tetrahedral site and force magnetic Fe^{3+} to migrate to octahedral site and, as x increases. As result, the net moment increases due to the decrease in fraction of moment of tetrahedral site and an increase in moment of octahedral sites [88].

FeCo MNPs usually exhibit high M_s values (122 - 230 emu/g) compared with CoFe_2O_4 MNPs [89], due to the absence of the non-magnetic oxygen component [90]. However, the ease of oxidation in the presence of air is the key issue for these alloys [90].

Palladium metal is a non-magnetic element but tends to order ferromagnetically when alloyed with a small amount of magnetic transition metal impurities (such as Fe, Co and Ni 3d metals) [91]. A polarization of Pd atom by a magnetic impurity is due to the hybridization and exchange between 4d and 3d orbitals (Figure 2-5) [92].

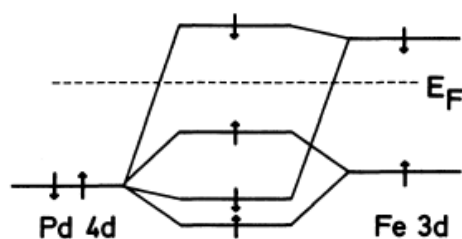


Figure 2-5 Illustration of the covalent interaction between Fe 3d and Pd 4d orbitals [92].

The appearance of ferromagnetism can be explained by the large density of states at the Fermi level (E_F).

Joseph A. Paulus and Robert D. Tucker proposed for the first time PdCo seeds for thermal treatment of tumors [93]. PdCo thermoseeds (typically rod shape where $d=1\text{mm}$ and $L=1-2\text{ cm}$) are permanently implanted into the cancerous tissue, and thus the patient can be scheduled for

activation of the thermoseeds at intervals of minimal thermotolerance [93]. The authors developed a new approach to treat prostate cancer, post-radiotherapy, using these thermoseeds. During thermotherapy, PdCo rods heat up when exposed to an alternative magnetic field (due to eddy current) to a specific temperature (Curie temperature), at which the alloy goes from being magnetic to non-magnetic, and ceases to heat up and it simply maintains the Curie temperature as long as it remains in the magnetic field [93].

Deger et al. [94] conducted a clinical study on the treatment of patients with localized prostate cancer with a magnetic hyperthermia, using self-regulating PdCo thermoseeds, after radiotherapy. During hyperthermia, PdCo thermoseeds heating temperatures were between 42 and 46°C with a curie temperature of 55°C. The initial median prostate specific antigen (PSA) value was 11.6 ng/ml, and then decreased to 1.3 ng/ml and 0.55 ng/ml after 12 and 24 months respectively after the therapy. Moreover, PdCo seeds proved to be biocompatible and do not show major complication during the treatment, and remain in the prostate during follow up [94].

According to Brezovich et al. [95], a heat production rate of 200 mW/cm is adequate for most clinical application. El-Sayed et al. calculate the power dissipated from $\text{Pd}_{89.2}\text{Co}_{10.8}$, $\text{Pd}_{73}\text{Ni}_{27}$ and $\text{Cu}_{29.6}\text{Ni}_{70.4}$ ferromagnetic seeds, having a rod shape with a diameter of 0.9 mm diameter and a 5.5 cm length as function of temperature [96]. At 20°C, the heating power of $\text{Pd}_{89.2}\text{Co}_{10.8}$ was about 171 mW/g, and 150 mW/g for $\text{Pd}_{73}\text{Ni}_{27}$. The $\text{Cu}_{29.6}\text{Ni}_{70.4}$ seed showed a much smaller heating power of 80 mW/g. Therefore, $\text{Pd}_{89.2}\text{Co}_{10.8}$ seed exhibit the highest heating power to treat localized tumors compared with the other two alloys, at 100 kHz and 4 kA/m.

Iron based-MNPs have been widely studied for nanomedicine (especially for cancer treatment) and palladium-cobalt alloys have not received significant attention. Although Pd and Co are toxic elements, PdCo alloy has a higher stability and resistance to corrosion [97] compared to Fe based-alloy [98]. Moreover, the researches done over PdCo thermoseeds are very promising and encouraging to develop new MNPs candidates for thermotherapy made of PdCo alloys.

2.1.4 Nanotoxicity of biomaterials

Upon administration into tumor tissue MNPs interact with blood components (e.g. Plasma and platelets), where thousands of biomolecules compete for limited space on a NP surface [99], due

to van der Waal's interactions, electrostatic interactions, hydrogen bonding and/or hydrophobic interactions [100]. As result, MNPs acquire a dynamic exchange plasma proteins layer, so-called 'corona' [99], in which competitive displacement of earlier adsorbed proteins (generally small molecular weight and highly concentrated proteins, such as serum albumin) by other proteins with stronger binding affinities (typically of a larger molecular weight, such as kininogen) take place and is referred to 'Vroman Effect' [101]. Thus, the identity, organization and residence time of these proteins determine the way cells interact with NPs [99]. Moreover, the adsorbed proteins identity and their total amount showed to be strongly dependent on the particle surface chemistry (like surface composition, charge, topography and area) [100].

Studies show that plasma proteins, including immunoglobulins and complement proteins, once adsorbed to NPs surfaces it target the particles as pathogens for clearance (called 'opsonization') by the reticulo-endothelial system and mononuclear phagocytic system [102]. In fact, the immune system may recognize the proteins as native or as foreign pathogen depending on whether the proteins bind or not to immune cells receptors. Following proteins adsorption, platelets cells adhesion and activation on NPs may occur via interaction of adhesion receptors with the adsorbed blood proteins such as fibrinogen, fibronectin, vitronectin, and the von Willebrand factor [103,104]. As result, inflammatory cells (primary polymorphonuclear leukocytes) migrate from the blood toward the NPs, triggered by chemoattractants released from activated cells [105]. Inflammatory cells adsorption over the protein-coated NPs surface, due to protein ligands of integrins, lead to an acute or chronic inflammation [106].

The concept of inert biomaterials points out the need of strategies for improving implant integration, to avoid foreign body reactions. It was shown that when macrophages are cultured on surface-modified polymers displaying hydrophobic, hydrophilic and/or ionic chemistries, they change their protein expression profiles and cytokine/chemokine responses [107]. Consequently, current studies in the design of such biomaterials include passive modulation of the surface chemistry, to limit immune responses. For example, polyethylene glycol (PEG)-modified surface prevents proteins adsorption due to its sterically hindered and hydrophilic coating [108], and are thus protected against cell adhesion and activation. On the other side, functionalization of the surface with bioactive molecule such as adhesion sites (e.g. Fibronectin) [109], anti-inflammatory

drugs (e.g. Glucocorticoid) [110] and growth factors (e.g. Platelet-derived growth factor) [111] is also a very interesting strategy for modulating or suppressing inflammatory responses.

MNPs can induce toxicity, not only by activating cells in a direct way as discussed above, but also indirectly by excessive tissue accumulation of free metal ions [112]. It was shown that reactive oxygen species (ROS) are generated by the cells as a result of leached ions after exposure to an acidic environment, such as lysosomes (pH= 4.5) [113]. In general, most cells can tolerate a certain amount of ROS, whereas higher levels of ROS persist over a longer time and may result in cell damage and subsequent induction of toxic effects [114].

The mechanism by which NPs cause cell apoptosis via ROS remains unclear. However, the intrinsic apoptosis pathway is generally proposed for superparamagnetic iron oxide-induced cell apoptosis [40]. In the intrinsic pathway, NPs infiltrate into the mitochondria and boost ROS production resulting in mitochondrial membrane disorder and subsequent release of pro-apoptotic proteins, cytochrome c, and apoptosis-inducing factor, which then activates caspase-9 and caspase-3 to boost cell apoptosis [41].

Since the toxicity of the NPs is affected by the level of induced ROS, the surface must be stable against degradation to limit the quantity of free metal ions.

Potential (Eh)-pH diagram or Pourbaix diagram is essential to investigate the thermodynamic of material corrosion, by monitoring the regions of potential and pH where the metal is: unreacted (region of immunity), protected by a surface film of an oxide or a hydroxide (region of passivity) or dissolved (region of corrosion) [115]. Figure 2-6 shows the Pourbaix diagram for both iron and palladium elements in water containing fluoride ions [116]. According to the diagram, iron will corrode and produce Fe(II) and/or Fe(III) at potential zero and at pH below 6, whereas palladium remains unreacted under these conditions. This difference in stability is due to the higher reactivity of iron towards oxidation ($E_{\text{Fe(II)/Fe}}^{\circ} = -0.44\text{V}$; $E_{\text{Fe(III)/Fe}}^{\circ} = -0.04\text{V}$), compared with palladium ($E_{\text{Pd(II)/Pd}}^{\circ} = +0.915\text{V}$). Moreover, iron forms a porous oxide layer when exposed to water or air [117], and consequently anodic (iron)/cathodic (iron oxide) sites created at the surface trigger the process of corrosion.

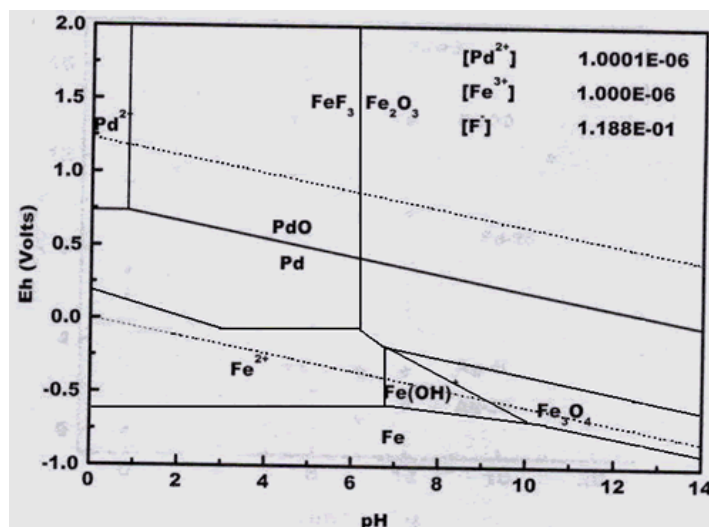
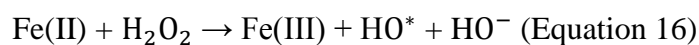
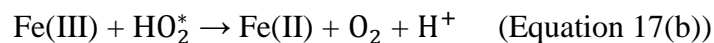
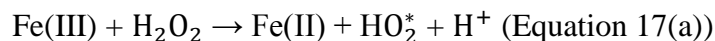


Figure 2-6 Pourbaix diagram showing iron and palladium species and water stability region [116].

The reactivity of iron towards oxidation reveals the toxicity of uncoated IONPs [118], and suggests more study into the biocompatibility of the coatings on the long term [119]. The most important source of toxicity of IONPs is described by ‘Fenton’ and ‘Fenton like’ reactions (equation 16 and equation 17 respectively) [39], in which the Fe(II) or Fe(III) reacts with H_2O_2 to produce ROS species.



$$k = 76 \text{ M}^{-1}\text{s}^{-1}$$



$$k = 0.01 \text{ M}^{-1}\text{s}^{-1}$$

Free ROS species exhibit a lack of specificity with which they react [120], and this makes the study of the oxidative mechanism in the toxicity of iron ions very complex [121]. However, ROS interactions with biological components have been classified into three types of reactions: electron transfer, radical addition and atom abstraction, and identified to cause cells damage [122].

The toxicity of Pd, Co pure metal and $\text{Pd}_{43}\text{Co}_{57}$ alloy was tested in vitro for dental casting (Figure 2-7) [123]. It was shown that the cells multiply in the presence of Pd as much as those for the control, and keep their natural form. Whereas in the presence of Co, the cells degenerate with time and approaches zero at 72h of incubation due to cytoplasmic shrinkage and blister formation. On the other hand, the binary alloy $\text{Pd}_{43}\text{Co}_{57}$ enhances the cells growth and morphology compared with pure Co, showing a monotonically increase of cell multiplication like the control. These results indicate that the toxicity of Co may be avoided when alloyed with Pd.

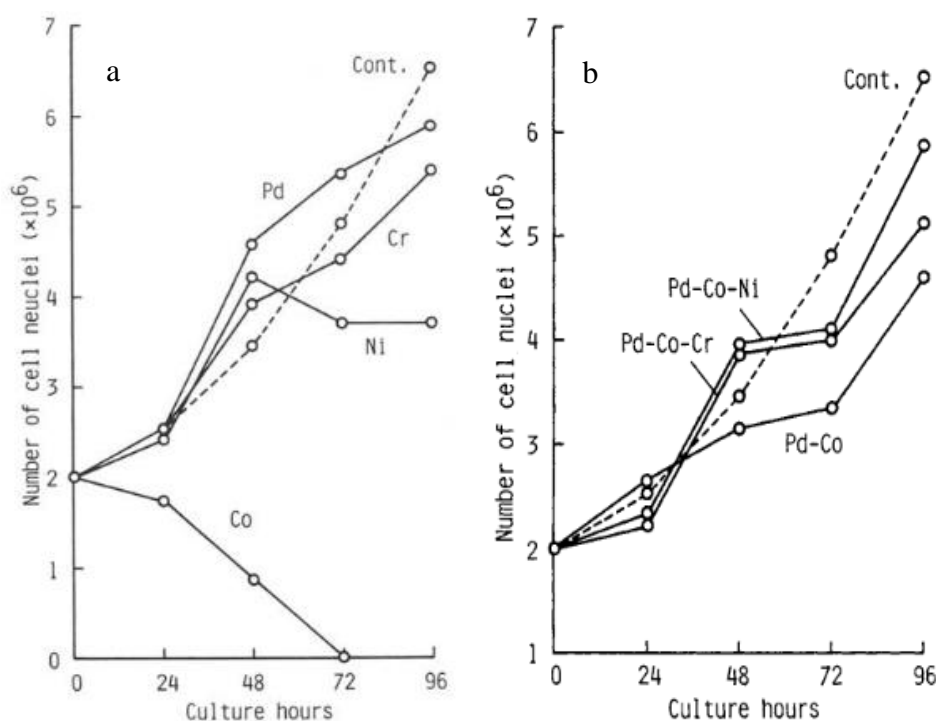


Figure 2-7 Growth curves for a) the pure metals composing the Pd-Co alloys, b) the $\text{Pd}_{34}\text{Co}_{57}$ alloys [117].

The corrosion of the binary alloy $\text{Pd}_{80.8}\text{Co}_{19.2}$ in synthetic saliva [124] produces a selective dissolution of the less-noble components 'Co' on the surface of the alloy, leaving a Pd-enriched layer on the surface. The results of corrosion are in accordance with that of toxicity, the safety of a biomaterial largely dependent on its corrosion resistance. Therefore, pure palladium is non-toxic due to the low dissolution rate of palladium ions [125], while pure Co is not stable and thus releases toxic cobalt ions.

Despite belonging to essential trace elements of the human body, the accumulation of cobalt ions is genotoxic and may cause induce necrosis with inflammatory response [126]. The oral median lethal dose (LD_{50}) for soluble Co salts has been estimated to be between 150 and 500mg/kg body weight [126]. Further, very low doses of Pd are sufficient to cause allergic reactions in susceptible individuals [127]. An allergy response is a hypersensitive immune reaction towards harmless allergens. At the first exposure to an allergen, B cells encounter the allergen and differentiate into a plasma cell to produce large amounts of antigen-specific IgE. The IgE molecules attach to mast cells inducing the release of large amounts of histamine and other inflammatory chemicals, which lead to swelling and redness.

Oral LD_{50} of palladium oxide is about 4.9g/kg body weight [128]. Also high concentrations of Pd ions are capable of eliciting a series of cytotoxic effects [127].

Electrochemical corrosion test and immersion test were performed at 37°C for $Pd_{93.85}Co_{6.15}$ alloy sample (with a density of 11.4g/cm³) in mammalian Ringer's solution [129]. The tests results showed a long-term corrosion rate of $7.7 \cdot 10^{-8}$ µm/year, and a release of 0.7µg/l of Pd(II) with 1.8µg/l of Co(II) per year, indicating a significantly high corrosion resistance of PdCo compared with standard surgical implants (0.04 µm/year) [129].

According to phase diagram of PdCo alloy (figure 2-7), a single phase solid solution of substitutional Co atoms in a Pd lattice is formed when the atomic percentage of Pd is higher than 53 %. Consequently, the corrosion behavior of the PdCo alloy will be similar to that of pure Pd. In fact, palladium remains unreacted at normal pH or even acidic environment, as stated in Pourbaix diagram (figure 2-6). Pure palladium corrodes only in extremely acidic medium, which is unlikely to occur in biological media. The selective dissolution of Co near or at the surface on the long-term is possible [129], and as result Co-depleted layer is formed. The alloy is then likely to exhibit passivation behavior of pure palladium. An additional dissolution of cobalt may occur by volume diffusion of these less noble atoms to the surface [130].

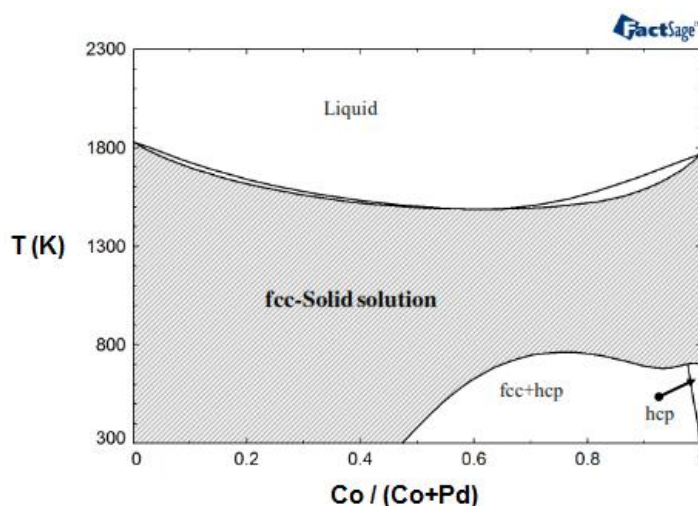


Figure 2-8 Phase diagram of PdCo system obtained from FactSage software [131].

Alloying Pd and Co not only induces ferromagnetism in Pd atoms but also enhances the corrosion resistance of Co atoms, which makes this alloy a good candidate for biomedical application.

2.1.5 Conclusions

In this study, we have reviewed the basics of magnetic properties and nanotoxicity of NPs for magnetic hyperthermia. Also, recent advances on the most used MNPs for biomedical application were discussed. From this study it can be seen that despite its corrosion problem, iron oxide NPs have received considerable attention. However, new candidates such as PdCo NPs may have a great potential for magnetic hyperthermia due to their high corrosion resistance and good ferromagnetic behaviour.

Acknowledgments

The authors thank the Fonds Québécois de la Recherche sur la Nature et les Technologies (FQRNT) and the Fondation Universitaire Pierre Arbour for their funding of this research.

CHAPTER 3 OBJECTIVES AND METHODOLOGY

Magnetic NPs are frequently employed in biomedical research as drug delivery systems and/or magnetic resonance contrast agents. Nevertheless, the safety issues of these particles have not been completely solved because it is difficult to compare the cytotoxicity data since the toxic effects of NPs are influenced by many parameters (such as size distribution, surface coating, magnetic properties, etc.) [132]. Also, numerous studies showed contradicting findings since different cell types will interact with the same particle in different ways [133]. Moreover, the lack of coherence between various research activities for establishing priorities among the research needs is one reason why a toxicological profile of these particles has not yet been well documented in the literature. Therefore, along with the expanding applications of NPs and the growing numbers of consumer products containing NPs, the release of these substances into the environment is expected, and the impact of these materials is increasing significantly [134].

Recent studies show that Fe_3O_4 NPs can affect the cellular functionality by altering the level of transferrin receptor expression and can change the cellular proliferation capacity by altering the expression of cyclins and cyclin-dependent kinases in cell cycle [135,136]. Other research has reported the cytotoxic effects of Fe_3O_4 NPs on the cytoskeleton of growing neurons [137], by increasing cytoskeletal disruption and decreasing their ability to form mature neurites in response to nerve growth factor exposure. Moreover, researchers are finding evidence that Fe_3O_4 NPs exposure can produce mutagenic effects including: chromosomal aberrations, DNA strand breakage, oxidative DNA damage and mutations [138]. It is worth noting that the excess of iron exposure has been found to cause elevated ROS generation through the Fenton reaction, resulting in oxidative stress that damages DNA, lipids and proteins, consequently resulting in carcinogenesis [139]. These findings confirm previous reports that the presence of intracellular Fe_2O_3 nanoparticle constructs can result in significant changes in cell behavior and viability [140].

Based on the above literature review, PdCo NPs produced by electrodeposition have never been considered as potential magnetic materials for cancer treatment using hyperthermia therapy.

On the other hands, magnetic nanoparticles can induce toxicity by excessive tissue accumulation of free metal ions [141], due to the high levels of reactive oxygen species (ROS) generated by the cells [142], as a result of leached ions, and which may result in cell damage and subsequent toxic effects [143]. Since the toxicity of the nanoparticles is affected by the levels of induced ROS, the surface of the nanoparticles must be stable upon degradation to limit the quantity of free metal ions. Corrosion tests done over Pd-rich PdCo alloys in oral simulated environment showed a high corrosion resistance [144]. Furthermore, Pd rich-PdCo seeds showed a heating temperatures between 42 and 46°C during the treatment of localized prostate cancer, as result of ferromagnetic properties of Co [145].

Therefore, Pd-rich PdCo NPs may have also a great potential for magnetic hyperthermia use, and thus it will be very interesting to investigate for the first time the synthesis and corrosion resistance of Pd-rich PdCo NPs.

From these interesting results, the main objective of this work is to develop magnetic PdCo NPs for cancer treatment using magnetic hyperthermia therapy.

Accordingly, the first step of this work is the synthesis of the PdCo nanoparticles by electrodeposition.

In fact, the nanofabrication processes can be divided into the two well-known approaches: bottom-up and top-down. The bottom-up approach (such as self-assembly of NPs or monomer/polymer molecules, chemical or electrochemical reactions for precipitation of nanostructures, sol-gel processing, laser pyrolysis, chemical vapor deposition (CVD), plasma or flame spraying synthesis, and atomic or molecular condensation) implies that the nanostructures are synthesized onto the substrate by stacking atoms onto each other, which gives rise to crystal planes, and then crystal planes stack onto each other, resulting in the synthesis of the nanostructures. Whereas, the top-down approach (such as photo-lithography and electron beam lithography, anodization, and ion- and plasma etching (PE)) implies that the nanostructures are synthesized by etching out crystals planes that are already present on the bulk material.

Top-down methods are generally not suitable for production on a very large scale because they presently encounter technological limitation and require extremely long and costly processes. In addition, the biggest issue with top-down approach is the imperfection of the surface structure and

the significant crystallographic damage to the processed patterns. While bottom-up approach promises a better chance to obtain nanostructures with less defects and more homogenous chemical composition.

Electrodeposition is a bottom-up method that uses electrical current to reduce dissolved metal cations into a thin layer of the material onto a conductive substrate surface. Typically, a conventional three electrodes electrochemical cell (Figure 3-1) is used for this purpose. It allows the application of the potential/current onto the working electrode (WE) without the contribution of the other electrodes. The counter electrode (CE) is used to complete the current path, while the reference electrode (RE) serves as potential control and measurement.

The strengths of electrodeposition technique are numerous, such as rapidity, simplicity, low-cost, scalability, manufacturability and does not require high vacuum facilities [146]. However, the powerful feature is its ability to control the composition, size and shape of the electrodeposited material.

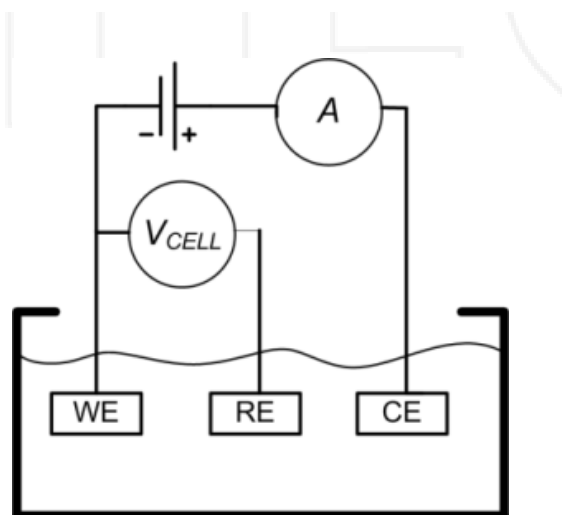


Figure 3-1: Schematic of three electrodes electrochemical cell [147].

Furthermore, the potential of degradation of metallic NPs and the subsequent release of cytotoxic metallic ions can be determined by using the same electrochemical setup.

According to the literature, the resistance of metallic NPs toward corrosion can be enhanced by heat treatments or surface passivation, as they reduce the surface reactivity towards oxidation.

Thus, it is very interesting to investigate the corrosion resistance of PdCo NPs and evaluate the effect of heat and alkanethiol layer on their stability.

In addition, no in-depth research has been performed so far neither on the electrodeposition of PdCo NPs onto graphite nor the study of the stability of these particles. Hence, this work consists of four main studies:

- Synthesis and characterization of magnetic PdCo films and nanoparticles.
- Optimization of the electrodeposition parameters during the synthesis of PdCo.
- Corrosion behaviour of PdCo nanoparticles in Ringer's solution.
- Effect of the heat and alkanethiol treatments on the corrosion resistance of PdCo nanoparticles.

To achieve these goals, we have developed a new method for the synthesis of PdCo NPs using a sequential electrodeposition on graphite electrode. Despite the difficulties to deposit PdCo on the highly oriented pyrolytic graphite, it was used as working electrode to obtain a 3D growth required to produce nanoparticles. To enhance the deposition on graphite electrode, small Pd particles were deposited by electroless on the graphite surface acting as an efficient particle-mediated electron transfer, from graphite to Pd(II) + Co(II) ions, for Pd and Co electrodeposition. Later, a sequential electrodeposition followed by 1-dodecanethiol coating was adopted to increase the number of nanoparticles. Moreover, electrodeposition parameters (such as graphite surface, bath composition, applied potential and time of electrodeposition) were optimized to produce spherical Pd-rich PdCo nanoparticles in the range 30-50 nm.

As a second step and this is the main goal of this study, the corrosion behaviour of the electrodeposited PdCo NPs was investigated. Polarization assays and surface analysis were done, as well as immersion test and corrosion electrolyte analysis. Also, the effect of heat and passivation layer of alkanethiol treatment on the corrosion resistance was studied. The heat treatment of metallic alloys can strongly influence the corrosion resistance because it is associated with the modification of the material microstructure and consequently the structure and the chemical composition at the surface, including the oxide layer. On the other hand, the corrosion passivation of metals using an electrically insulating layer of self-assembled alkanethiol monomers may also

affect the corrosion resistance due to their ability to resist to electron transfer at the metal-solution surface, as result of the hydrophobicity of the alkyl chain.

Several methods were used to characterize and study the properties of PdCo nanoparticles. The surface morphology of the NPs was examined by scanning electron microscope (SEM), while the composition was analyzed by energy dispersive X-ray analysis (EDX). X-ray diffraction (XRD) was performed to obtain information on the crystalline structure of the PdCo films. X-ray photoelectron spectroscopy (XPS) is used in order to measure the elemental composition, and chemical state of the atoms at the NP's surface. The open circuit potential (OCP) was adopted to monitor the potential over the time and thus to determine initial surface changes and stabilization of corrosion conditions. Corrosion analysis was done by potentiodynamic polarization assays, where Tafel plot is used to calculate the corrosion parameters (corrosion potential (E_{corr}) and current (I_{corr})). Contact angle measurements were realized on PdCo samples with water, in order to evaluate to wettability of the material and determine if it affects its corrosion behaviour.

In general, the surface reactivity of a biomaterial increases with increasing its surface area. In addition, studies showed that a hydrophilic surface allows the establishment of contact between the body environment (e.g. blood proteins) and the biomaterial's surface, and thus contributes to cell and biomolecule migration and adhesion [148]. Therefore, the value of the contact angle indicates whether the surface is hydrophilic or hydrophobic and thus evaluates the interface area between solution and sample, which determine the behavior of a biomaterial towards corrosion.

Atomic force microscope (AFM) images before and after the corrosion assay were essential to study the roughness of the surface, and therefore have an idea about the corrosion type. The corrosion solution analysis by atomic absorption spectroscopy (AAS) is used to identify and quantify the ion release before and after the corrosion experiment.

Pourbaix diagram, also known as a potential/pH diagram or equilibrium diagram, provides information about the regions of stability and instability of a metal. These regions are determined from the curve of the variation of the potential (V) as a function of the pH of the electrolyte in which it is immersed. This diagram of the variation of V vs pH is used to identify the region of the active state (corrosion behavior) of a metal and also the region of its passivity (formation of oxide/hydroxide layer) and immunity (thermodynamic stability). Thus, this diagram is used to

estimate the corrosion product compositions at various potential-pH combinations, and to determine the environmental pH and potential essential to prevent corrosion.

Potentiodynamic polarization method involves changing the potential of the working electrode and monitoring the current produced as a function of potential. This method is used for corrosion testing because it can provide useful informations regarding the corrosion mechanisms, rate and susceptibility of specific materials in designated environments.

The Tafel plot is a plot of the electrochemical kinetics which relates the rate of an electrochemical reaction of an electrode immersed in an electrolyte to its over potential. The Tafel equation was first deduced experimentally and was later shown to have a theoretical justification.

Experimentally, in the case of this study, the Tafel plot is performed on a PdCo specimen by potentiodynamic polarization about 250 mV anodically (above the open circuit potential) and 250 mV cathodically (below the open circuit potential). The corrosion current (i_{corr}) is obtained by extrapolating the linear portion of the Tafel plots to the zero overpotential, and then calculated using Stern-Geary equation (Equation 18).

$$i_{corr} = \frac{(\beta_a)(\beta_c)}{2.3 (R_p)(\beta_a + \beta_c)} \quad (\text{Equation 18})$$

The value of β_a can be determined by taking the slope for the anodic portion of the Tafel plot and β_c for the corresponding cathodic part.

The polarization resistance (R_p) is defined as the slope of the potential-current density plot near E_{corr} and is equal to $\frac{\Delta E}{\Delta i}$.

Ringer's solution, also known as physiological salines or balanced salt solutions, is a solution of a mixed of several salts (NaCl, KCl, CaCl and NaHCO₃) dissolved in water. This solution was used as electrolytic bath during potentiodynamic polarization (corrosion test) for the purpose of simulating the in vivo fluid environment.

Finally, magnetization measurements, such as magnetic moments and Curie temperatures, were carried out to obtain the basic magnetic properties of the PdCo samples. As the saturation magnetization can be calculated from the maximum magnetic moment of the hysteresis loop, the

hysteresis loop will inform us on the heat-generation efficiency of PdCo NPs. Giving that the specific loss of power is proportional to the saturation magnetization, according to Rosensweig relationship. In addition, the coercivity obtained from the hysteresis loop will indicate if the PdCo NPs exhibit a ferromagnetic or a superparamagnetic behaviour. Therefore, it will show if these NPs are suitable for biomedical applications or not.

Each magnetic alloy has its characteristic Curie point. Thus, Curie point measurements were used to determine if PdCo NPs are composed of PdCo alloys and evaluate the homogeneity of the composition in the deposited PdCo particles.

PdCo NPs are deposited onto 0.7 mm x 0.7 mm (0.3 mm thickness) graphite substrate. However, these particles must be transferred to a culture medium in order to study their biocompatibility. For this purpose, we tested the feasibility of separating the NPs from the graphite using ultrasonic bath. The time of sonication and the temperature of the bath were also evaluated to study their effect on the quantity of the particles transferred into the solution.

CHAPTER 4 SUMMARY OF THE WORKS

4.1 Article 2: Electrodeposition of PdCo nanoparticles onto Pd-modified graphite electrode for future medical nanodevices

Lina Kafrouni^{1,2}, Rosa Rego³ and Oumarou Savadogo^{1,2*}

¹ Department of Chemical Engineering, Polytechnique Montréal, C.P. 6079, Succursale Centre-ville, Montréal, Québec, H3C 3A7, Canada.

² Laboratory of New Materials for Energy and Electrochemistry systems (LaNoMat).

³ Chemistry Department and CQ-VR, University of Trás-os-Montes e Alto Douro, Quinta de Prados, 5000-801 Vila Real, Portugal.

* Phone: +1-514-340-4725; fax: +1-514-340-4468; e-mail: osavadogo@polymtl.ca

Submitted to Journal of Electroanalytical Chemistry, on February 23rd, 2016. (JELECHEM-D-16-00211)

Abstract: A method involving a sequential electrodeposition of PdCo nanoparticles, onto Pd-modified graphite, followed by 1-dodecanethiol (DDT) coating has been developed for the first time. The electrodeposition parameters such as activation seeds, bath composition, applied potential, and time of deposition were investigated. The comparative study performed on the electrochemical properties of graphite and Pd-modified graphite showed that Pd seeds increase the electrocatalytic activity for the reduction of Pd(II) and Co(II) to PdCo alloy, compared to clean graphite. Furthermore, the co-deposition of PdCo starts at a potential lower than -0.375 V. The scanning electron microscopy (SEM) results showed that coating PdCo nanoparticles with 1-dodecanethiol (DDT) for 19 hours, before subsequent electrodeposition, will increase the concentration and the stability of the deposited PdCo nanoparticles. The SEM images and the energy dispersive x-ray spectroscopy (EDS) results showed that when the applied potential decreases from -1.0 V to -1.3 V the morphology of PdCo nanoparticles changes from clusters to spherical and agglomeration-of-spheres, and the Co content increases to reach a maximum of 35.6 %. According to the x-ray diffraction (XRD) patterns, the presence of glycine in the bath solution enhances the crystalline structure of the deposited PdCo films.

Keywords— Electrodeposition; graphite electrode; medical nanodevices; PdCo nanoparticles.

4.1.1 Introduction

The advantage of the magnetic targeted nanoparticles is the automatic navigation in the blood vessels, for targeting regions that are inaccessible or at high risks with existing interventional tools. In addition to the external manipulation by the magnetic field, the net field inhomogeneity created by the disruption of the local magnetic field can be picked up as a negative contrast in magnetic resonance imaging (MRI), which is essential for monitoring the navigation of these nanoparticles (NPs) in the human body [149].

Moreover, the heat generated by the exposition of the magnetic NPs to an alternating magnetic field can be used to destroy tumor tissue, because tumor cells are more sensitive to a temperature increase than healthy ones [150].

Iron oxide-based magnetic nanoparticles (MNPs), composed of magnetite (Fe_3O_4) or maghemite ($\gamma\text{-Fe}_3\text{O}_4$), continue to attract attention for magnetic hyperthermia application due to their lack of toxicity, excellent biocompatibility, ability to escape from the reticuloendothelial system, and low protein adsorption [151]. However, iron is the most corrosion vulnerable metal. A variety of methods have been employed to functionalize the iron-based particles with a coating of inert polymers including dextran, polysaccharides, polyethylene glycol, and polyethylene oxide [152,145] in order to increase their stability, and biocompatibility. In addition to polymer coatings, biocompatible silica becomes another attractive approach for developing iron oxide- based MNPs for biomedical applications.

The main drawbacks of capping the MNPs with silica are the synthesis of uniform silica shells with controlled thickness on the nanometer scale and the risk of oxidization [153]. Moreover, the use of physically adsorbed polymers, such as dextran, is limited by the lack of stability; this issue have involved cross-linking to form cross-linked iron oxide particles [154].

Another consideration to take into account is the effect of polymer or other non-magnetic coating on the nanoparticles magnetic properties, where the saturation magnetization (M_s) decreases when the thickness coating increases. This reduction has been mainly associated with the existence of a

magnetically dead layer on the surface of particles [155]. Accordingly it is very important to develop other magnetic nanodevices which are not limited by this dead layer.

PdCo alloys rich in Pd have demonstrated excellent corrosion resistant properties [156], and Co-based alloys such as Co-Fe achieved an extremely high heating performance of 1300–1600 W/g [157].

The ultimate objective of this project is to synthesize PdCo based MNPs for magnetic hyperthermia, with better magnetic properties than iron oxide due to less corrosion-related problems, and uselessness of coating material. To achieve this goal, the electrodeposition method is used because of its great capability in optimizing the composition, size, and shape of the NPs in order to enhance their stability, magnetic performance, and nanotoxicity for biomedical applications.

4.1.2 Materials and methods

4.1.2.1 Chemicals

Highly oriented pyrolytic graphite plate was purchased from Alfa Aesar (China), and then cut into cuboid electrodes. The graphite substrate had a surface area of 0.7 cm².

Acetone (CH₃COCH₃, Sigma-Aldrich) and nitric acid (HNO₃, 68 %, Fluka) were used as organic and metals solvents, respectively, during the cleaning process of the graphite electrodes.

The wettability of graphite substrate was improved by dipping its surface in sodium dodecyl sulfate (SDS) (CH₃ (CH₂)₁₁OSO₃Na, ≥ 99 %, Sigma-Aldrich).

Tin(II) chloride (SnCl₂, ≥ 99.99 %, Aldrich) and/or chromium potassium sulfate dodecahydrate (CrK(SO₄)₂·12H₂O, ≥ 98 %, Aldrich) were used to sensitize the graphite substrate before its activation with Palladium(II) chloride (PdCl₂, 99 %, Aldrich) and/or cobalt(II) chloride hexahydrate (CoCl₂·6H₂O, 99 %, Fluka), respectively, by electroless.

PdCl₂ and CoCl₂·6H₂O were used also for electrochemical deposition. The supporting electrolytes used during electrodeposition were: hydrochloric acid (HCl, 37 %, Fluka), ammonium hydroxide (NH₄OH, 50 %, Fluka) and glycine (NH₂CH₂COOH, ≥ 99 %, Aldrich). The pH was adjusted to 10 by the addition of concentrated ammonium hydroxide.

For the Self-Assembled Monolayers (SAMs) of alkanethiols, 1-dodecanethiol (DDT) ($\text{CH}_3(\text{CH}_2)_{11}\text{SH}$, $\geq 98\%$, Aldrich) was used.

Sulfuric acid (H_2SO_4 , 98 %, Fluka) is used as electrolyte during the linear scan voltammetry.

Nitrogen gas was purchased from Air Liquide, Canada (99.9 % purity). Aqueous solutions were prepared using Milli-Q water (18.2 M Ω cm). Ethanol (96 %, Scharlau) was used for the preparation of DDT solution and for washing the electrodes after treatment with DDT.

All chemicals were provided by Aldrich (Ontario, Canada) and used as received.

4.1.2.2 Electrode preparation

Prior to the PdCo alloy electrodeposition, graphite substrates were hand-polished with 180 grit microcloth of aluminum oxide and silicon carbide wetted with deionized water, until a mirror-like surface was obtained. It is then immersed in 68 % nitric acid for 1 minute and rinsed with acetone and deionized water thoroughly.

After cleaning the graphite surface from organic and metals impurities, it is necessary to provide a hydrophilic surface as well as a high density of nucleation sites for the subsequent electrodeposition process. To achieve this goal, graphite surface was immersed in 0.004 M sodium dodecyl sulfate (SDS) solution for 1 hour, and then modified with Pd and/or Co seeds.

4.1.2.3 Preparation of Pd (and/or Co) modified graphite

In order to prepare Pd-modified graphite, electroless deposition of Pd precursors is performed after up to three pretreatments with Sn sensitization followed by Pd activation. This process involved the immersion of graphite surface sequentially in two solutions consisting of: 25 mL of 0.56 mM palladium(II) chloride in 0.166 M hydrochloric acid solution and 25 mL of 10 mM tin(II) chloride in 0.166 M hydrochloric acid solution, for 30 minutes in each solution at room temperature. After the Sn sensitization - Pd activation process was completed, the samples were washed thoroughly again with distilled water to remove residual used electrolyte followed by drying in air.

The tin(II) chloride solution was aged for more than 3 months [158] before it was used, for improving its sensitizing performance due to the formation of uniform colloidal compound of Sn(IV) and Sn(II).

The sensitizing solution for Co-modified graphite consists of: 25 mL of 10 mM chromium(III) potassium sulfate dodecahydrate in 20 ml ammonium hydroxide solution (pH=13.8), and the activating solution includes: 25 mL of 10 mM cobalt(II) chloride hexahydrate in 20 ml ammonium hydroxide solution (pH=13.8).

The sensitization and activation process for the preparation of PdCo -modified graphite involved Sn sensitization-Pd activation followed by Cr sensitization-Co activation.

4.1.2.4 Electrochemical measurements

Electrochemical experiments were conducted on a PAR 273A potentiostat (Princeton Applied Research, Oak Ridge, TN). A conventional three-electrode system is employed, in which a Pd (and/or Co) -modified graphite electrode and a platinum plate are used as the working and counter electrodes, respectively. The reference electrode is a saturated calomel electrode (SCE). All potentials in this work are reported with respect to SCE. All the experiments are carried out at room temperature.

4.1.2.5 PdCo films and PdCo nanoparticles synthesis

The electrodeposition of PdCo films onto Pd (and/or Co) modified graphite substrate were accomplished by dipping the graphite surface in a solution of Pd(II) and Co(II) with electrolytes deaerated with nitrogen atmosphere, and then a constant negative potential less than -0.375 V is applied for 1 hour to the graphite electrode.

PdCo NPs are obtained by reducing the time of deposition to 1 minute. Sequential electrodeposition of PdCo NPs is realized by dipping the graphite surface in a deaerated solution of Pd(II) and Co(II) as electrolytes, and then a constant potential is applied for 1 minute to the graphite electrode, followed by coating the deposited PdCo NPs with DDT before subsequent electrodeposition for 1 minute. This method of successive rounds deposition-DDT treatment has been developed to: maintain a narrow size distribution and increase the number density of the PdCo NPs at the graphite surface by using SAMs of DDT strategy.

The concentration of DDT and the exposure time to these monomers were tested by evaluating the size distribution of PdCo NPs treated with DDT under three different conditions.

During the first treatment (T1), a 50 μL of the 0.002 M DDT solution was immobilized for 2 hours on graphite substrate immediately after the deposition of PdCo NPs. The electrodes were carefully washed in stirred ethanol for 20 minutes to remove any DDT that was not chemisorbed onto the electrode surface. Subsequently, the substrate is immersed in 25 mL of 0.004 M SDS solution to enhance the wettability of the graphite for 30 minutes.

The second treatment (T2) is similar to the first one but the electrode substrate was immersed in the DDT solution for 2 hours and then washed with ethanol for 5 minutes without stirring. The third treatment (T3) is similar to the second treatment but the immersion in 0.004 M DDT solution was kept for 19 hours.

The three different treatments are summarized in figure 4-1.

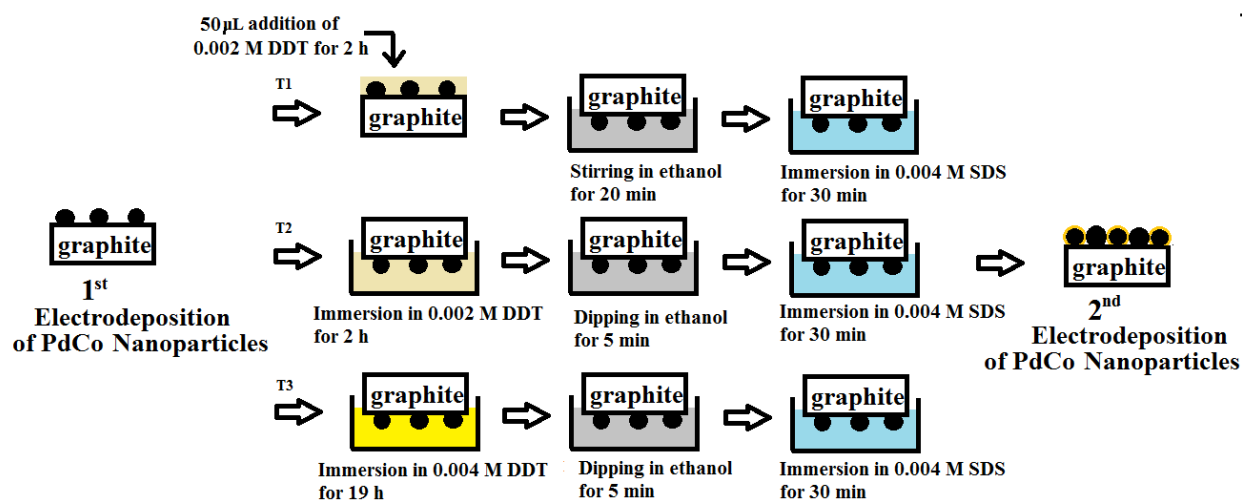


Figure 4-1 Illustration of the three treatments (T1, T2, and T3) for coating PdCo nanoparticles by self-assembled monolayers of DDT.

4.1.3 Results and discussion

4.1.3.4 Impact of sensitization – activation process on PdCo deposition

According to figure 4-2, the clean graphite surface didn't show any cathodic or anodic peak during the cyclic voltammetry test in 0.003 M Pd(II) + 0.006 M Co(II) solution. On the other hand, Pd-modified graphite exhibits an increase in electrocatalytic activity for oxidation-reduction reactions (four cathodic peaks (A-D) and three anodic peaks (E-G)) compared to clean graphite.

In fact, small Pd particles have a large surface-to-volume ratio compared to bulk graphite. As a result, adsorption of large number of Co(II) + Pd(II) ions onto the small particles surface is possible. Furthermore, the passage of an electron is slow between graphite surface and Pd(II) + Co(II) ions due to the low density of states in the basal plane of the highly ordered pyrolytic graphite used [159].

However, small Pd particles act as an efficient particle-mediated electron transfer, from graphite to Pd(II) + Co(II) ions. This may be related to the decrease of the open circuit voltage (OCP) (OCP(graphite)= 0.768 V, OCP(Pd-modified graphite)= 0.465 V) of the graphite electrode after Pd modification. This allows the decrease of the overvoltage of the PdCo electrodeposition.

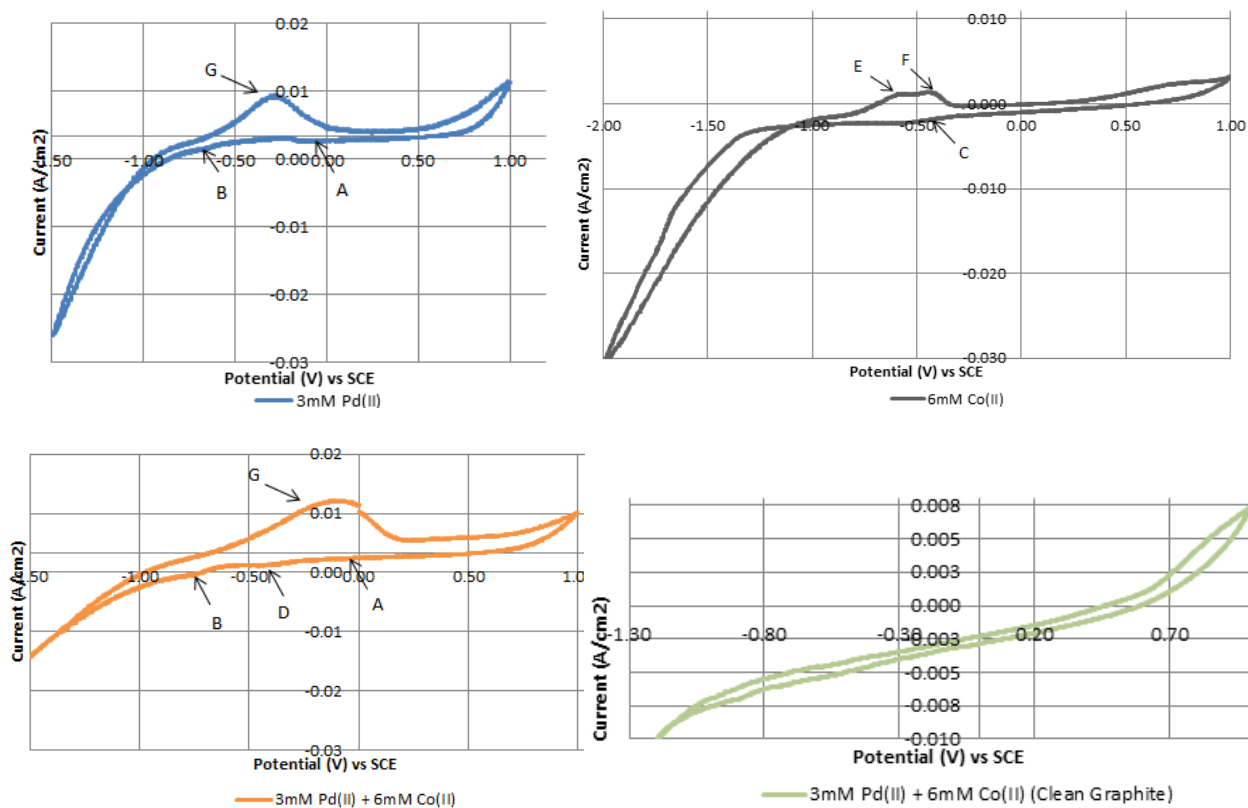


Figure 4-2 Cyclic Voltammograms (10th cycle) curves of clean and Pd-modified graphite registered in the electrolytes with different composition of both palladium (II) and cobalt (II) ions. (Scan rate: 50 mV/s)

4.1.3.5 Determination of the codeposition potential

Cyclic voltammograms (CVs) shown in figure 4-2 illustrate the electrochemical behavior of a Pd-modified graphite electrode in an aqueous solution (pH = 10) containing palladium chloride (0.003 M) with/without cobalt chloride (0.01 M), or cobalt chloride (0.01 M) in hydrochloric acid (0.5 M), ammonium hydroxide (0.5 M) and glycine (0.6 M), at a scan rate of 50 mV/s.

In the cathodic current regions, there are four visible peaks currents (figure 4-2) identified as: A, B, C and D, whereas in the anodic part three peaks are identified as: E, F and G can be seen. In Pd(II) solution, the sharp increase of the cathodic current at potentials below 0 V (peak A) indicates the onset of Pd electrodeposition. At more cathodic potentials, the appearance of peak B (below -0.625 V) can be attributed to the reduction of hydrogen adsorbed on Pd surface. The significant

increase of the cathodic current below -1.0 V can be associated to the hydrogen evolution reaction (HER) process.

Following the addition of cobalt chloride to Pd(II) solution, peak A disappeared and a new cathodic peak rises at -0.25 V (peak D). Comparing peak D with peak C (below -0.375 V, characteristic of the reduction of Co(II) to Co(0)) and peak A, the electrodeposition of the alloy PdCo occurs at a potential that lies between the deposition potentials of the pure metals. This behavior is classically and, of course, frequently observed for the electrodeposition of binary alloys [160].

The anodic peaks at -0.6 V and -0.55 V (peaks E and F, respectively) can be attributed to the oxidation reactions of different Co phases deposited during the direct scan. The increase of anodic current in the region of peak G, above -0.4 V, is related to the oxidation of hydrogen adsorbed on electrodeposited palladium surface. The comparison of the cathodic current peaks position allows to conclude that a potential lower than -0.375 V is needed for the co-electrode position of PdCo particles.

4.1.3.6 Optimization of the electrodeposition parameters

4.1.3.6.1 Activation seeds

The aim of Sn sensitization - Pd activation (and/or Cr sensitization - Co activation treatment) was to investigate the effect of the Pd (and/or Co seeds) on the epitaxial growth. According to DRX patterns (figure 4-3), the three broad diffraction peaks present at $2\theta = 40.6^\circ, 46.6^\circ$, and 68.4° can be indexed to the (111), (200), and (220) facets diffractions of face-centered cubic (fcc) of pure Pd, respectively. The other diffraction peaks at 42.4° , 44.5° , 51.7° , 54.4° , and 59.7° corresponding to the (100), (101), (102), (004), and (103) diffraction of graphite, respectively. In addition, Co standards peaks at 2θ values of 44.3° , and 51.6° corresponding to the (111), and (200) crystal planes peaks, respectively, cannot be found. This indicates that all the PdCo samples prepared exhibit the characteristics of a single-phase face-centered cubic (FCC) crystalline structure, and are substitution solid solutions where some atoms of Pd are replaced by Co atoms. A small positive shift was observed and can be related to the alloy formation.

Also, it can be seen from figure 4-3 that PdCo films deposited on Pd-modified graphite exhibit slightly higher crystallinity compared to those deposited on Co or PdCo modified graphite. The

shifted peak to high angle means that the crystal lattice is compressed and thus the FCC structure of the deposited PdCo is modified.

EDS results in table 4-1 shows that the activation of the graphite surface with Co precursors and PdCo precursors increase the Co content in the deposited films, when compared with electrodeposited films obtained prior to the surface activation with Pd seeds.

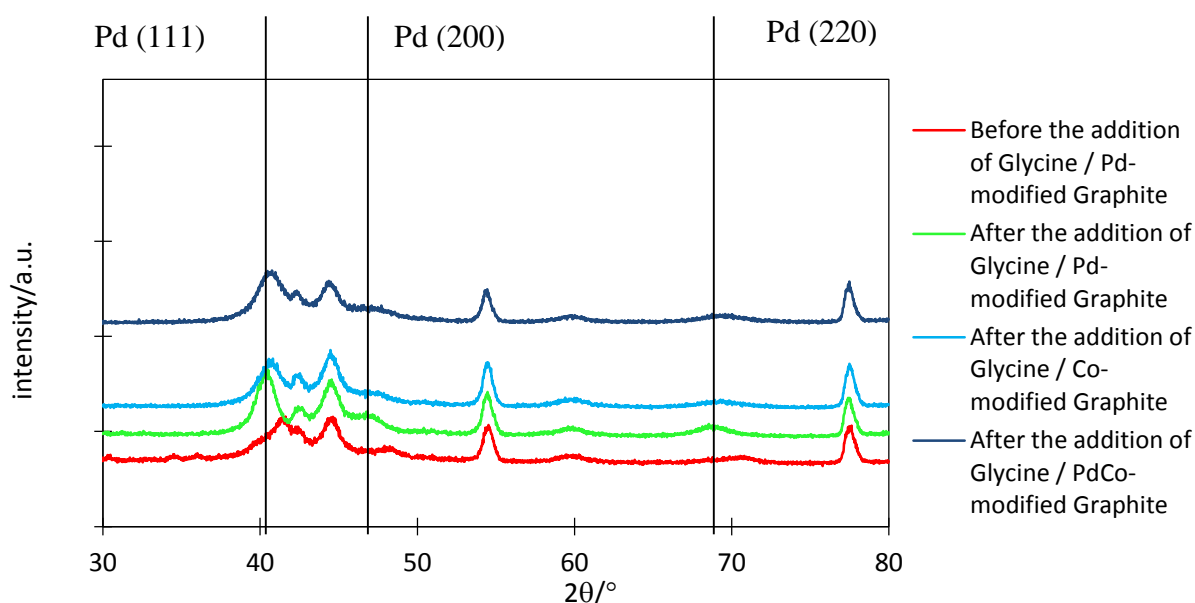


Figure 4-3 XRD patterns of electrodeposited PdCo films at different electrodeposition parameters, after addition of glycine.

These results can be explained by the fact that more there is Co atoms in the seeds more there is the Co nucleation in the deposited films. As a result of the increase of the Co content in the film, the FCC crystalline structure starts to change towards FCC + hexagonal structures.

4.1.3.6.2 Bath composition

Glycine is an amino acid molecule and was chosen as a complexing agent since it exists in many forms depending on the pH of the bath solution. Accordingly, Co-Glycine and Pd-Glycine complexes depend strongly on the pH of the solution. In the pH investigated in this work (pH = 10), Pd and Co are mainly complexed with anionic and zwitterionic forms of glycine [160].

The effect of the addition of glycine in the PdCo alloy composition is shown in Table 4-1. At low time of electrodeposition (30 minutes) there is more cobalt in the electrodeposited films, whereas at high electrodeposition time (1 h) palladium-rich alloy is obtained.

Preferential electrodeposition may take place depending on the stability constant (K) of the individual complexes and ease of electron transfers. The anionic form of glycine forms a tris-glycinato complexes with cobalt [161] and very stable bis-glycinato complexes with palladium, this stability makes difficult the reduction of Pd(II) compared with Co(II), case on 30 min deposition samples. As the pH fluctuates at the graphite surface during the electrodeposition, because the hydroxide ions are consumed by the graphite electrode during hydrogen evolution, some glycinato ligands become zwitterionic complexes with similar stability constant with Pd and Co. This feature of glycine molecule pH dependent seems responsible of the variation in the ratio Pd/Co during the eletrodeposition time [162].

SEM images (Figure 4-4) show that the glycine favors the dendritic morphology over the time, as a result of easy directions for electron transfer. This complex structure can explain the reason why before adding glycine to the electrodeposition bath the deposit is compact and flat and in the presence of glycine the electrodeposited film is less dense with a 3D shape.

Furthermore, it can be seen from figure 4-3 that the degree of crystallinity increases when the glycine is added to the bath solution. The increase in crystallinity can be attributed to the deposit uniformity controlled by glycine molecule.

Table 4-1 Energy dispersive x-ray spectroscopy (EDS) results of electrodeposited PdCo at different electrodeposition parameters before and after addition of Glycine.

Activation	Bath composition	Overpotential (V)	Time of deposition	EDS (Co at. % in PdCo)
Pd modified graphite	Before addition of Glycine	-1.2	1 h	22.10
	After addition of Glycine		30 min	31.00
			1 h	9.87
Pd modified graphite	After addition of Glycine	-1.2	1 h	9.87
Co modified graphite				15.00
PdCo modified graphite				22.20
Pd modified graphite	After addition of Glycine	-1.0	1 min (two sequential deposition, treatment 3)	13.45
		-1.1		35.65
		-1.2		38.41
		-1.3		34.47

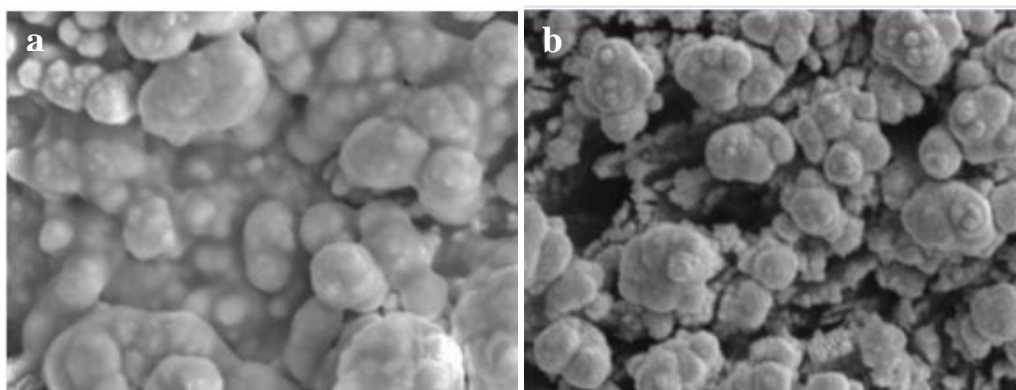


Figure 4-4 SEM images of electrodeposited PdCo films before (a) and after (b) the addition of glycine to the bath solution. (Magnification of 3K x)

4.1.3.6.3 Applied potential

To investigate the effect of the applied potential on the Pd/Co ratio in the deposited PdCo films, four potentials were applied: E1= -1.0 V, E2= -1.1 V, E3= -1.2 V, E4= -1.3 V vs SCE. Table 4-1 shows that the Co content increases to reach a constant value (around 35 %) with the applied negative potential. According to the CVs curves shown in figure 4-2, the hydrogen evolution reaction (HER) is much more pronounced during Pd electrodeposition (CV in 0.003 M Pd(II)) than

during the electrodeposition of Co (CV curve obtained in 0.006 M Co). This is due to the better electrocatalytic activity of Pd than Co for the HER. This good electrocatalytic feature of Pd for the HER makes the electrodeposition of Pd difficult. This explains why at high applied potential there is a decrease in the ratio Pd/Co in the electrodeposited PdCo films.

Furthermore, the applied potential not only controls the composition ratio but also affects the particle size and shape of metallic deposits, because the ratio of the nucleation rate/growth rate of the nuclei depends on the applied potential.

According to figure 4-5, when the applied potential decreases from -1.0 V to -1.3 V, the morphology of PdCo nanoparticles changes from clusters to spherical and agglomeration-of-spheres.

4.1.3.6.4 Sequential electrodeposition

For magnetic hyperthermia application, PdCo NPs with Co content between 10 and 48 %, and crystalline FCC structure are needed [163]. To achieve this goal, graphite surface was modified with Pd small particles, glycine was added to the bath solution, the applied potential was fixed at -1.2 V, and the time of deposition was decreased till 30-40 nm uniform PdCo NPs are obtained.

Three samples were synthesized at different times of deposition: 5, 2 and 1 minute. SEM images in figure 4-6 show that 1 minute deposition is enough to obtain nanoparticles in the range of 30-50 nm.

During sequential electrodeposition, the treatment with DDT was investigated by varying the concentration of DDT and the exposure time to this compound, to enhance the size distribution of the PdCo on the graphite surface. SEM images in figure 4-7 were used to measure the size distribution of the deposited PdCo NPs with and without treatments with DDT.

Figure 4-7 shows that two successive electrodepositions of 1 minute without treatment with DDT increase the ratio size/number of NPs, compared to one electrodeposition of 1 minute. After treatments T1 and T2, the NPs are dispersed but bigger than those obtained in the case of one electrodeposition during 1 minute. Even though T1 and T2 were not efficient, sample treated with T3 has a high concentration of PdCo NPs with a uniform particle size distribution.

These results allow us to conclude that the nanoparticles must be treated with DDT for 19 hours to obtain a self-assembly monolayer on the PdCo surface.

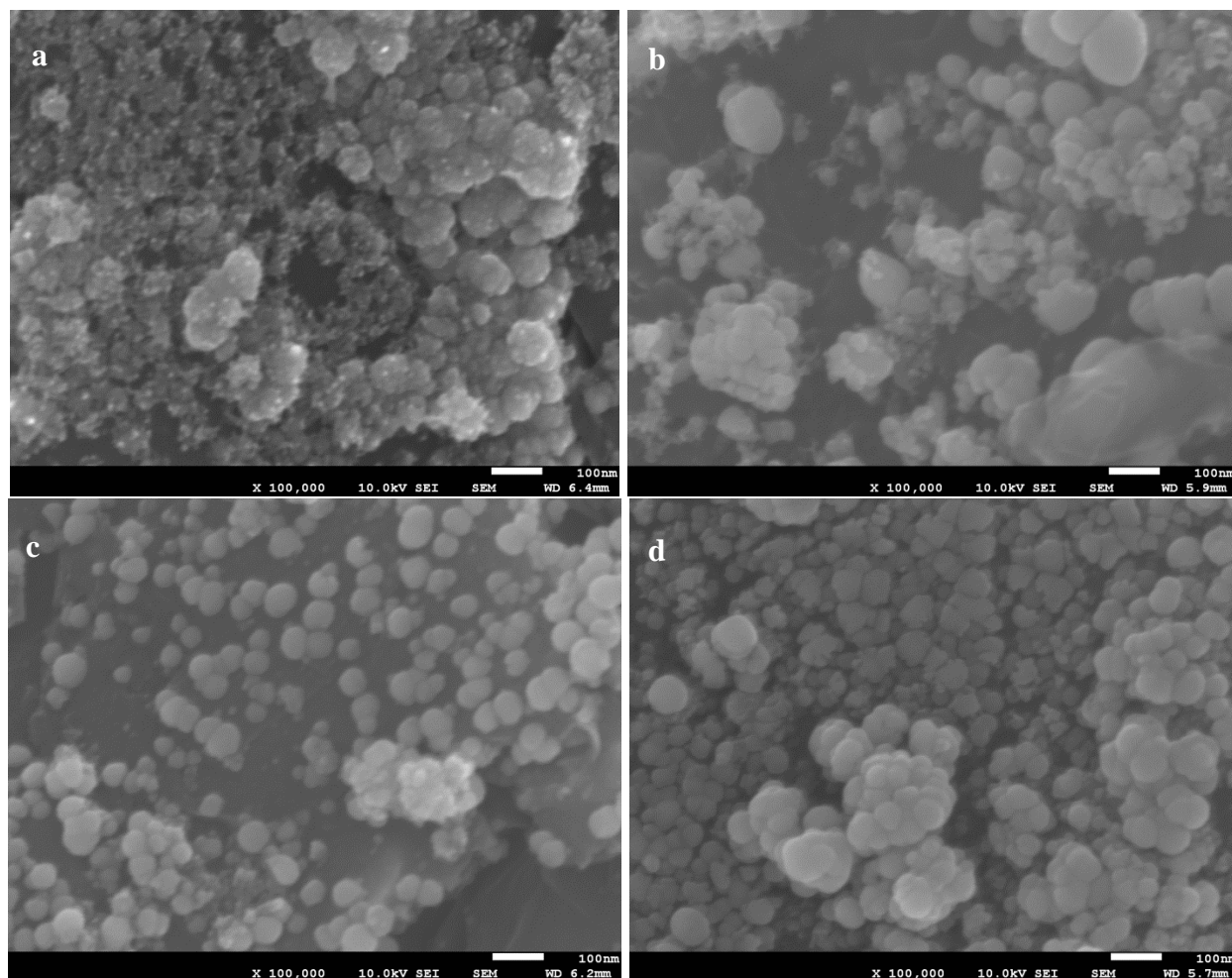


Figure 4-5 SEM images of electrodeposited PdCo NPs at: -1.0 V (a); -1.1 V (b); -1.2 V (c) and -1.3 V (d). (magnification of 100k x)

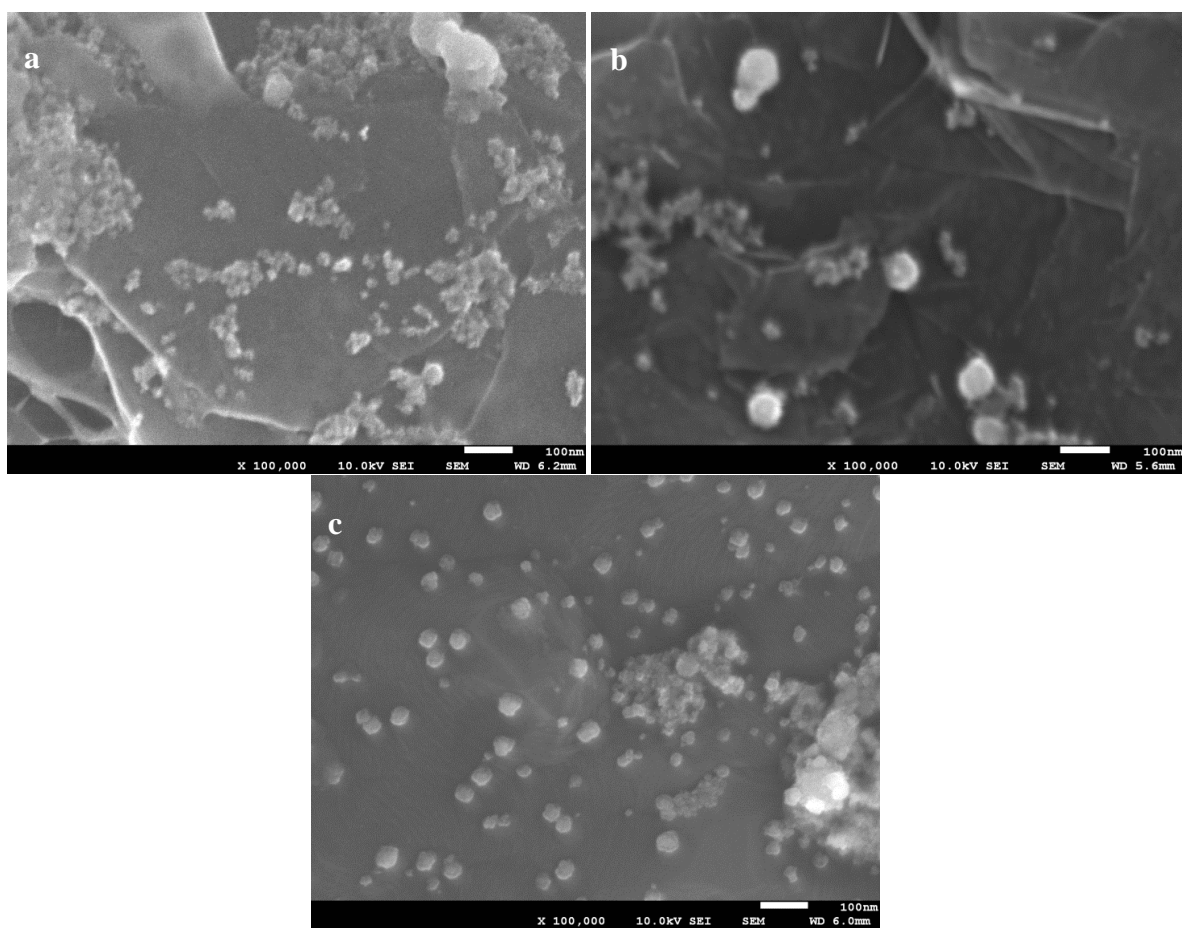


Figure 4-6 SEM images of electrodeposited PdCo at different time of deposition: 5 minutes (a); 2 minutes (b); and 1 minute (c). (magnification of 100k x)

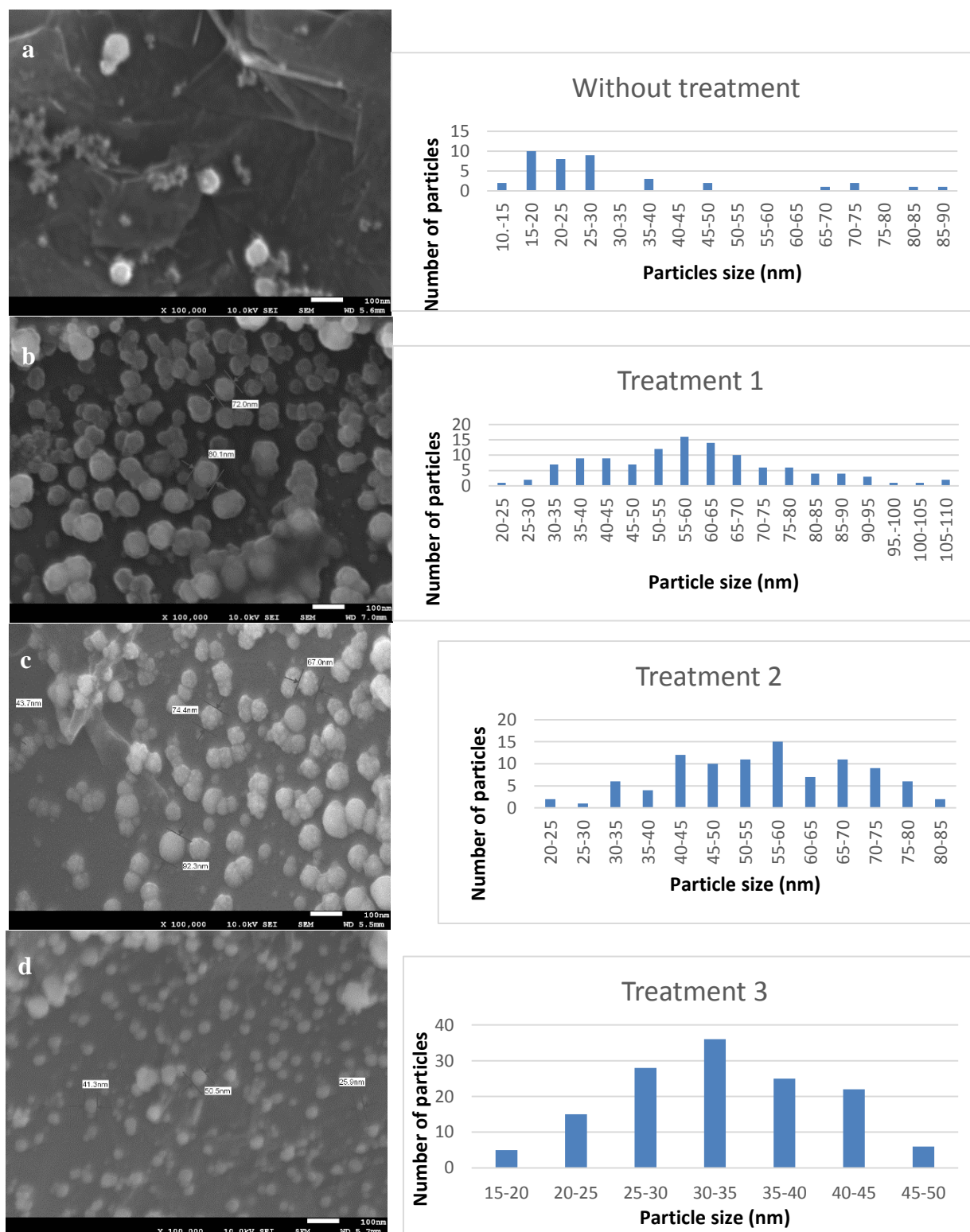


Figure 4-7 SEM images and the corresponding size distribution histograms of two sequential electrodeposition of PdCo with and without treatment with 1-dodecanthiol (DDT): without treatment (a); treatment 1 (b); treatment 2 (c); and treatment 3 (d). (magnification of 100K x).

4.1.4 Conclusion

In this work, the electrodeposition of spherical PdCo NPs, in the range of 30-50 nm, with a ratio Pd/Co = 65.3:34.7 (accuracy ± 2 %) was achieved on Pd-modified graphite using 19 h of surface treatment with 0.004 M DDT (as coating) between two successive deposition at -1.2 V for 1 minute in a bath solution containing: 0.003 M Pd(II) + 0.006 M Co(II) + 0.5 M (ammounium hydroxide + hydrochloric acid) + 0.6 M glycine.

Future studies must be done on the stability, magnetic behaviour and biocompatibility of these MNPs. This will help to evaluate whether these PdCo NPs can be used as medical nanodevices, because biomaterials must be biofunctional and biocompatible in order to perform well for the purpose which it was designed for.

Acknowledgments

The authors thank the Fonds Québécois de la Recherche sur la Nature et les Technologies (FQRNT) and the Fondation Universitaire Pierre Arbour for their funding of this research. Rosa Rego acknowledges FCT for grant SFRH/BSAB/1337/2013.

4.2 Article 3: Corrosion behavior of Palladium-Cobalt nanoparticles for the design of new hyperthermia implants

Lina Kafrouni^{1,2}, Taraneh Javanbakht^{1,3}, Oumarou Savadogo^{1,2 *}

¹ Department of Chemical Engineering, Polytechnique Montréal, C.P. 6079, Succursale Centre-ville, Montréal, Québec, H3C 3A7, Canada.

² Laboratory of New Materials for Energy and Electrochemistry systems (LaNoMat).

³ Department of Chemistry, Université de Montréal, Montréal, Québec, H3C 3J7, Canada.

* Phone: +1-514-340-4725; fax: +1-514-340-4468; e-mail: osavadogo@polymtl.ca

Submitted to *Electrochimica Acta*, on February 23rd, 2016. (Manuscript number: PA-16-131)

Abstract: The main toxicity of metallic nanoparticles comes from their ability to corrode and release metallic ions. Therefore, their potential degradation and release of cytotoxic ions has to be determined. In this study, the corrosion resistance of newly developed Pd₆₅Co₃₅ nanoparticles (NPs) for magnetic hyperthermia was evaluated. Furthermore, the influence of heat treatment at 200 °C, 300 °C and 400 °C and surface passivation with 1-dodecanethiol (DDT) monomers on the corrosion resistance of PdCo NPs was investigated. We compared the corrosion behaviour of the treated samples with the as-deposited sample. The corrosion parameters of the samples were determined using potentiodynamic polarization assay in Ringer's solution, followed by surface and corrosion electrolyte analysis. During polarization test, PdCo NPs treated with heat at 400 °C displayed the lowest corrosion current density i_{corr} of 0.022114 $\mu\text{A}/\text{cm}^2$, while the sample treated with DDT monomers exhibited the highest corrosion density of i_{corr} of 0.87202 $\mu\text{A}/\text{cm}^2$. According to AAS, the heat and alkanethiol treatments significantly decrease the release of Pd and Co ions in the supernatant after the polarization assay in the order 200 °C > 400 °C > 300 °C > DDT > Untreated. XPS analysis showed that the corrosion of treated/untreated PdCo samples varies upon the chemical composition at the surface, which revealed to be treatment-dependent. Moreover, the immersion test in Ringer's solution for both treated and untreated samples exhibited an excellent corrosion resistance ([Pd(II)]<0.01 ppm; [Co(II)]<0.01 ppm). This study concluded that PdCo NPs could be used as a medical micro-device if they are treated with heat to prevent high Pd and Co ions release in biological environment and subsequent nanotoxicity.

Keywords— Corrosion, palladium-cobalt alloy, biocompatibility, magnetic hyperthermia.

4.2.1 Introduction

The use of palladium-based alloys has increased in the late 1970s due to the increasing price of gold (Price of Pd :110 \$US/oz; Price of Au: 500-1000 \$US/oz), after deregulation of gold in USA. As result, palladium-silver alloys have increasingly been used in Germany and worldwideas dental prosthesis, such as crowns and bridges, as leading alternative to gold [164]. In the 1990s and following publications [165] on chronic illnesses and periodontal inflammation caused by corrosion of Pd alloys, there have been major warning in Germany about the safety of using Pd in dental casting alloys [166,167]. In the late 1990, Pd cost increased to over 1000 \$US/oz after political crisis in Russia, the major producer of Pd ore, and eliminate the advantage of low cost Pd alloys. Since then the price of Pd has decreased, and documented studies showed that metallic Pd didn't exhibits cytotoxicity effects and the risk of releasing Pd ions in Pd-rich dental casting alloys appears to be extremely low [168], except allergic reactions for some individuals.

Palladium-cobalt binary alloy was firstly introduced to medicine, more precisely for thermal treatment of tumor, in 1993 by Paulus and Tucker [169]. They proposed Pd rich-alloy for this purpose due to the relative corrosion resistance of Pd and ferromagnetic behaviour of Co. In fact, the corrosion resistance of Pd [170] is attributable to its stable electronic configuration $5s^0 4d^{10}$, where the outer 4d shell orbitals are paired. Despite that 5s orbitals are lower in energy and thus should be filled first, the 5s electrons are transferred to the 4d orbitals because the two orbitals are close enough in energy. Furthermore, the face centered cubic (fcc) lattice structure of Pd forms stable solid solutions with Co in Pd-rich PdCo alloys (figure 4-8), which exhibits a low corrosion tendency because it has the same composition throughout and thus avoids galvanic corrosions between the microscopic areas of different composition [170].

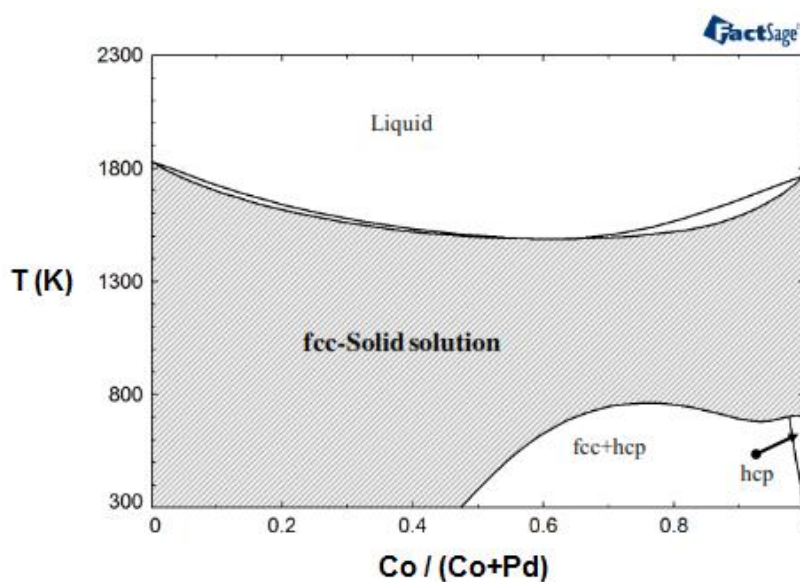


Figure 4-8 Phase diagram of PdCo system obtained from FactSage software [171].

Polarization tests done over Pd-rich PdCo alloys in oral simulated environment showed a lower corrosion behaviour and the presence of potential region where the current density is potential-independent, compared with Co-rich PdCo alloys [172]. This potential region was attributed to the palladium enriched surface, formed as consequence of Co selective dissolution at the surface [173]. Pourbaix diagrams of Pd-water and Co-water in figure 4-9 show that the stability region of Pd is bigger than that of Co, and thus confirm the proposed mechanism of selective dissolution of Co in Pd rich-PdCo alloys.

Furthermore, studies showed that oxygen chemisorbed layer of PdO may form at the Pd rich surface during the current-voltage polarization curves, due to the existence of the electron vacancies in the PdCo 3d orbitals, and can strongly limit the dissolution rate of Co atoms [174].

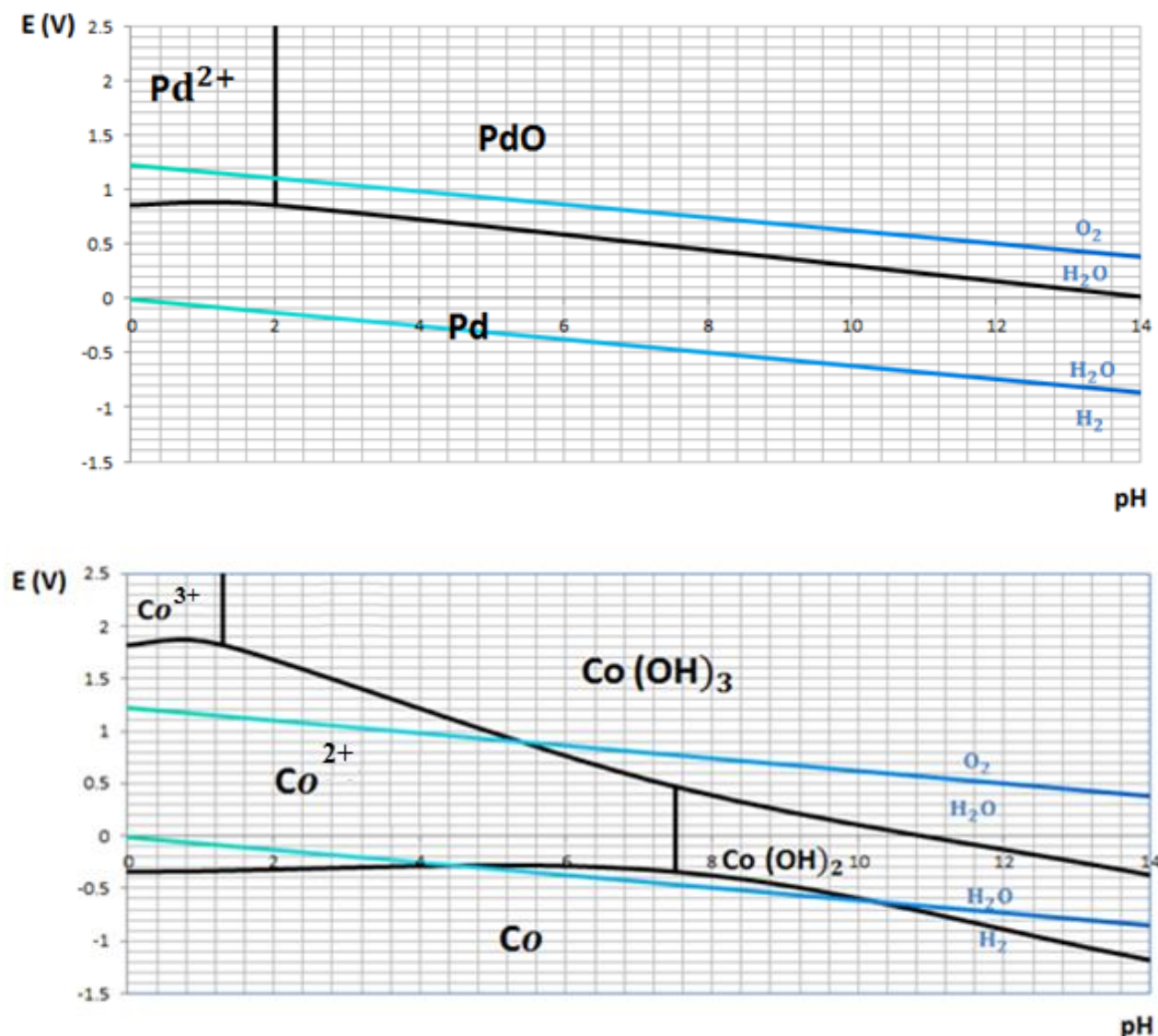


Figure 4-9 Pourbaix diagram showing palladium and cobalt species and water stability region.

Heat treatments of metallic alloys are usually associated with the modification of the material microstructure in order to obtain a single phase (figure 4-8), in which the alloying elements are dissolved. The resulting phase transformation influences the structure and the chemical composition of the surface, including the oxide layer, and therefore the resistance toward corrosion [175]. Our laboratory developed for the first time, PdCo alloys for the oxygen reduction reaction in acid medium for polymer electrolyte fuel cell applications [176,177]. It was shown that the chemical surface composition might have an important effect on the stability of the palladium alloys against corrosion in this medium. On the other hand, the corrosion passivation of metals

using an electrically insulating layer of self-assembled alkanethiol monomers showed to protect gold from the corrosion in aqueous Br^- solution [178]. The effectiveness of these monomers in corrosion resistance is due to their ability to resist to electron transfer at the metal-solution surface, as result of their hydrophobic alkyl chain.

The degradation of PdCo NPs by electrochemical corrosion and the release of cytotoxic Pd(II) and Co(II) ions can limit their use for biomedical applications. To the best of our knowledge, the corrosion resistance of PdCo NPs in physiological solution was not yet investigated. In order to study the effect of heat and alkanethiol monomers treatments on the corrosion resistance of PdCo NPs, three heated samples at 200 °C, 300 °C and 400 °C, and one sample treated with 1-dodecanethiol (DDT) for 19 hours were tested in this manuscript.

The corrosion behaviour of the four treated samples was compared to the untreated sample of PdCo NPs (the control) using polarization assays followed by the characterizations of their surface chemical compositions. To achieve this goal, scanning electron microscopy (SEM), atomic force microscopy (AFM), X-ray Photoelectron Spectroscopy (XPS) and static contact angle (SCA) measurement were used to evaluate the surface modification after the polarization assay. Also, atomic absorption spectroscopy (AAS) was adopted to quantify the ions release.

4.2.2 Materials and methods

4.2.1.1 Materials and sample preparation

Palladium- 35 % Cobalt NPs used in this study were synthesized using the electrodeposition method onto Pd-modified graphite developed in our previous work [179]. Hence, chemicals and electrochemical equipment are used according to the latter study [179].

The electrodeposition was accomplished by dipping the graphite surface in a solution of Pd(II) and Co(II) with electrolytes deaerated with nitrogen atmosphere, and then a constant negative potential of -1.2 V was applied for 1 minute to the graphite electrode.

Five samples of Pd-35 % Co NPs were synthesized and four of them were subsequently treated with heat at 200 °C, 300 °C and 400 °C (under nitrogen atmosphere) for one hour or treated with 4 mM DDT monomers (in ethanol solution) for 19 hours. Untreated sample was used as control in

order to study the effect of the heat and electrically insulating layer on the corrosion resistance of the PdCo alloy.

4.2.1.2 Surface analysis

The morphologies of the five samples were observed on a scanning electron microscopy (SEM, JEOL JSM7600F) at 10.0 kV. Sample's topography was measured by atomic force microscopy (AFM, Topometrix discoverer), and the average roughness was determined using the software embedded within the AFM system having an absolute accuracy of 0.5 nm.

X-ray photoelectron spectroscopy (XPS) was done with ESCALAB 3 MKII de VG. Survey and C 1s, O 1s, Pd 3d and Co 2p high resolution spectra of the samples were obtained, using nonmonochromated Mg K α radiation (1253.6 eV), at a power setting of 300 W, having an instrument resolution of 0.7 eV. The samples were deposited onto graphite, using two-sided adhesive Cu tape. The base pressure during scanning was less than 1×10^{-9} torr. Electrons were detected at a perpendicular take-off angle, using 0.05 eV steps, and spectra were analyzed using the VG Advantage software. The sputtering of the untreated PdCo alloy was carried out using the Ar beam and XPS survey and high resolution spectra were obtained after sputtering. During the sputtering, the Ar energy and sputtering duration were 1kV and 2 minutes. The absolute accuracy of this instrument is 0.1-0.2 %.

The high resolution spectra of the chemical elements, including Pd and Co, after the sputtering were obtained.

4.2.1.2.1 Contact angle

The contact angle measurements were achieved by placing 2 μ L of water on the Pd/Co alloys deposited on the graphite. The sessile drop contact angle being stable on the minute time frame, one measurement per location was taken immediately using a NRL C.A. Goniometer (Model No. 100-00 115). The measurements were carried out on several spots on the un-treated and treated PdCo alloys and graphite in *triplicata*. The accuracy of the instrument is $\pm 2^\circ$.

4.2.1.2.2 Potentiodynamic polarization assay

Polarization measurements were performed by a standard three-electrode cell, in which a platinum plate, saturated calomel electrode (SCE), and PdCo NPs sample (graphite supported) were used as counter, reference, and working electrodes respectively, with a microprocessor-controlled electronic potentiostat (PAR 273A, Princeton Applied Research, Oak Ridge, TN). All measured potentials presented in this work were referred to SCE.

The electrolyte was 50mL of Ringer's physiological solution (Sigma-Aldrich) with the following composition: 0.12 g/L CaCl_2 , 0.105 g/L KCl, 0.05 g/L NaHCO_3 , 2.25 g/L NaCl, to simulate the body fluid. The electrolyte solution was deaerated with nitrogen gas for 1 hour before the polarization assay. During the polarization, the latter solution was maintained at 37 °C under a low flow of nitrogen atmosphere.

The open circuit potential (E_{ocp}) of the samples, immersed in deaerated Ringer's solution, was monitored for 1 hour. Polarization tests were carried out with a sweep rate of 0.17 mV/s, sweeping potential from -250 mV under E_{ocp} to +250 mV above E_{ocp} . The corrosion parameters, corrosion current density (i_{corr} (A/cm²)) and corrosion potential (E_{corr} (V/SCE)), were determined by Tafel extrapolation using CorrWare version 3.4e.

4.2.1.2.3 Immersion test

An immersion test was performed to determine the short-term corrosion behaviour of the PdCo NPs samples. The five samples were placed into separate vials of 100 ml Ringer's solution at 37 °C. A control of Ringer's solution was prepared and similarly stored to measure baseline levels of constituent element ions. 11 Samples of supernatant were collected during 7 days and stored for atomic absorption spectroscopy analysis of Pd and Co concentrations (Lambda 19 Spectrometer). Ion concentrations in the test solutions were compared to standard solutions containing known ranges of the constituent ions for instrument calibration. Absolute accuracy of the instrument is within 10 ppb for the ions tested.

4.2.3 Results and discussion

4.2.3.1 Polarization assay

Figure 4-10 shows the variation of the open circuit voltage (E_{ocp}) of the PdCo alloy with time for the five samples of PdCo. This E_{ocp} is created at the working electrode's surface as result of the formation of the electrical double layer of ions and subsequent electrochemical reactions at the electrode-Ringer's solution interface [180]. The E_{ocp} value varies as function of time until it reaches equilibrium, where the oxidation and reduction currents are equal. Measuring E_{ocp} (vs SCE reference electrode) as function of time is essential to evaluate the kinetics of electron transfer on the sample's surface. As shown in figure 4-10, untreated sample of PdCo exhibits the highest value of E_{ocp} , among those of the other treated samples, with a significant increase to reach a plateau value of 0.368 V vs SCE in 1 hour. It seems that untreated PdCo surface exhibits spontaneous passivity in Ringer's solution. On the other hand, after a short decrease during the first 800 s the E_{ocp} of the PdCo samples treated increases (in the case of 300 °C) or remain stable (in the case of 200 °C and 400 °C). The decrease may be due to the oxidation of the Co at the surface. Following the decrease, the increase of E_{ocp} can be attributed to the passivation of the sample of Pd-rich treated at 300 °C, whereas the stability of E_{ocp} in samples treated at 200 °C and 400 °C can be explained by the stability of the Pd-rich surface in this range of potential. The E_{ocp} of the sample treated with DDT remains stable during the first 2100 s and then increases significantly. This behaviour can be explained by a first step protection of the physisorbed DDT monomers at the surface of the sample, which prevents the dissolution of the sample, and in a second step the dissolution of the physisorbed DDT monomers from the surface of the sample in Ringer's solution and resulted in some bared regions of the surface. Bared surface will behave like untreated surface and thus exhibits a spontaneous passivity.

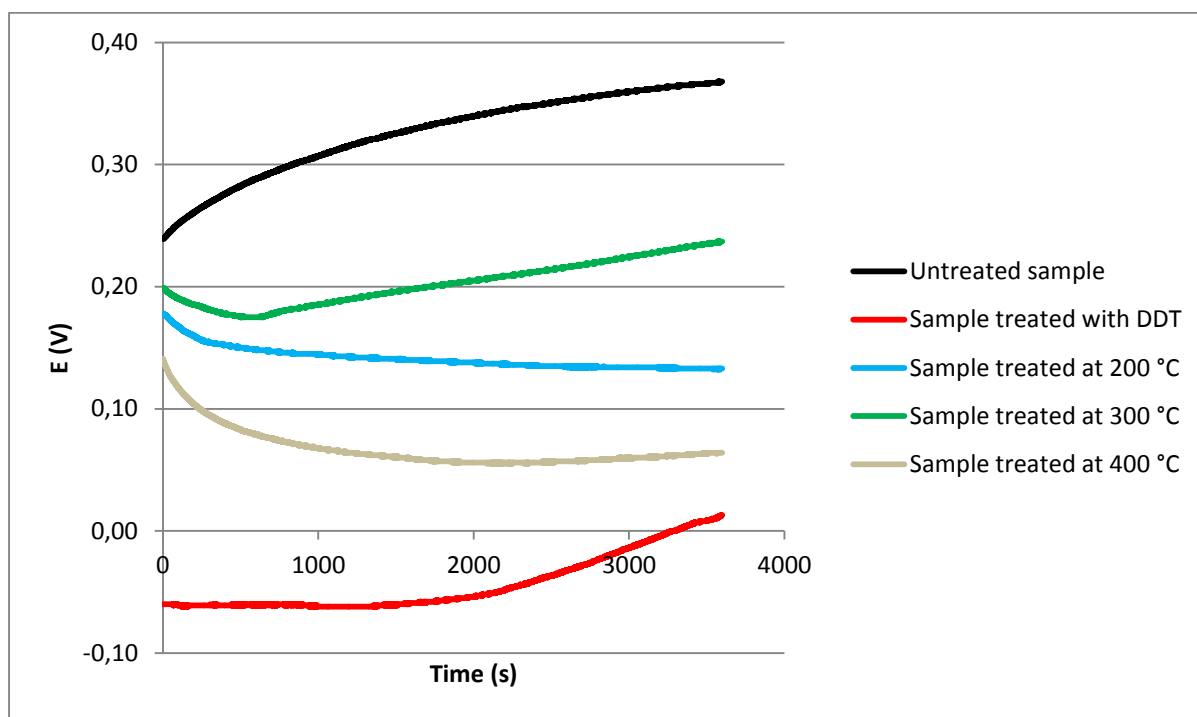


Figure 4-10 Open circuit potential (vs E_{SCE}) as function of time for the 5 differently treated PdCo NPs samples, immersed in 37 °C Ringer's solution.

The potentiodynamic polarization curves of the PdCo untreated/treated samples are shown in figure 4-11, and the derived electrochemical parameters extracted from these curves are summarized in table 4-2. It could be seen that the samples which exhibit passivation behaviour in OCP test, sample heated at 300 °C, DDT treated and untreated samples, have the highest corrosion current densities (I_{corr}) compared with stable behaviour samples (treated at 200 °C and 400 °C). These results suggest that the passive layer formed on these PdCo surfaces is inhomogeneous, maybe due to the non-homogeneity of the material, which induces galvanic cells at the interface which enhances corrosion of the surface and consequently increases the I_{corr} .

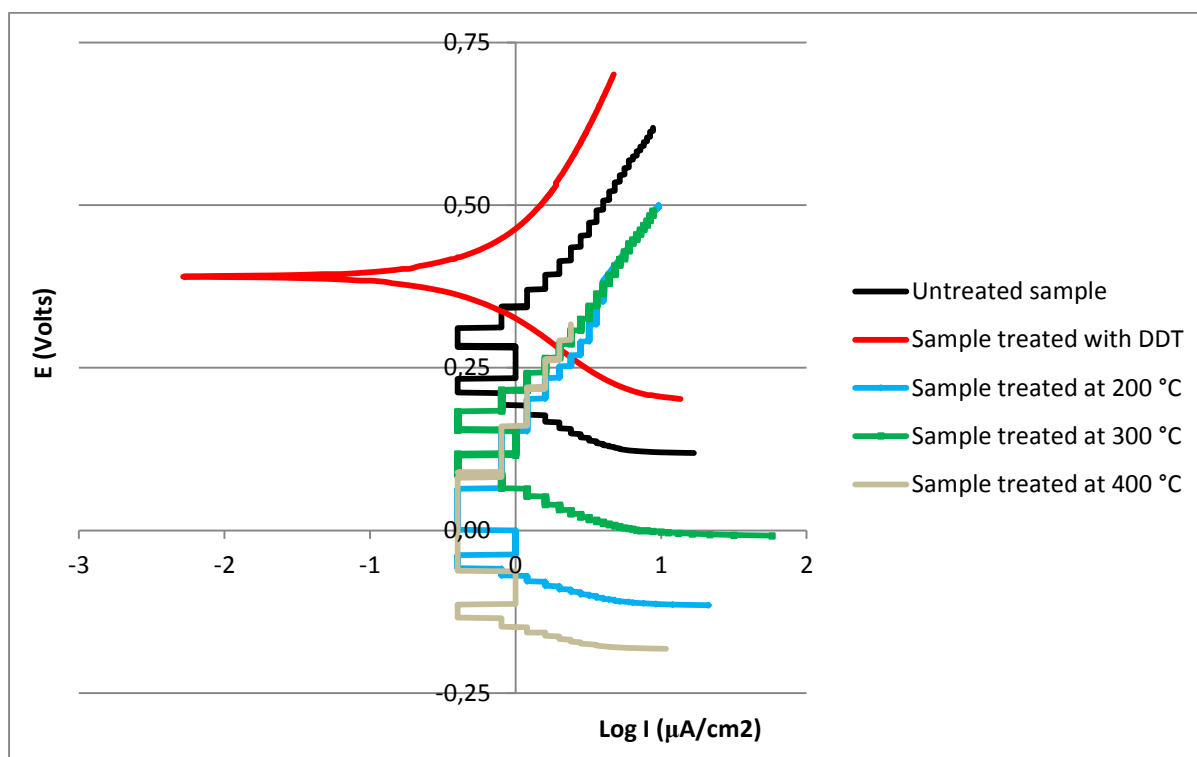


Figure 4-11 Polarization curves of PdCo NPs samples in Ringer's solution.

Table 4-2 Corrosion parameters for the PdCo samples extracted from Tafel curves.

	OCP	E_{corr} (V)	I_{corr} ($\mu\text{A}/\text{cm}^2$)
Untreated	0.368	0.24888	0.23874
Protection with DDT	0.013	0.39037	0.87202
Heated at 200°C	0.133	-0.015252	0.027084
Heated at 300°C	0.237	0.13457	0.065828
Heated at 400°C	0.064	-0.081646	0.022114

4.2.3.2 Atomic absorption spectroscopy

According to atomic absorption spectroscopy analysis (table 4-3) following polarization test, the Pd and Co concentrations in the supernatant decrease significantly after heat treatments. This indicates heating at 200 °C, 300 °C and 400 °C for 1 hour may have a significant impact on the crystallinity enhancement of PdCo.

On the other hand, DDT treatment also reduces the release of Pd and Co by 2 times in comparison to those of the untreated sample. But the concentration of the released Pd and Co ions is higher for DDT treated samples than those of heat treated samples. This can be explained by the loss of physisorbed DDT monomers from the sample surface during the polarization test. This loss allows formation of non-protected areas at the surface of the sample, which are more sensitive to corrosion.

Table 4-3 Corrosion supernatants analysis by atomic absorption spectroscopy.

	Pd (ppm)	Co (ppm)
Untreated	0.07	0.055
Protection with DDT	0.03	0.029
Heated at 200°C	0.01	0.013
Heated at 300°C	0.02	0.019
Heated at 400°C	0.02	0.012

4.2.3.3 Contact angle

Contact angle measurements were done with water on graphite (the support of PdCo samples) and treated/untreated PdCo samples (figure 4-12). The average values of the right and left contact angles are presented in table 4-4. According to table 4-4, the surface of graphite and DDT treated sample were hydrophobic because hydrophobic areas are obtained for samples which contact angles are higher than 90° [181]. In contrary, the surfaces of the untreated and heat treated samples at 200 °C and 300 °C were hydrophilic because the contact angle are lower than 90 ° [181]. In fact, hydrophobic long carbon chain and methyl tail group of DDT monomers are responsible of the high contact angle of DDT treated sample. Hydrophobicity is a great feature of this sample because it reduces the contact between PdCo and Ringer's solution and thus decreases the ions release, compared with untreated sample. Despite the hydrophobicity of the DDT treated sample, the higher release of ions compared with the hydrophilic samples treated with heat can be explained by the presence of bared regions. The results above indicate that the wettability of the surface might not be an appropriate parameter to probe the corrosion behaviour of biomaterials in Ringer's solution, because it will predict the average of the surface hydrophobicity regardless of the non-homogeneity of the composition at the surface.

The wetting behaviour of the untreated and heated samples suggests that the chemical composition of the surface vary upon the treatment, and becomes more hydrophilic when treated at 200 °C than at 300 °C. The surface may contain different type of oxides such as hydrophobic PdO and hydrophilic $\text{Co}(\text{OH})_3$ which exhibit different solubility in water.

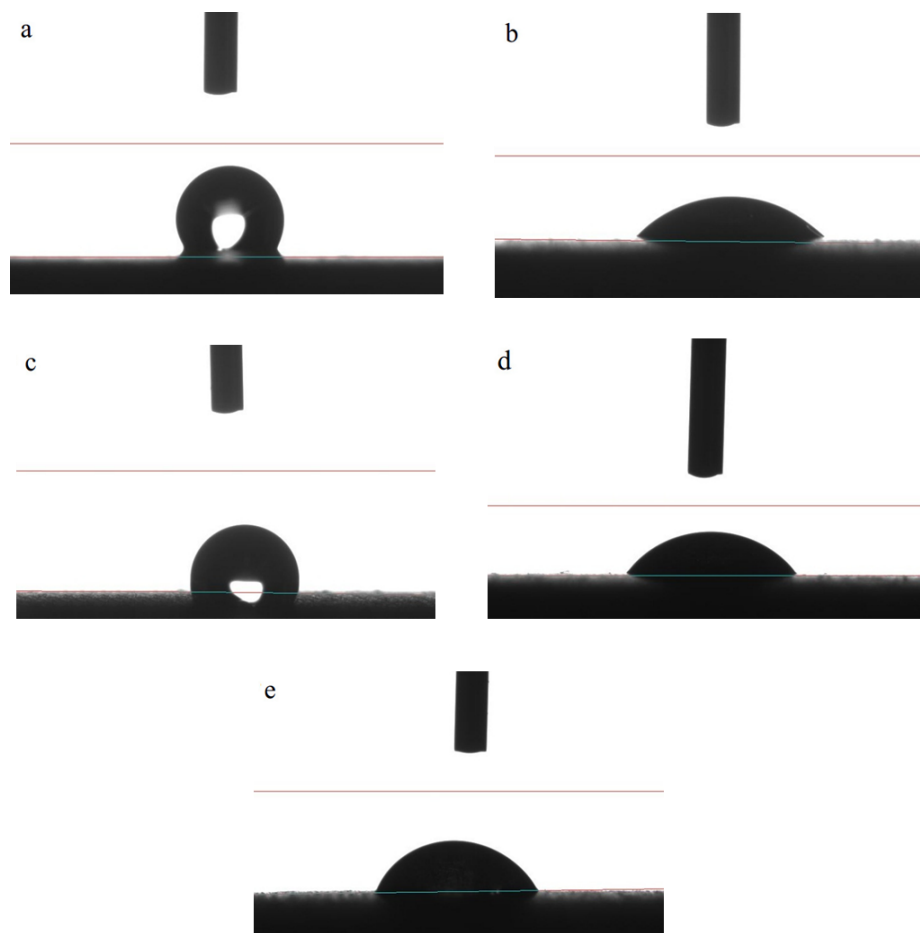


Figure 4-12 Contact angles of a) graphite, PdCo NPs b) untreated, c) DDT treated and d) treated with heat at 200 °C and e) at 300 °C.

Table 4-4 Static contact angle measurements before the corrosion assay on the PdCo samples.

	Contact Angles (°)
Graphite	125.2
Untreated	50.7
Protection with DDT	96.4
Heated at 200 °C	41
Heated at 300 °C	58

4.2.3.4 SEM and AFM

The corrosion of the samples was also evaluated qualitatively by the analysis of the surface morphology using SEM and AFM microscopy and by measuring the surface roughness (R_q) from AFM images. SEM images of the untreated/treated samples, before and after polarization test, are showed in figure 4-13. According to SEM images, the spherical morphology of the PdCo NPs samples didn't appear visibly different for untreated and treated surfaces. They do not also show any sign of pitting corrosion after the polarization test. AFM images (figure 4-14) confirm that the samples were uniformly degraded, and thus the surface of PdCo samples resists to the attack from aggressive species (such as chloride ions) in Ringer's solution.

Surface roughness may have a strong influence on the corrosion resistance of the material; therefore the average roughness of PdCo samples (before and after polarization test) was estimated (in table 4-5) using AFM images. Before the polarization assay, untreated and 200 °C heated samples exhibited an average roughness (42.2 nm and 40.1 nm, respectively) lower than samples treated with DDT or heated at 300°C ($R_q = 59.2$ nm and 81.9 nm, respectively). After the polarization assay, the samples with higher initial surface roughness showed an increase by 150.8 nm (for DDT treated) or a reduction by 55.5 nm (for the heat treated at 300 °C) of the surface roughness, whereas the samples with lower initial surface roughness didn't show a significant change of their surface roughness. This behavior can explain the higher Co^{2+} ions released ($[\text{Co}^{2+}] = 0.029$ ppm) and corrosion current density ($i_{\text{corr}} = 0.87202 \mu\text{A}/\text{cm}^2$) of the DDT treated and 300°C heat treated ($[\text{Co}^{2+}] = 0.019$ ppm; $i_{\text{corr}} = 0.065828 \mu\text{A}/\text{cm}^2$) samples when compared to those obtained with the 200 °C heat treated sample ($[\text{Co}^{2+}] = 0.012$ ppm; $i_{\text{corr}} = 0.027084 \mu\text{A}/\text{cm}^2$).

Despite that the untreated sample, which exhibit an average initial roughness (42.2 nm), didn't show a difference in the roughness after the polarization assay, it displays the highest release of Co^{2+} ions and a high corrosion current density ($[\text{Co}^{2+}] = 0.055$ ppm; $i_{\text{corr}} = 0.23874 \mu\text{A}/\text{cm}^2$) among all the samples. This might be an indication that the surface roughness might reveal the type of corrosion (pitting or uniform) involved in a corrosion process rather the corrosion rate value.

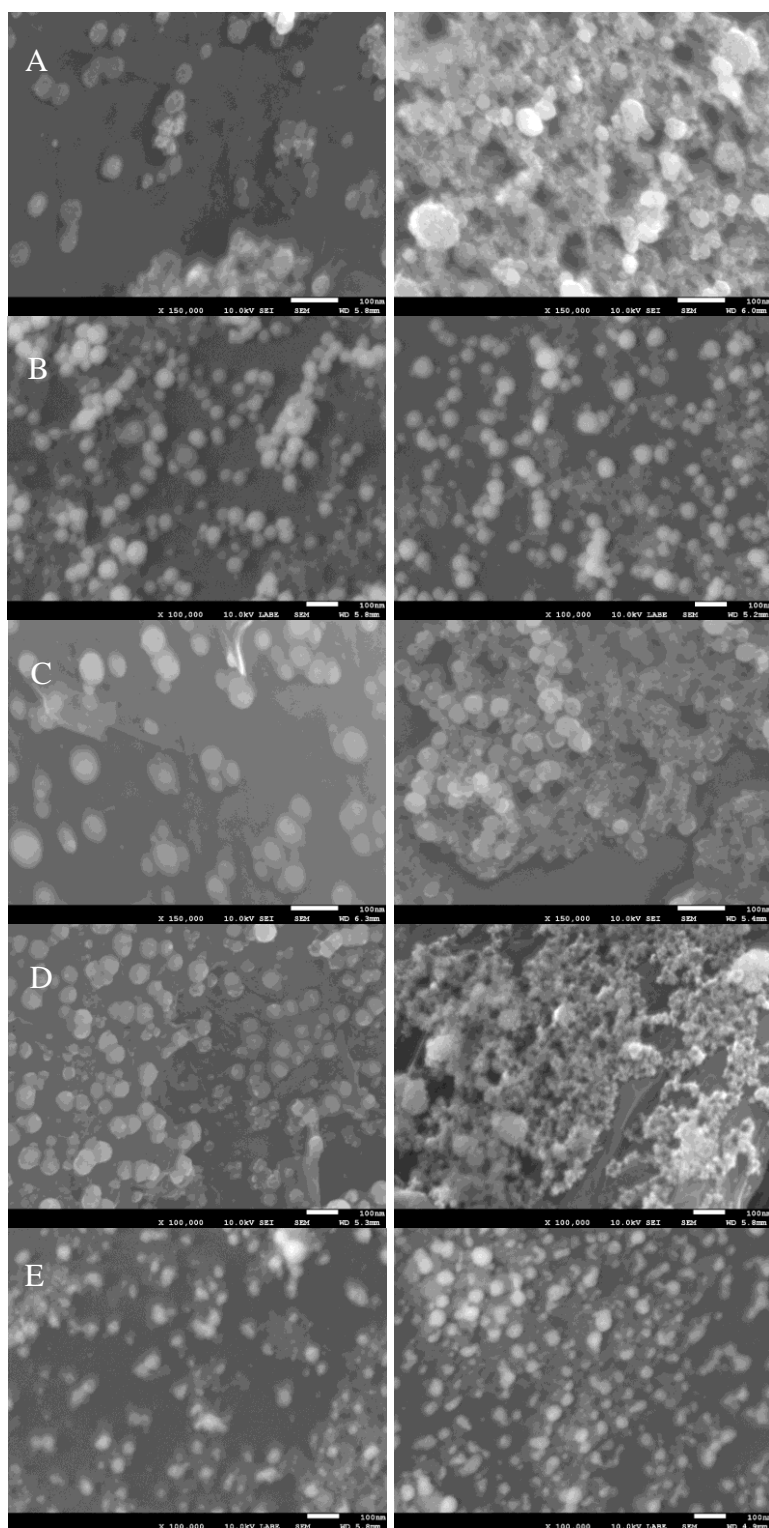


Figure 4-13 SEM micrographs of PdCo NPs before (left) and after (right) polarization assay. (A): untreated, (B): treated with DDT, (C): heated at 200 °C, (D): heated at 300 °C, and (E): heated at 400 °C.

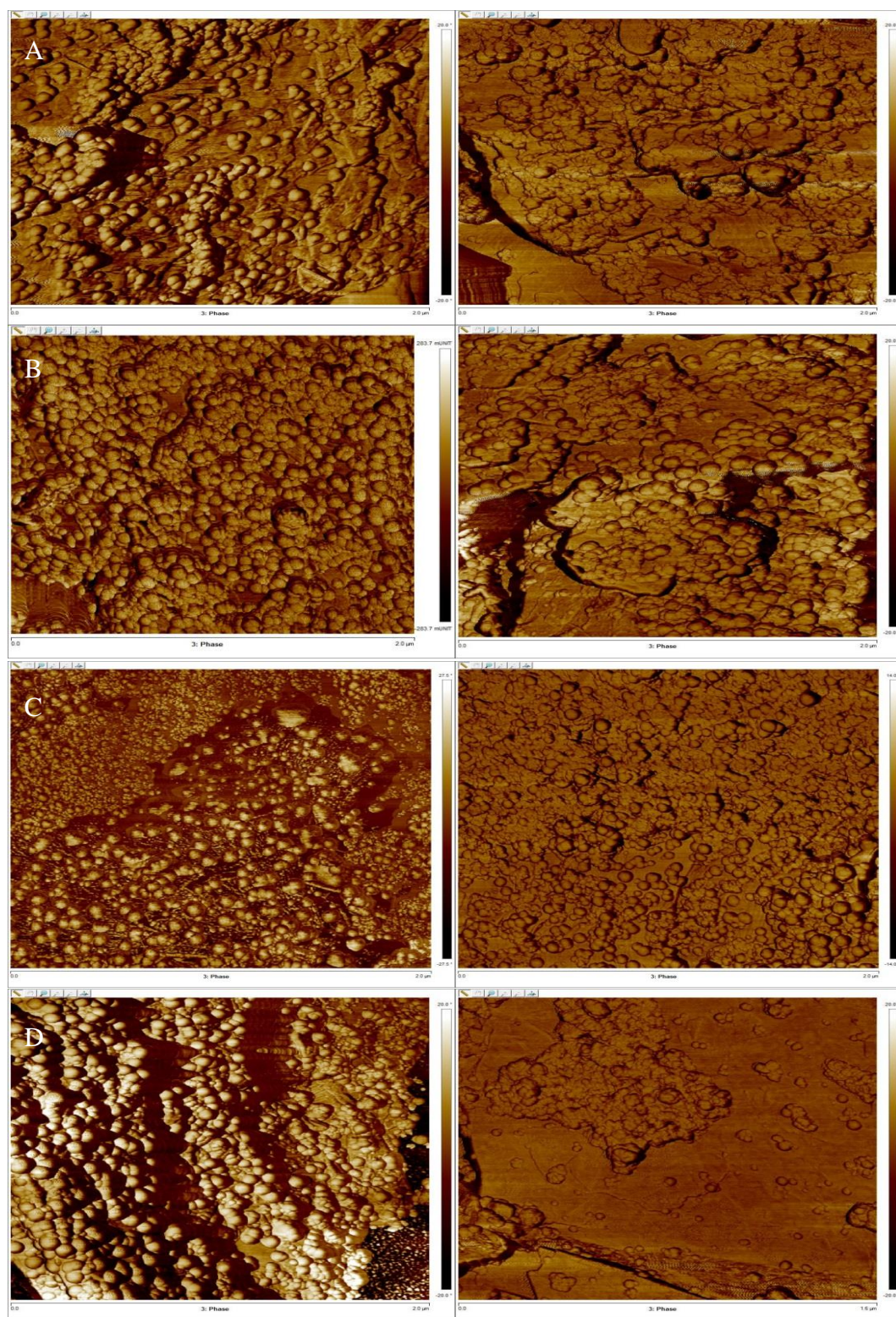


Figure 4-14 AFM images of PdCo NPs before and after polarization assay, left and right respectively. (A): untreated, (B): treated with DDT, (C): heated at 200 °C, and (D): heated at 300 °C.

Table 4-5 Surface average roughness (Rq) of the 4 samples, obtained from AFM images before and after the polarization test.

PdCo Samples	Rq (nm)	
	Before corrosion	After corrosion
Untreated	42.2	42.9
Protection with DDT	59.2	210
Heated at 200°C	40.1	41.1
Heated at 300°C	81.9	26.4

4.2.3.5 X-ray Photoelectron Spectroscopy (XPS)

The typical XPS survey spectra of the PdCo samples before and after polarization are shown in figure 4-15 (a-d). The XPS data allows the identification of the chemical composition of the alloy surface before and after polarization and the oxidation states of Pd and Co at the surface of the PdCo samples, including the passive layer. According to the elemental composition obtained from XPS spectra (table 4-6), palladium (Pd), cobalt (Co), carbon (C), oxygen (O), nitrogen (N), silica (Si), sodium (Na), chloride (Cl), sulfur (S) and tin (Sn) were shown to be present on the sample's surfaces. Nitrogen (N) may arise from the laboratory's environment whereas Na and Cl may come probably from the synthesis electrolytes (NaOH and HCl, or Pd and Co salts) and Ringer's solution during polarization. Sn contamination results from the Pd-sensitization/activation of the graphite before the synthesis, S is present in DDT monomers. Si and C may refer to the graphite electrode and DDT monomers.

High resolution analysis of the XPS spectra allows the determination of binding energies (table 4-7) of Pd3d5/2, O1s and Co2p3/2 involved in chemical species at the surface of the various PdCo samples.

Pd metallic is present on the surface of the heat treated samples before the polarization test, whereas Co metallic appears only on the DDT treated sample before the polarization test. Moreover, Pd is more stable than Co in aqueous medium as predicted by the Pourbaix diagram (figure 4-9). Therefore, the surface of the sample treated with DDT is less stable than that of samples treated with heat. The results of XPS are in good agreement with the results of the polarization assays, where the corrosion current density of DDT treated samples ($i_{\text{corr}} = 0.87202 \mu\text{A}/\text{cm}^2$) is

significantly higher than those of the samples treated with heat ($i_{\text{corr}}(300\text{ }^{\circ}\text{C}) = 0.065828\text{ }\mu\text{A}/\text{cm}^2$, $i_{\text{corr}}(200\text{ }^{\circ}\text{C}) = 0.027084\text{ }\mu\text{A}/\text{cm}^2$).

The composition of the passive layer seems to be dependent on the sample's treatment. For example, the energy binding of Pd3d5/2 corresponding to PdO appears only in untreated and 300 °C heat treated samples. The hydrophobic property of PdO explains the higher contact angle values of these samples among the other samples.

It can be clearly seen from table 4-6 that Pd is enriched and Co is depleted at the surface of 200 °C and 300 °C heat treated samples after the polarization assay. It should be noted that these samples exhibited a Co(hydroxide)-rich surface and Pd⁰ content before the corrosion study. In addition, the Pd metallic content is higher on the 200 °C heat treated sample than on the 300 °C heat treated sample. Moreover, the sample treated at 300 °C contains a high quantity of Pd in the form of PdO. These results may explain the lower concentration of Pd and Co ions released from the heat treated sample at 200 °C in comparison to those from the heat treated sample at 300 °C.

However, Pd (oxide)-rich surface with Co (oxide, hydroxide) content exhibit a higher decrease in Co than in Pd (case of untreated sample). Pd (metallic)-rich surface with PdCl₂ contamination and Co metallic contents show a small decrease in Pd and a subsequent increase in Co (case of DDT treated sample). These results indicate that the corrosion of PdCo NPs varies upon the chemical composition at their surfaces, which is related to the method of the sample's treatment.

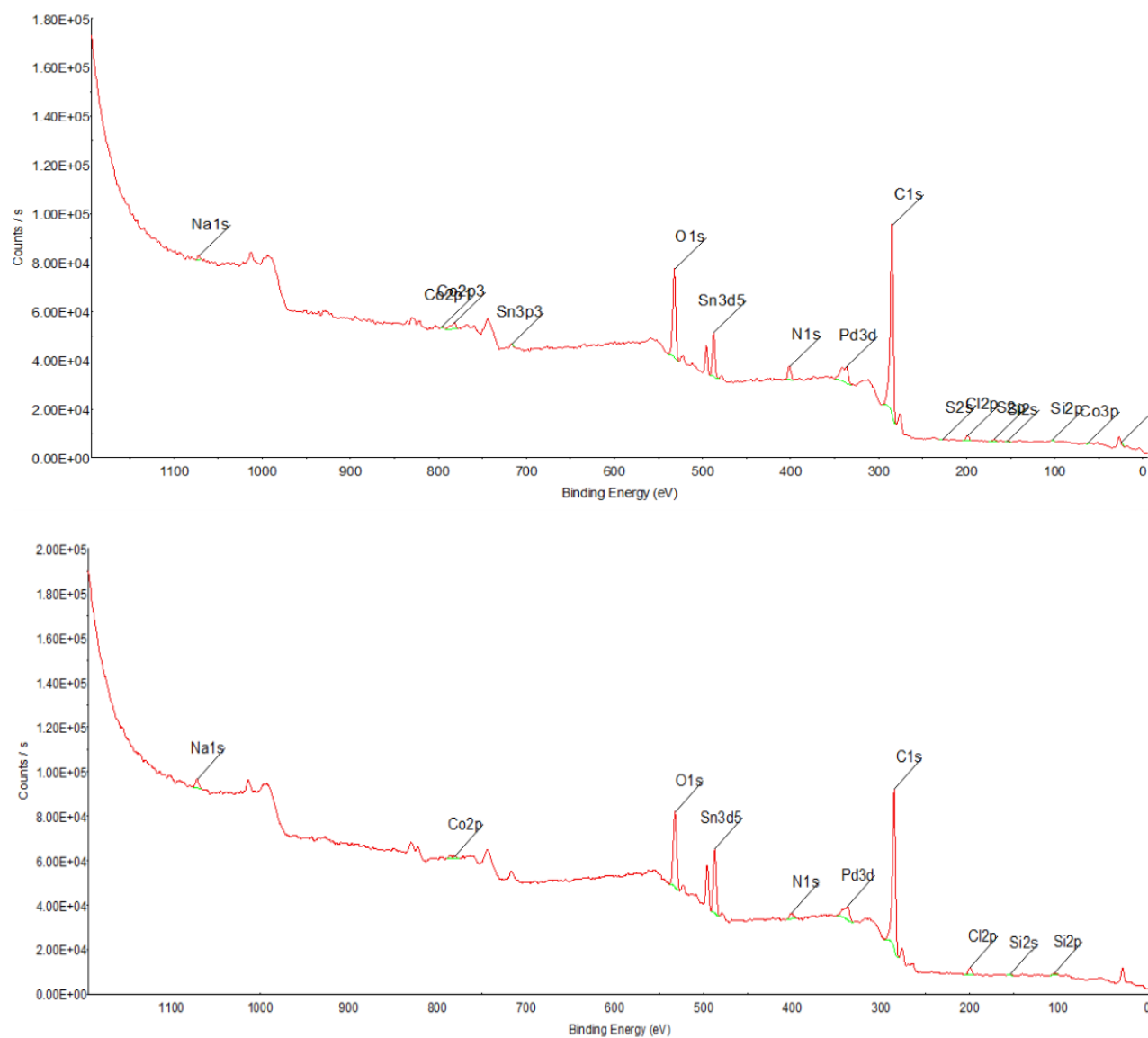


Figure 4-15.a XPS survey spectra before (upper) and after (lower) polarization of untreated PdCo samples.

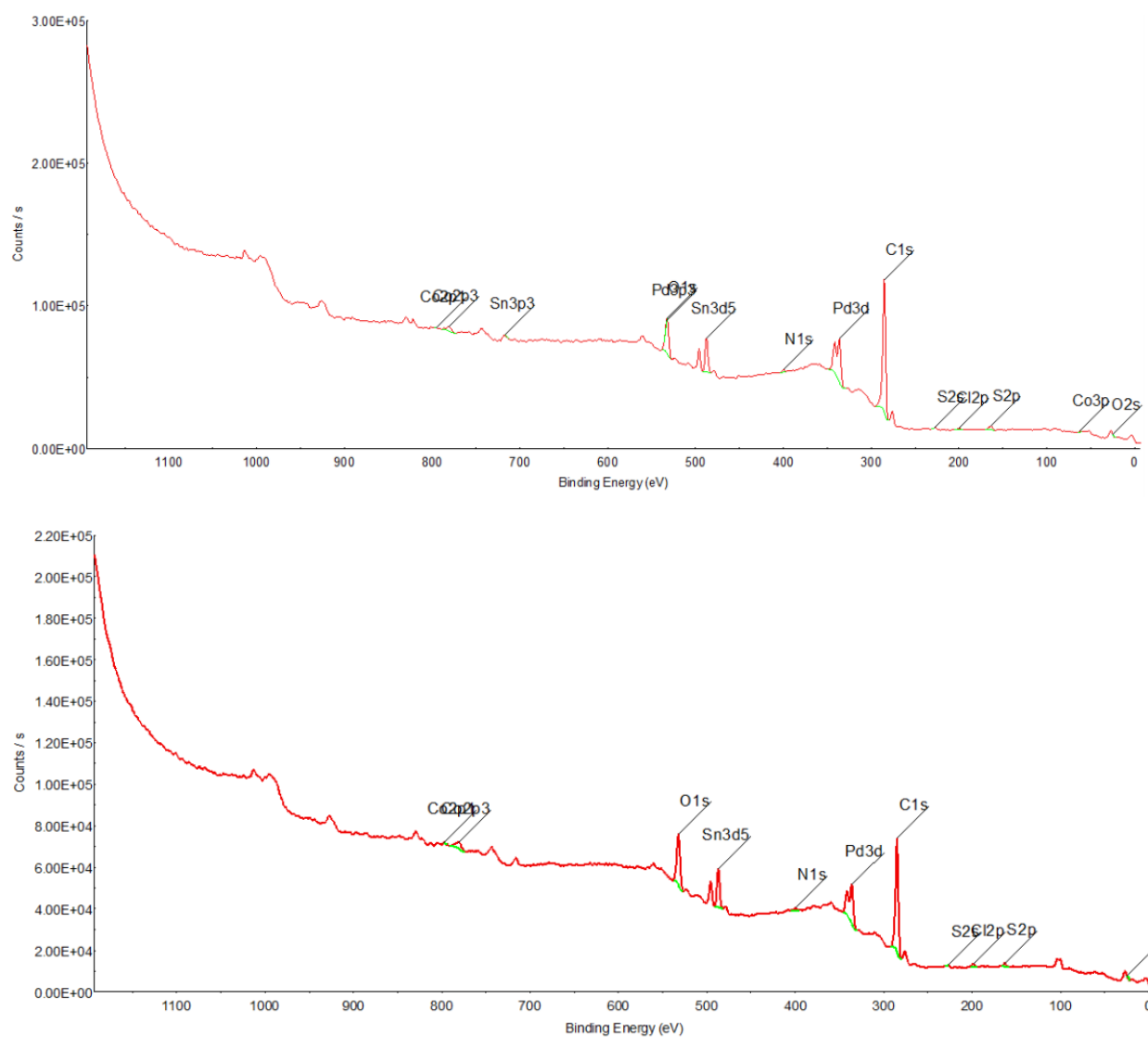


Figure 4-15.b XPS survey spectra before (upper) and after (lower) polarization of PdCo samples protected with DDT.

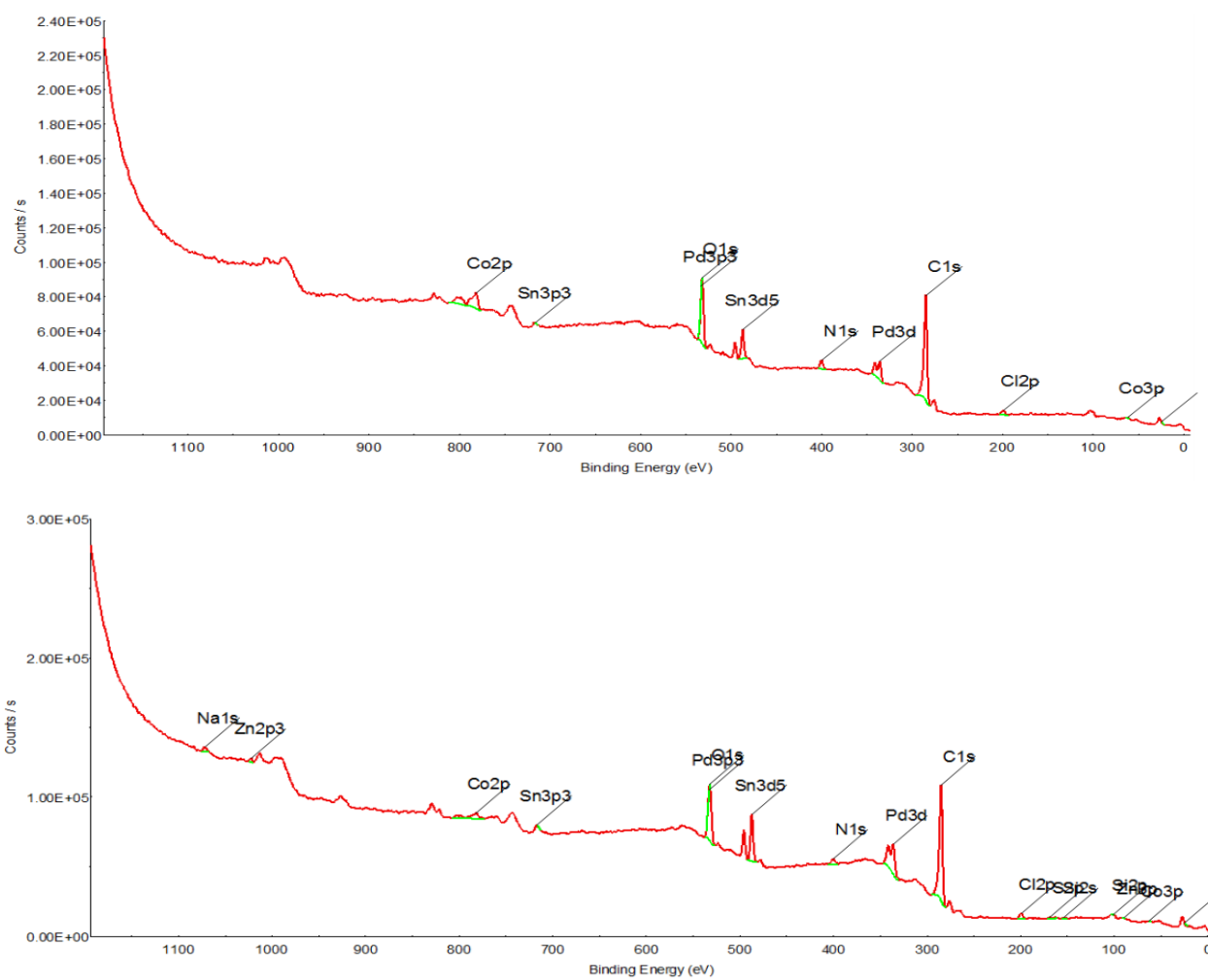


Figure 4-15.c XPS survey spectra before (upper) and after (lower) polarization of PdCo samples heated at 200 °C.

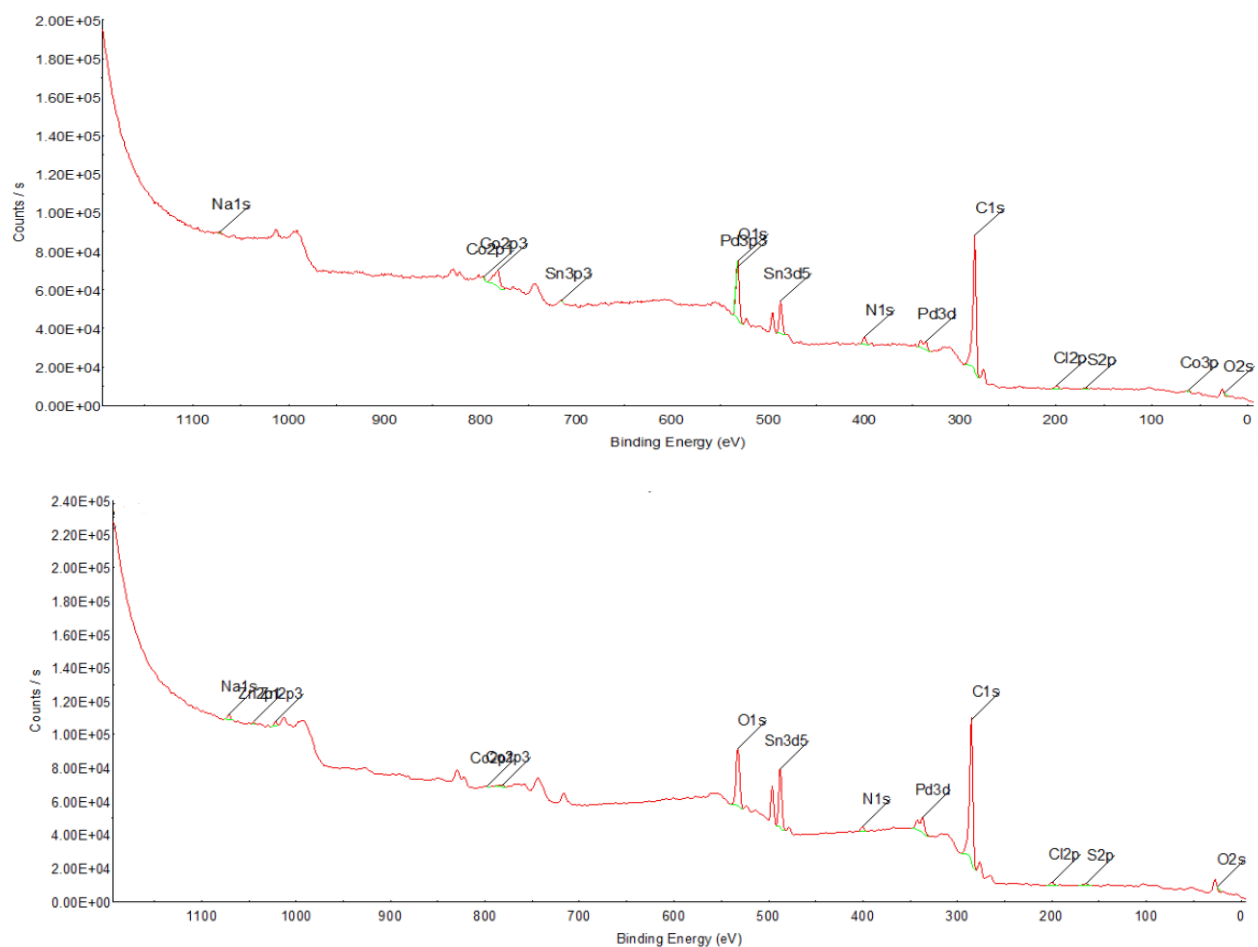


Figure 4-15.d XPS survey spectra before (upper) and after (lower) polarization of PdCo samples heated at 300 °C.

Table 4-6 Chemical composition of the elements for PdCo samples surface before (B.P.) and after polarization (A.P.).

Atomic composition %		C	O	N	Na	Cl	S	Pd	Co	Si	Sn
Untreated	B. P.	76.9	15.3	3.5	0.3	0.7	0.4	0.9	0.6	0.4	1.0
	A. P.	76.2	16.4	2.0	1.0	1.2	---	0.7	0.2	0.3	1.8
Protection with DDT	B. P.	81.5	11.4	0.8	---	0.4	1.2	2.7	0.7	---	1.3
	A. P.	75.0	17.2	1.1	---	0.6	0.9	2.4	1.2	---	1.6
Heated at 200 °C	B. P.	72.2	18.0	3.4	---	1.2	---	1.1	3.0	---	1.1
	A. P.	73.0	16.6	2.6	0.7	1.2	0.4	1.9	1.1	0.5	1.7
Heated at 300 °C	B. P.	77.9	14.4	2.4	0.1	0.8	0.3	0.5	2.5	---	1.1
	A. P.	79.5	14.4	1.3	0.6	0.6	0.5	0.8	0.2	---	1.9

Table 4-7 Identification and quantification of the binding energies of Pd3d5/2, O1s and Co2p3/2, involved in chemical species at the surface of the various PdCo samples, from high energy resolution.

Elements	Binding Energy (eV)	Chemical Bonds	Atomic composition %							
			Untreated sample		Protection with DDT		Heat treated at 200 °C		Heat treated at 300 °C	
			B.P.	A.P.	B.P.	A.P.	B.P.	A.P.	B.P.	A.P.
Pd3d5/2	335.2	Pd-Pd°	-	-	-	2.1	-	-	-	-
	335.7		-	-	2.2	-	1.3	1.7	-	-
	335.8		-	-	-	-	-	-	0.5	-
	336	Pd-O	0.5	-	-	-	-	-	-	-
	336.1		-	-	-	-	-	-	-	0.7
	336.2		-	0.4	-	-	-	-	-	-
	337.1	Pd-O or Pd-Cl	-	-	-	0.6	-	-	-	-
	337.6	Pd-Cl ₂	-	-	0.7	-	-	0.6	-	-
	338		-	-	-	-	-	-	0.1	-
	338.1		-	-	-	-	-	-	-	0.2
	338.4		0.4	0.4	-	-	-	-	-	-
O1s	530.9	M-O	-	-	-	5.4	-	-	-	-
	531.1		-	3.3	-	-	-	6.5	-	6.2
	531.3		2.4	-	4.3	-	-	-	-	-
	531.4		-	-	-	-	6.3	-	4.8	-
	532	M-OH and C=O	9.1	7.3	4.3	8.1	-	-	-	5.2
	532.3		-	-	-	-	10.6	7.7	7.8	-
	533	C-O	4.2	5.5	-	-	1.6	1.4	2.7	3.9
Co2p3/2	778	Co-Co°	-	-	-	0.6	-	-	-	-
	778.4		-	-	0.4	-	-	-	-	0.2
	778.8	Co°, Co-O in Co ₃ O ₄ , Co-C or Co-M	-	-	-	-	-	0.4	-	-
	779.3	Co-O in Co ₃ O ₄ , Co-C or Co-M	0.2	-	-	-	-	-	-	-
	780.8	Co-O in Co ₃ O ₄ , Co-OH in Co(OH) ₂ or Co-Cl in CoCl ₂	-	-	0.4	1	-	-	-	-
	781.5	Co-OH in Co(OH) ₂ or Co-NH ₃ in Co(NH ₃) ₃ Cl ₃	-	-	-	-	-	-	-	0.4
	781.7		0.4	-	-	-	3.7	1	-	-
	781.8		-	0.2	-	-	-	-	3.2	-
	782.8	Co-Cl in CoCl ₂ .xH ₂ O	-	-	0.1	-	-	-	-	-

As untreated sample didn't show Pd metallic atoms at the surface, therefore sputtering were done to investigate the oxidation states of palladium below the passive layer. The atomic composition (%) of the chemical elements observed in the survey spectra of the untreated PdCo sample before and after sputtering are summarized in table 4-8.

Table 4-8 Atomic composition of the chemical elements observed in the survey spectra of the untreated PdCo alloy before and after sputtering.

Atomic composition (%)	Pd	Co	C	O	Sn	N	Si	S	Cl	Na
Before sputtering	0.9	0.6	76.9	15.3	1	3.5	0.4	0.4	0.7	0.3
After sputtering (1 kV; 2 minutes)	0.3	0	97.1	1.5	0.3	0	0.2	0	0.2	0.4

No amount of Co, S and N was observed after the sputtering of the untreated PdCo alloy, whereas these elements were present on the surface before the sputtering. The amounts of Pd, O, Si, Sn and Cl were decreased, whereas that of C increased on the surface of the sample due to the sputtering. It should be noted that Co element was not detected in the survey spectra after sputtering, while peaks for Co were identified from XPS high resolution spectra. The peak shapes obtained in high resolution mode are more accurate, and consequently quantification is also better.

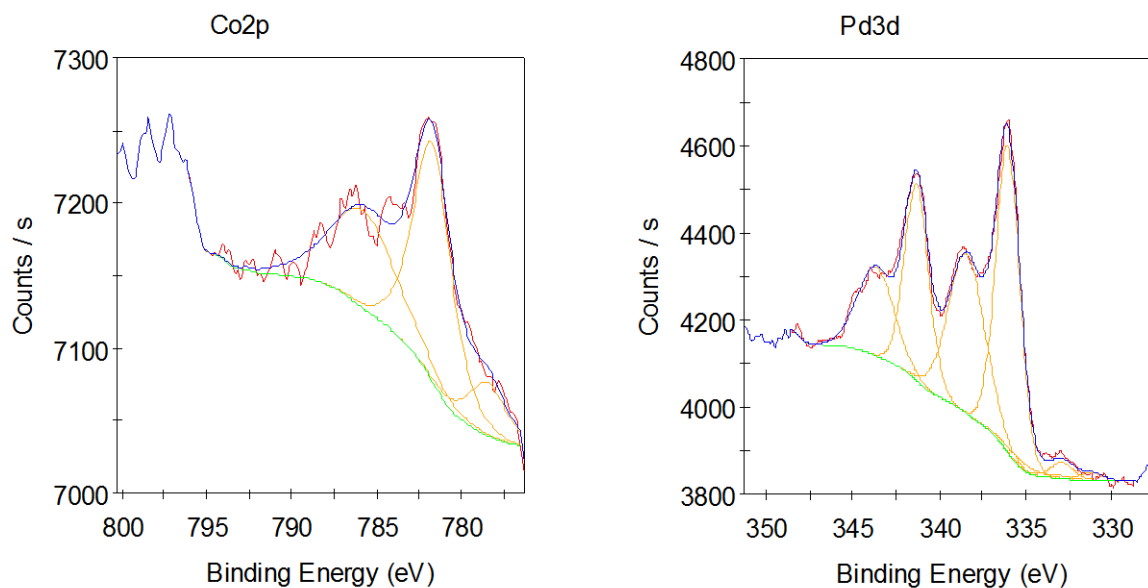
The high resolution XPS spectra of Pd 3d and Co 2p before and after sputtering are illustrated in figure 4-16. Co 2p XPS spectrum before sputtering is comprised of three main peaks at about 779.8 eV, 781.7 eV and 786.2 eV assigned to Co 2p_{3/2}. The peak at 779.8 eV is characteristic of cobalt oxides (e.g. Co₂O₃, Co₃O₄), cobalt oxyhydroxide (e.g. CoO(OH)) and cobalt hydroxide (Co(OH)₂) [182]. The peak at 781.7 eV can be attributed to cobalt hydroxides or trichlorotriamminecobalt (Co(NH₃)₃Cl₃), and the peak at 786.2 eV (shake up) is associated to cobalt oxides and cobalt chloride [182]. After sputtering, the peaks of Co 2p_{3/2} are observed at 778.6 eV and 782.1 eV (shake up), they are assigned to metallic Co only [182].

It is worth noting that after sputtering at 1 kV for 2 minutes, the amount of Co oxides and hydroxides calculated from the high resolution XPS data decreased from 0.6 % to a very low atomic

%, and the amount of Co metallic increased from 0 to 0.7 %, at the surface of the untreated PdCo sample. These results suggest two possibilities, whether sputtering method induced the reduction of the cobalt oxides/hydroxides at the surface to cobalt metal or eroded the surface elements (including cobalt oxides/hydroxides) and thus metallic Co in the underlayer shows up.

On the other hand, Pd 3d XPS spectrum before sputtering is comprised of four main peaks at about 336.1 eV, 338.7 eV, 341.5 eV and 344 eV. The peaks at 336.1 eV and 341.5 eV are attributed to Pd 3d_{5/2} and are characteristic of Pd–O species [182]. However, those at about 338.7 eV and 344 eV correspond to Pd 3d_{3/2} and are assigned to Pd–Cl species [182]. After sputtering, the peaks of Pd 3d_{5/2} are observed at 336.7 eV and 341.7 eV, and are characteristic of Pd–O species [182,182].

It is important to mention that the atomic % of palladium oxide (PdO), calculated from the high resolution XPS data, increased from 0.5 to 0.9 % whereas the % of palladium chloride (PdCl₂) decreased from 0.4 to 0 % after sputtering the surface of the untreated PdCo sample. Therefore, untreated PdCo NPs consist of PdO core and PdO with PdCl₂ shell.



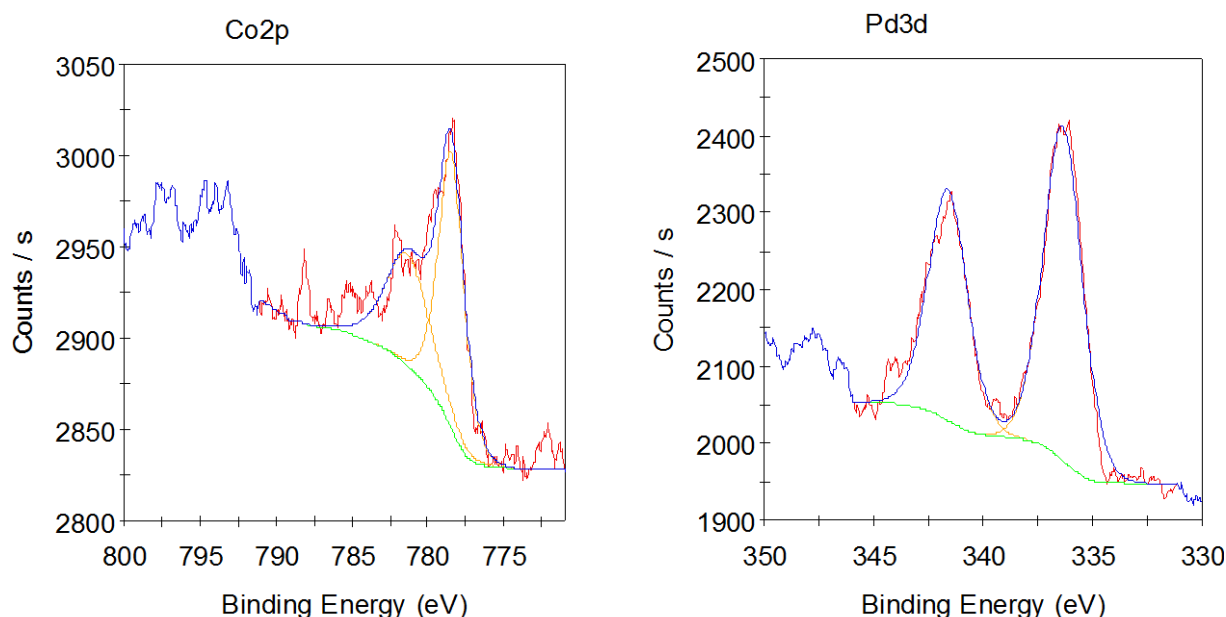


Figure 4-16 High resolution XPS of Pd 3d_{5/2} and Co 2p_{3/2} before (upper) and after sputtering (lower).

4.2.3.6 Immersion test

The quantity of Pd and Co ions released during the immersion of PdCo samples in 37 °C Ringer's solution for 7 days are indicated in table 4-9. The concentrations of both Pd and Co ions are less than 0.01 ppm for all the samples, indicating that PdCo samples exhibit a very good resistance to corrosion on the short-term.

Table 4-9 Quantity of metal ions released during 166 hours.

Ion release (ppm)	Untreated	Protected with DDT	Heated at 200 °C	Heated at 300 °C
Pd	<0.01	<0.01	<0.01	<0.01
Co	<0.01	<0.01	<0.01	<0.01

4.2.4 Conclusions

Palladium-cobalt is a very good candidate for magnetic hyperthermia because of the stability of palladium and ferromagnetic properties of cobalt. Few studies were done on the corrosion of PdCo alloys [124,183,184,185]. They showed a good stability for Pd rich PdCo alloys. However, the

stability of Pd rich PdCo NPs was not investigated. Thus, it is very interesting to investigate for the first time the corrosion resistance of PdCo NPs. Moreover, the effect of heat and alkanethiol layer on the stability of PdCo NPs was evaluated.

Based on the results of this work, it can be concluded that:

1) PdCo based alloys were produced by electrodeposition under a constant negative potential of -1.2 V applied for 1 minute to the graphite electrode, as a supporting electrode, in a three electrochemical cell configuration. The supporting electrode was immersed in a solution containing Pd(II) and Co(II) salts and de-aerated with nitrogen atmosphere.

2) The PdCo NPs samples treated with heat displayed the lowest corrosion current densities (i_{corr}) of 0.022114 $\mu\text{A}/\text{cm}^2$ for 400 °C, 0.027084 $\mu\text{A}/\text{cm}^2$ for 200 °C and 0.065828 $\mu\text{A}/\text{cm}^2$ for 300 °C. On the contrary, the sample treated with DDT monomers and untreated sample exhibited the highest corrosion densities of i_{corr} of 0.87202 $\mu\text{A}/\text{cm}^2$ and 0.23874 $\mu\text{A}/\text{cm}^2$ respectively.

3) According to AAS, the heat treated and alkanethiol treated samples exhibited a low release of Pd and Co ions, which may reach [Pd] = 0.01 ppm; [Co] = 0.013 ppm, in the Ringer's solution after the polarization assay. The increase in the ions concentrations is in the following order for heat treated (at 200 °C, 300 °C and 400 °C) samples, DDT treated sample and untreated samples: heat treated at 200 °C < heat treated at 400 °C < heat treated at 300 °C < treated with DDT < Untreated. XPS analysis showed that the corrosion of treated/untreated PdCo samples varies upon the chemical composition at the surface, which revealed to be treatment-dependent. Moreover, after 7 days of immersion in 37 °C Ringer's solution both treated and untreated samples exhibited an excellent corrosion resistance ([Pd]<0.01 ppm; [Co]<0.01 ppm).

This study concluded that PdCo NPs could be used as a medical micro-device if they are treated with heat, because this treatment showed to be very efficient in the enhancement of the PdCo NPs stability upon corrosion in Ringer's solution, and thus prevent high Pd and Co ions release in biological environment and subsequent nanotoxicity.

Acknowledgments

The authors thank the Fonds Québécois de la Recherche sur la Nature et les Technologies (FQRNT) and the Fondation Universitaire Pierre Arbour for their funding of this research.

CHAPTER 5 GENERAL DISCUSSION

This discussion helps to make relation between the various parts of the thesis; the originality of work and the correlations between the method of the PdCo alloys synthesis, their chemical composition to their resistance to corrosion and magnetic properties. An electrochemical method for the synthesis of new medical micro-device of PdCo NPs was developed for the first time, using a sequential electrodeposition on graphite electrode. Despite the difficulties to deposit PdCo on the highly oriented pyrolytic graphite, we modified its surface with Pd particles by electroless to enhance the deposition of PdCo (due to the efficient Pd particles-mediated electron transfer) and then used it as working electrode to obtain a 3D growth required to produce nanoparticles. Later, a sequential electrodeposition followed by DDT coating was adopted to increase the number of nanoparticles. Moreover, the electrodeposition parameters (such as graphite surface, bath composition, applied potential and duration of electrodeposition) were optimized to produce spherical Pd-rich PdCo nanoparticles, with a ratio Pd/Co= 65.3:34.7, in the range 30-50 nm.

To the best of our knowledge, no in-depth research has been performed so far on the stability of Pd₆₅Co₃₅ NPs. Therefore, it was very interesting to investigate for the first time the corrosion resistance of PdCo NPs. Moreover, we studied the effect of heat and alkanethiol layer treatment on the corrosion behaviour of these NPs. The heat treatment showed a strong influence on the corrosion resistance, reducing the release of Pd and Co ions ([Pd] = 0.01 ppm and [Co] = 0.013 ppm) during polarization assay by enhancing the microstructure of the alloy and thereby the passive layer at the surface. On the other hand, the treatment with alkanethiol layer also enhances the corrosion resistance of the PdCo NPs by protecting Pd and Co metallic states from oxidation after the corrosion test, as long as the hydrophobic DDT are chemisorbed at the PdCo surface. The immersion of the treated and untreated samples of PdCo NPs done in 37 °C Ringer's solution revealed an excellent corrosion resistance ([Pd] < 0.01 ppm; [Co] < 0.01 ppm).

From the results of this work, we can conclude that PdCo NPs must be treated with heat or alkanethiol monomers to prevent high Pd and Co ions release in biological environment and subsequent nanotoxicity.

As limitations are inevitable in a research, these nanoparticles cannot be used directly neither for biocompatibility tests nor for magnetic investigations because of their deposition onto 0.7 mm x 0.7 mm (0.3 mm thickness) graphite substrate and their ferromagnetism behaviour due to the

presence of agglomerated particles. Furthermore, the concentration of PdCo NPs is very low resulting in difficulties for studying the crystalline structure using XRD analysis.

Despite the drawbacks mentioned above, the hysteresis loop and Curie point measurements were done over two samples A and B of PdCo. Samples A (Pd-14 % Co) and B (Pd-12 % Co) are both synthesized in the same conditions using two sequential electrodepositions at -1.2 V (vs SCE), for 1 min each followed by DDT protection (19h).

The hysteresis loop (magnetic moment versus the applied magnetic field) and the Curie point measurements were measured using a vibrating sample magnetometer (VSM).

According to the hysteresis loop (in figure 5-1), both samples are ferromagnetic and the maximum induced magnetic moments are about 0.60 and 0.55 memu for sample A and sample B respectively. The saturation magnetization (memu/g) of the sample can be obtained by dividing the maximum magnetic moment (memu) by the deposited PdCo mass (g), estimated from equation (19).

$$Q (C) = I (A) \times t (s) \quad (\text{Equation 19})$$

$$1 F = 96\,500 C = 1 \text{ mole of } e^-$$

For example, $Q(\text{sample A}) = 7.66 C$ during the electrodeposition, so the number of moles of e^- passed through the graphite electrode is $\frac{7.66 C}{96\,500 C} = 7.938 \times 10^{-5}$.

It takes 2 moles of e^- to form 1 mole of Pd ($\text{Pd(II)} + 2e^- \rightarrow \text{Pd}$), which contribute to 86 % of the alloy, therefore $n(\text{Pd}) = \frac{7.938 \times 10^{-5}}{2} \times \frac{86}{100} = 3.413 \times 10^{-5}$ mole, and $m(\text{Pd}) = n.M = 3.413 \times 10^{-5} \text{ mole} \times 106.42 \text{ g} = 3.6 \text{ mg}$.

Also, it takes 2 moles of e^- to form 1 mole of Co ($\text{Co(II)} + 2e^- \rightarrow \text{Co}$), which contribute to 14 % of the alloy, therefore $n(\text{Co}) = \frac{7.938 \times 10^{-5}}{2} \times \frac{14}{100} = 0.556 \times 10^{-5}$ mole and $m(\text{Co}) = n.M = 0.556 \times 10^{-5} \text{ mole} \times 58.93 \text{ g} = 0.327 \text{ mg}$.

The total deposited mass of PdCo in sample A is $m(A) = m(\text{Pd}) + m(\text{Co}) = 3.927 \text{ mg}$.

Thus the saturation magnetization of sample A is about $\boxed{M_s(A) = \frac{0.6}{0.003927} = 152.78 \text{ memu/g}}$

Using the same calculation above we obtained
$$M_s(B) = \frac{0.55}{0.002355} = 233.54 \text{ memu/g}$$

Although samples A and B are deposited in the same conditions and have almost the same composition, they exhibit different saturation magnetizations. The higher magnetization of sample B ($M_s = 233.54 \text{ memu/g}$) can be attributed to the agglomeration of particles seen in SEM images (figure 5-2) and subsequently higher particle size of PdCo particles compared with sample A ($M_s = 152.78 \text{ memu/g}$).

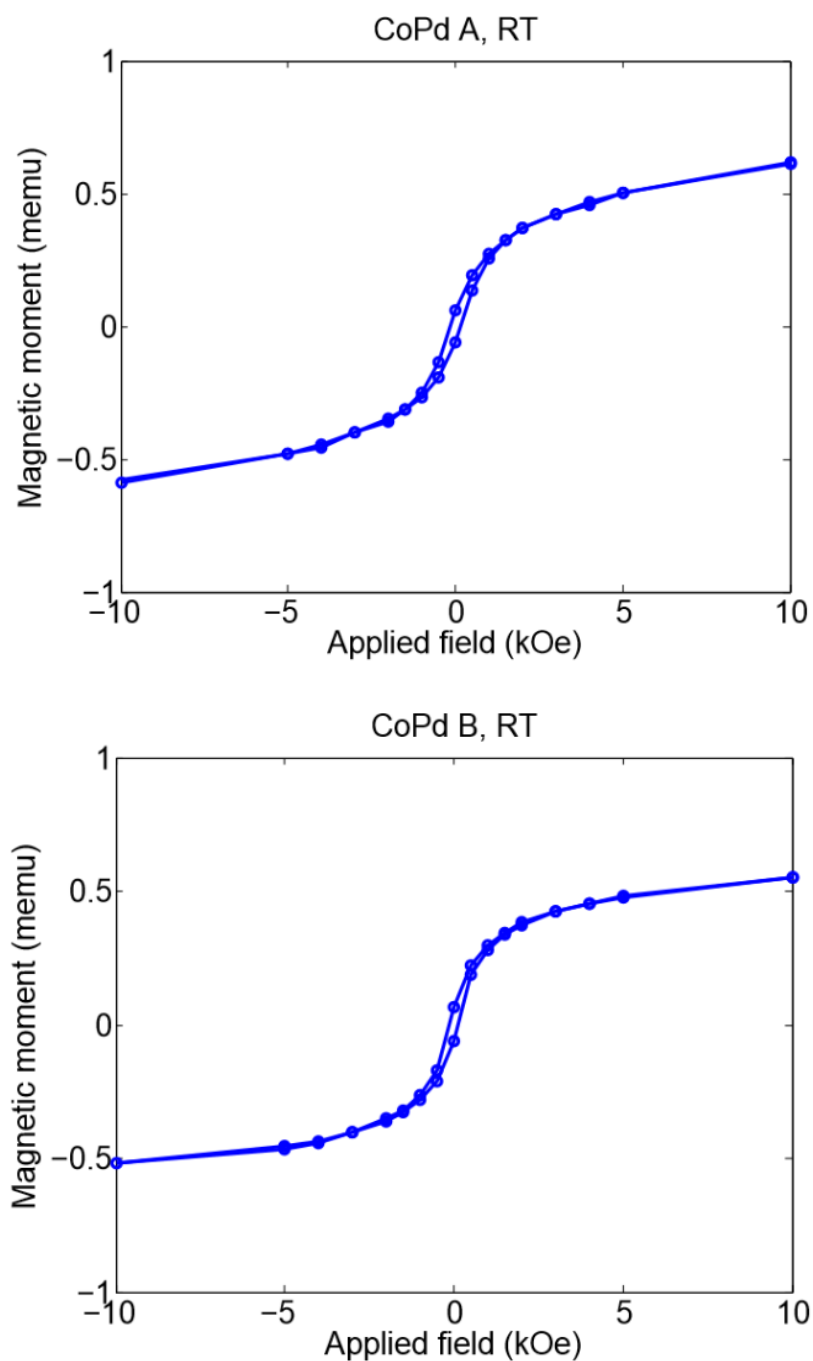


Figure 5-1 Longitudinal M-H hysteresis loop for Pd-14 % Co (A) and Pd-12 % Co (B) alloys, obtained by two sequential electrodepositions at -1.2 V, during 1 minute each and followed by DDT protection (19 h).

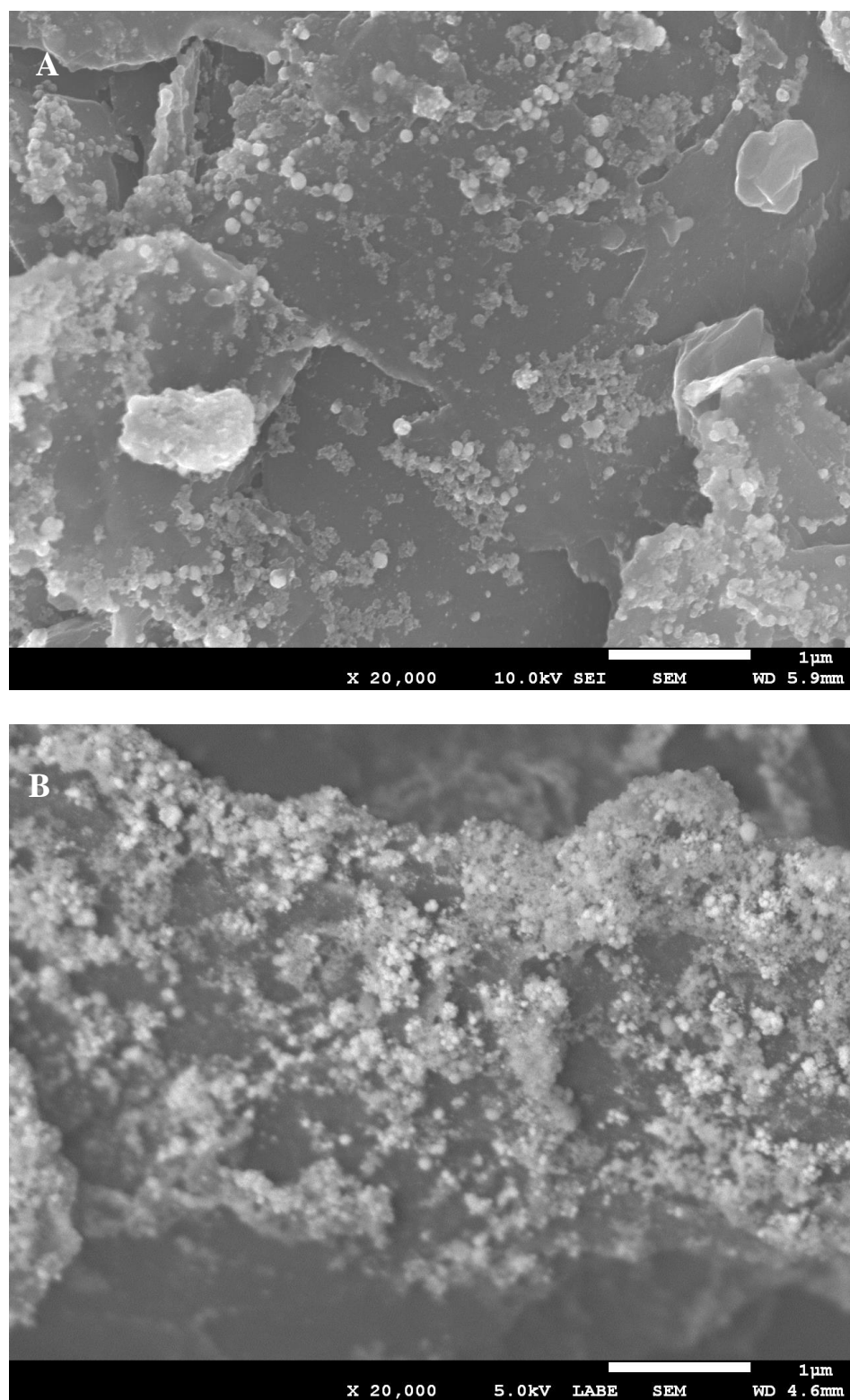


Figure 5-2 SEM images of electrodeposited Pd-14 % Co (A) and Pd-12 % Co (B) alloys obtained by two sequential electrodepositions at -1.2 V, during 1 minute each and followed by DDT protection (19 h). (magnification of 20k x)

The above results showed that the saturation magnetization of untreated PdCo NPs is about 200 memu/g, because both samples have a very low mass of NPs. This is another reason why the quantity of deposited NPs must be increased to enhance their magnetization, which is 450 times lower than those of the bulk material ($M_s = 90$ emu/g). [38].

Curie point measurements were done on the sample B (figure 5-4), sample of Pd-30 % Co deposited at -1.2 V for 45 s (figure 5-5), and on the graphite as well (figure 5-5). As expected, the graphite didn't undergo phase transitions and thus detected Curie points will belong to PdCo NPs. The Curie measurement showed that sample B exhibits a Curie temperature between 450 K and 475 K. According to Curie point graph of PdCo (figure 5-3) and EDX analysis (12 % Co), the Curie temperature is probably due to $\text{Pd}_{87}\text{Co}_{13}$ phase. However, it is not the only Curie temperature and other Curie temperature(s) is (are) expected.

The sample of Pd-30 % Co, deposited at -1.2 V for 45 s, showed at least two Curie temperatures. The first one is between 700 K and 850 K indicating a phase of 30 % Co, according to Curie point graph and EDX analysis. The second one is between 400 K and 450 K and reveals lower percentage of cobalt (about 10-15 %). The percentage of cobalt seems to vary significantly in the deposited NPs.

Therefore, neither sample B nor sample Pd-30 % Co are a single phase and this confirms the usefulness of the heating treatment after electrodeposition to enhance the microstructure of the alloy, which should be a single phase FCC solid solution.

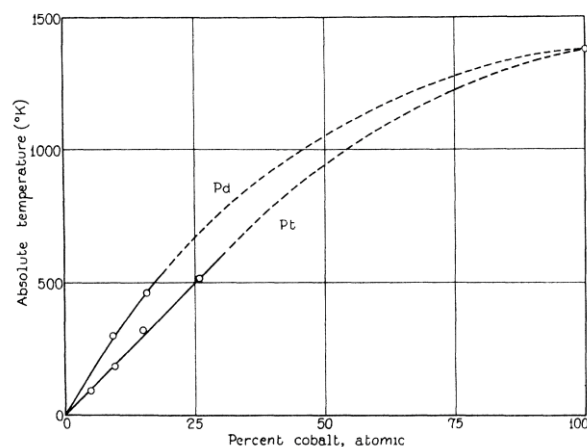


Figure 5-3 Curie point as a function of the atomic percentage of cobalt [186].

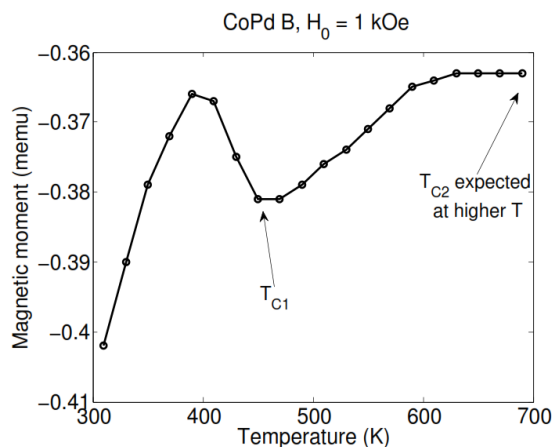


Figure 5-4 Magnetic moment as a function of temperature for sample B (Pd-12 % Co), obtained by two sequential electrodepositions at -1.2 V, during 1 minute each and followed by DDT protection (19 h).

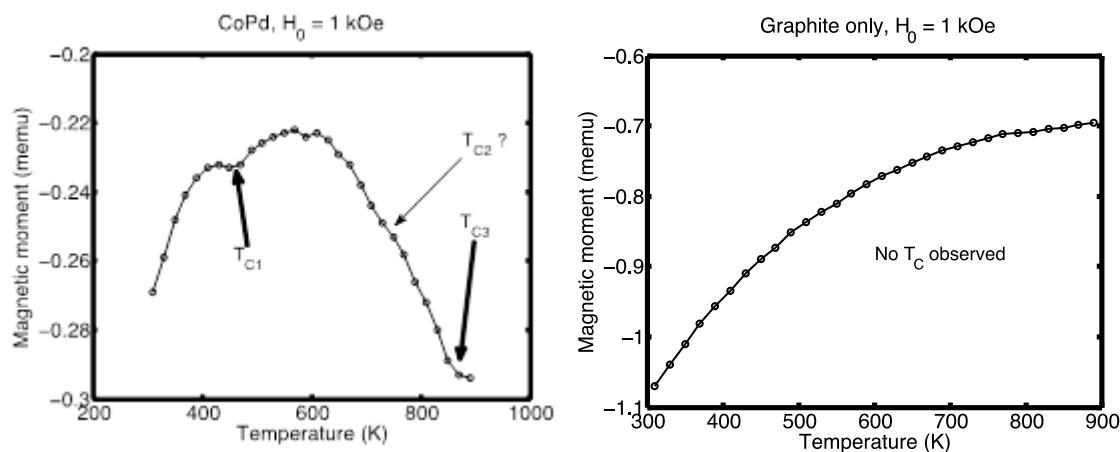


Figure 5-5 Magnetic moment as a function of temperature for Pd-30 % Co (left), deposited at -1.2 V for 45 s, and for graphite (right).

Based on Curie temperature results, we can conclude that samples treated with DDT (sample B or sample Pd-30 % Co) have a heterogeneous composition and also generally exhibit a lower corrosion resistance than the samples which have homogeneous composition. When a sample has two chemical compositions is immersed in an electrolyte, the component of the sample with the

lower potential is attacked. The lower corrosion resistance of the heterogeneous composition, compared with homogeneous composition, is the reason of the higher corrosion current of the sample treated with DDT ($i_{\text{corr}} = 0.87202 \mu\text{A}/\text{cm}^2$) compared with the samples treated with heat ($i_{\text{corr}} = 0.022114 \mu\text{A}/\text{cm}^2$ for 400°C). This highlights again the effectiveness of the heat treatment after the synthesis of NPs to obtain samples exhibiting one uniform chemical composition sample. The development of this family of samples consequently will increase the corrosion resistance of the NPs. Hysteresis loop, Curie temperature and XRD tests have to be done over PdCo NPs samples treated with heat to confirm if the enhanced crystallinity and homogeneity of the composition will increase the saturation magnetization.

On the other hand, the form of the magnetisation vs temperature curve and the negative magnetic moments obtained during these Curie point measurements come from the low magnetic moments of the graphite substrate. Therefore, a simple subtraction of the graphite magnetic moments from the overall magnetic moments of the samples was achieved (figure 5-6) in order to show the magnetic behavior of PdCo NPs as function of temperature.

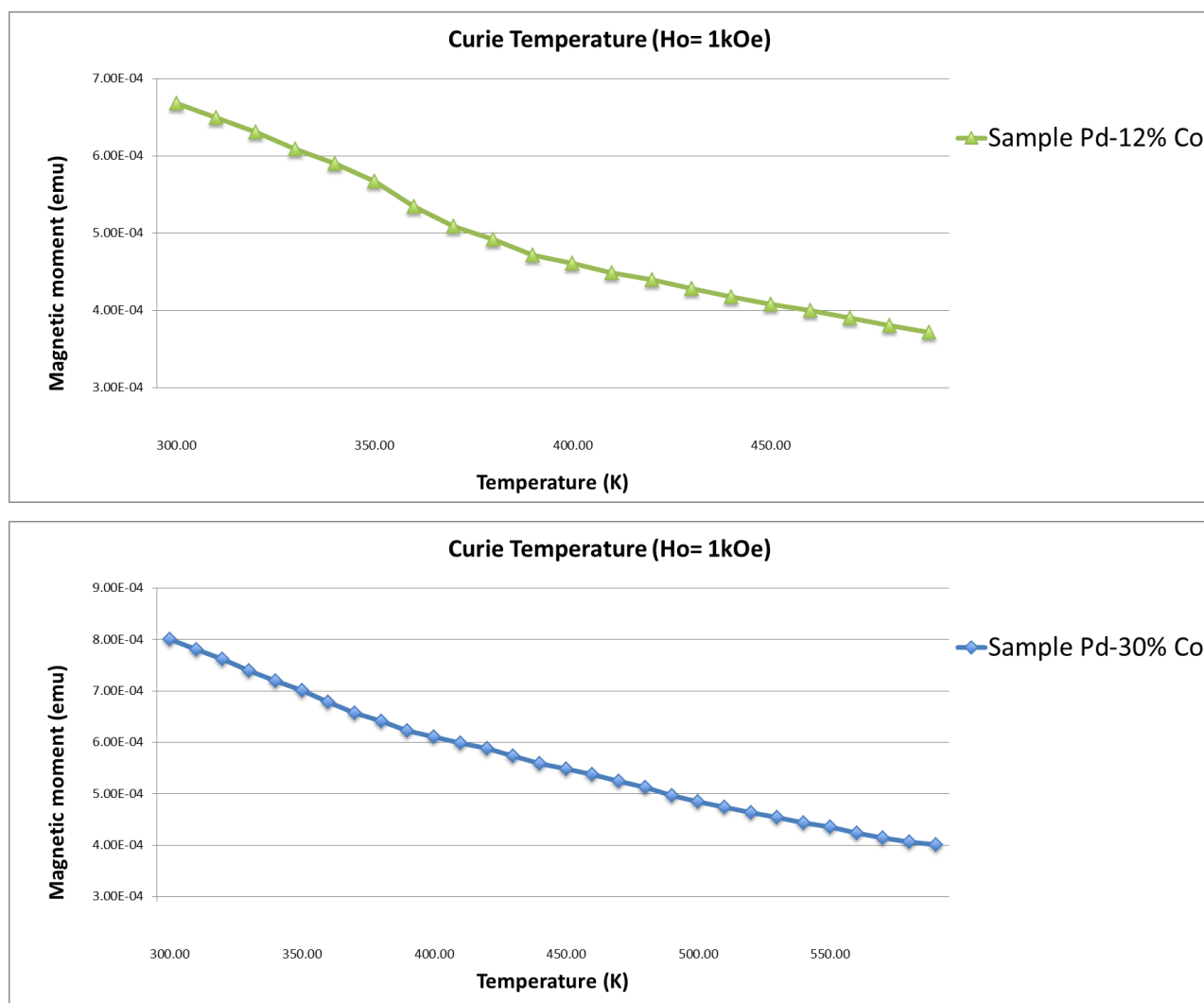


Figure 5-6 Magnetic moment as a function of temperature for sample B (Pd-12% Co) and sample Pd-30 % Co after subtraction of the graphite magnetic moments.

The NPs investigated exhibit a ferromagnetism behavior as result of agglomerated particles. To solve this problem and obtain superparamagnetic behavior, NPs must be transferred to a solution and then the solution of dispersed NPs is filtered to eliminate the big and very small particles.

We tested the feasibility of separating the NPs from the graphite using ultrasonic bath.

The PdCo NPs sample was placed in a vial containing 2 mL ethanolic solution of 50 mM DDT monomers. It can be seen from figure 5-7 that 30 minutes sonication at room temperature remove a visible mass of NPs from a certain region of the graphite surface; however the concentration of

PdCo particles is very low in the 36 μL solution evaporated on a clean graphite surface (used for SEM analysis).

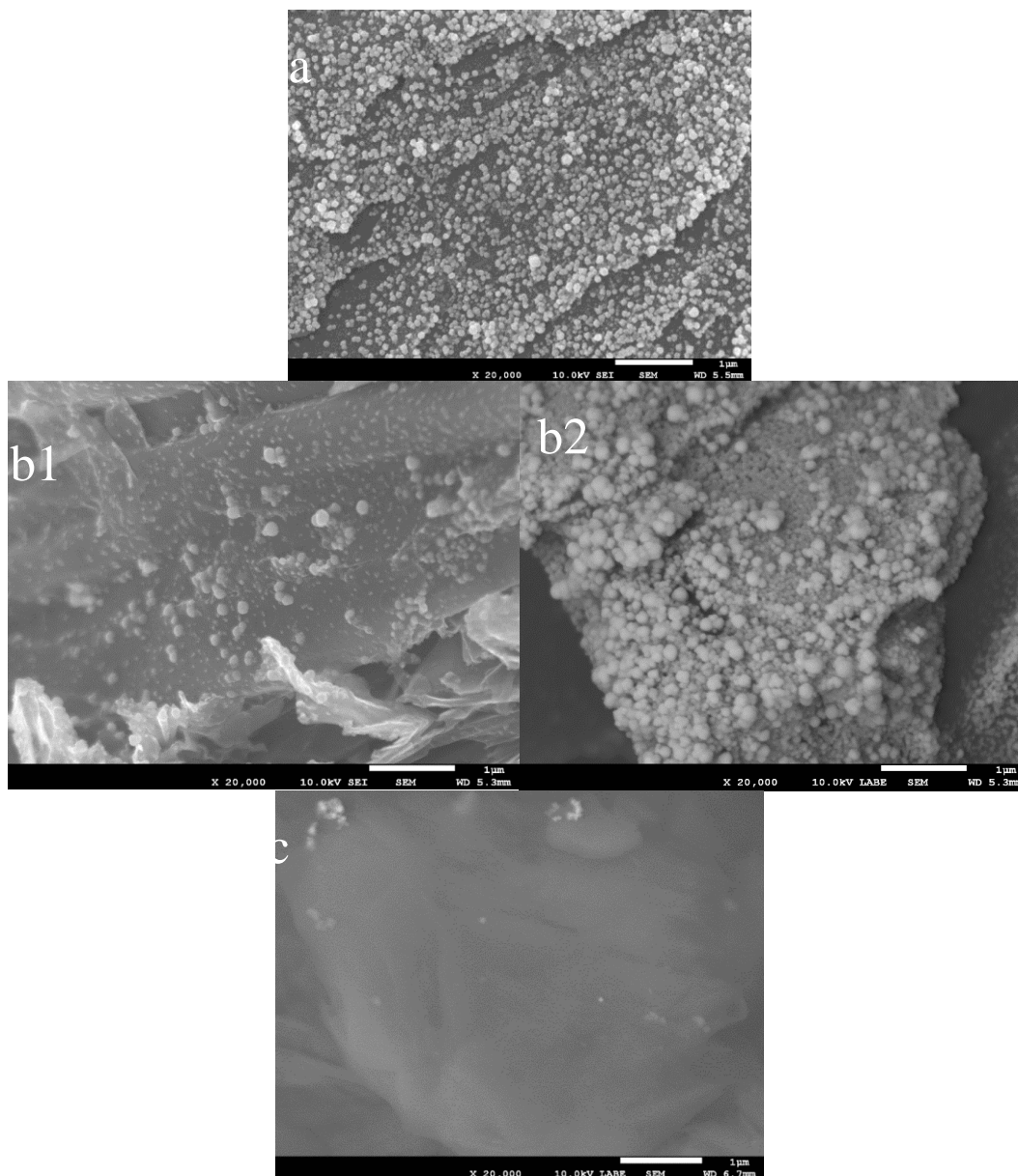


Figure 5-7 SEM images of (a) PdCo sample before sonication, (b) PdCo sample after sonication for 30 minutes at room temperature and (c) 36 μL solution of PdCo on graphite.

To understand the controversy in the SEM analysis, the time of sonication was increased more 7 hours to enhance the concentration of PdCo in the ethanolic solution and a brass substrate was used

instead of graphite, as a flat surface, to enhance the concentration of PdCo in the ethanolic solution. As seen from figure 5-8, the quantity of NPs in the solution increased significantly and the bared regions of graphite become more frequent.

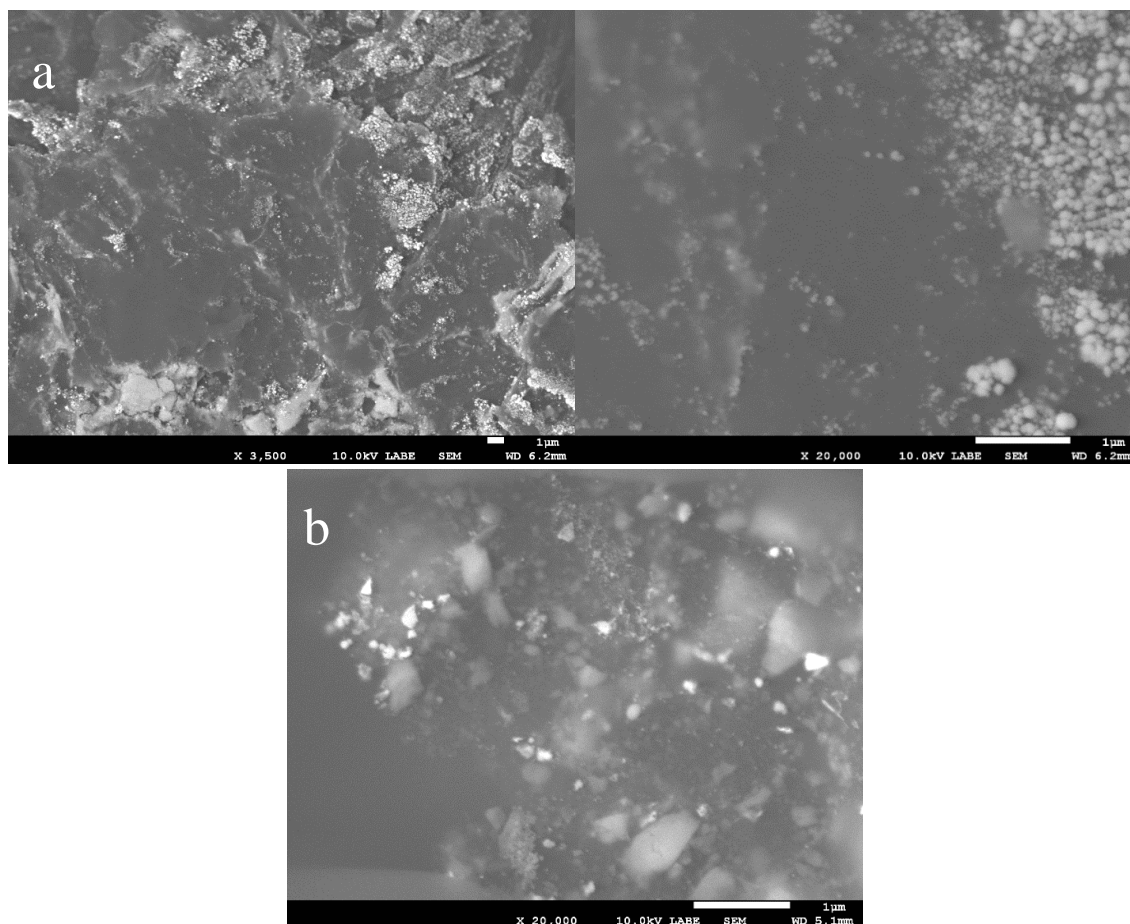


Figure 5-8 SEM images of (a) PdCo sample after sonication for 7 hours and 30 minutes at room temperature and (b) 36 μ L solution of PdCo on brass.

To evaluate the effect of the temperature during the sonication, the same sample of PdCo was sonicated during 6 hours at 55 $^{\circ}$ C (figure 5-9). SEM images have shown a very high concentration of NPs in the ethanolic solution as result of the very low concentration of the remaining electrodeposited PdCo NPs.

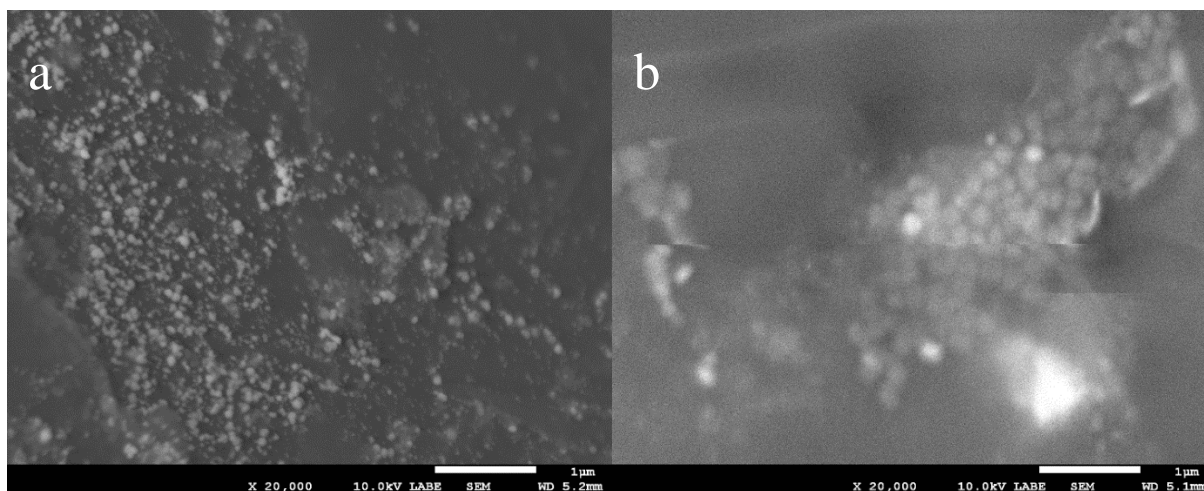


Figure 5-9 SEM images of (a) PdCo sample after sonication for 7 hours and 30 minutes at room temperature and more 6 hours at 55 °C, and (b) 36 μ L solution of PdCo on brass.

It can be concluded from the sonication test that it is possible to obtain a solution of dispersed PdCo NPs using a sonicator. Also, this test showed that the separation of the NPs from the graphite surface is time and temperature dependent.

Unfortunately, the cytotoxicity of Pd₆₅Co₃₅ NPs was not evaluated in this study due to the adsorption of these NPs onto graphite support and the sonication technique must be optimized. Furthermore, filtration technique is required to separate the NPs in a size range of 10-50 nm from those in higher ranges. Once these limitations are overcome and 10-50 nm Pd₆₅Co₃₅ NPs are obtained, the cellular toxicity of these NPs can be investigated. Therefore, in vitro exposure of cultured cells to NPs (prior to in vivo translation) is necessary to understand the cell-NP interaction and thus improve the biocompatibility of the NPs.

In the biomedical field, palladium has primarily been used as a component of alloys for dental prostheses, and current evidence suggests that palladium alloys (such as Au–Cu–Ag–Pd) are safe [187]. In addition, the growth curves of FL cells (epithelial cell strain derived from human amnion tissue membrane [188]) for the PdCo alloy showed that the toxicity of the alloy is very weak [123]. However, the toxic effects of NPs are influenced by many parameters (such as size distribution, surface coating, magnetic properties, etc) so it is very important to evaluate the nanotoxicity of Pd₆₅Co₃₅ NPs and compare it with the toxicity of PdCo bulk material.

An important challenge in realizing magnetic hyperthermia using magnetic nanoparticles is controlling the temperature during treatment. A ferromagnetic material having a Curie temperature just above the target temperature range (42 - 45 °C) would stop dissipating heat at the target temperature [188]. This is believed to explain why so much attention has been devoted to the study of ferromagnetic elements, such as Fe, Ni and Co (with Curie points far above the therapeutic range) mixed with non-magnetic elements to lower the Curie point [169]. Various candidate materials have been suggested, such as Co mixed with Pd (50 % – 30 %) which exhibits a Curie temperature in a therapeutic range from about 42 °C to about 100 °C [169] and thus can be used to treat many types of cancer. For example, the therapeutic range can vary from 42 °C up to 65 °C in the treatment of prostate tumors, whereas the range may extend to 100 °C in ablating a portion of brain tissue.

However, 23% Co mixed with 77% Pt has a Curie temperature about 500 °C, and it has only slight loss of magnetism at 350 °C [189]. Moreover, PtCo has a coercitive force above 341.850 A/m, and a residual induction of 0.645T [189]. Thus, PtCo alloy is of current interest in magnetic storage devices and there is no current research on its usefulness for magnetic hyperthermia applications. In addition, the platinum is an expensive metal compared with palladium (Pt: 1269\$/Oz, Pd: 775\$/Oz) and the values of the saturation magnetization for PtCo alloys are lower than that of PdCo (M_s (Pt-3.5 % Co)= 5.17 emu/g, M_s (Pd-3.5 % Co)= 15.12 emu/g) [38]. For the reasons mentioned above, PdCo is chosen instead of PtCo for investigating its properties in order to use it in magnetic hyperthermia.

According to Bagguley et al. [38], the saturation magnetization of PdCo FCC alloys (5 mm diameter and 0.1 mm thickness disk) fluctuate between 24.66 emu/g and 40.58 emu/g with increasing cobalt content from 8.9 to 23.0 at. %. However, the saturation magnetization of untreated Pd- 12% Co NPs synthesized in this project is about 0.23 emu/g. This 100 times lower value of magnetization can be attributed to the following reasons:

- 1) Decreasing size of PdCo particles: the saturation magnetization decreases with the size of a ferromagnetic particle. This is due to the growth of the disordered spin layer at the surface of the particle when it size decreases [56].
- 2) Usefulness of heating treatment: Pd- 12% Co NPs sample was not treated with heat (as the PdCo tested by Bagguley et al.) and thus showed a heterogeneous composition during Curie

temperature measurements. The heating treatment is necessary to enhance the microstructure of the alloy in order to obtain a homogeneous single phase FCC solid solution. Generally, a heterogeneous composition exhibits a lower corrosion resistance than the sample which has homogeneous composition. Hence, the magnetization of the homogeneous composition is higher than that of heterogeneous composition.

- 3) Low deposited mass of 0.00235 g of Pd- 12% Co NPs was deposited onto graphite during the sequential electrodeposition. As the magnetic moment of a sample is proportional to the number of particles, the overall magnetization increases with the increasing number or mass of the deposited PdCo particles. Thus, the synthesis method of PdCo NPs must be optimized to enhance the deposited mass of particles.

CHAPTER 6 CONCLUSION AND RECOMMENDATIONS

6.1 Conclusion

In this project, a new synthesis method of PdCo NPs has been developed. This method involves a sequential electrodeposition onto Pd-modified graphite, followed by 1-dodecanethiol (DDT) coating. Pd-modified graphite showed that Pd seeds increase the electrocatalytic activity for the reduction of Pd(II) and Co(II) to PdCo alloy. On the other hand, coating PdCo nanoparticles with 1- dodecanethiol (DDT) for 19 hours, before subsequent electrodeposition, increases the concentration and the stability of the deposited PdCo nanoparticles.

The SEM images and the EDS results showed that when the applied potential decreases from -1.0 V to -1.3 V, the morphology of PdCo NPs changes from clusters to spherical and agglomeration-of-spheres, and the Co content increases to reach a maximum of 35.6 %. On the other hand, the presence of glycine in the bath solution enhances the crystalline structure of the deposited PdCo films, according to the x-ray diffraction (XRD) patterns

As a second step and this is the main goal of this study, the corrosion resistance of newly developed Pd₆₅Co₃₅ NPs was evaluated. Furthermore, the influence of heat treatment at 200 °C, 300 °C and 400 °C and surface passivation with 1-dodecanethiol (DDT) monomers on the corrosion resistance of PdCo NPs was investigated. Based on the results of this study, it can be concluded that PdCo NPs treated with heat at 400 °C displayed the lowest corrosion current density i_{corr} of 0.022114 $\mu\text{A}/\text{cm}^2$, while the sample treated with DDT monomers exhibited the highest corrosion density of i_{corr} of 0.87202 $\mu\text{A}/\text{cm}^2$. However, the heat and alkanethiol treatments significantly decrease the release of Pd and Co ions in the supernatant after the polarization assay in the order 200 °C > 400 °C > 300 °C > DDT > Untreated.

XPS analysis showed that the corrosion resistance of treated/untreated PdCo samples varies upon the chemical composition at the surface, which revealed to be treatment-dependent. In addition, the immersion test for both treated and untreated samples exhibited an excellent corrosion resistance in Ringer solution ([Pd(II)]<0.01 ppm; [Co(II)]<0.01 ppm).

This study concluded that Pd₆₅Co₃₅ NPs could be used as a medical micro-device if they are treated with heat, because this treatment showed to be very efficient in the enhancement of the PdCo NPs

stability upon corrosion in Ringer's solution, and thus prevent high Pd and Co ions release in biological environment and subsequent nanotoxicity.

The hysteresis loop and Curie point measurements were done over two samples of PdCo NPs. The results of the hysteresis loop measurements are very promising. They showed a ferromagnetic behavior, and good saturation magnetizations (152.78 memu/g and 233.54 memu/g) compared to the very low mass of NPs. Besides, Curie point measurements confirmed the usefulness of the heating treatment after electrodeposition to enhance the microstructure of the alloy.

The sonication test showed that it is possible to obtain a solution of dispersed PdCo NPs using a sonicator. Also, this test showed that the separation of the NPs from the graphite surface is time and temperature dependent.

As limitations are inevitable in a research, these nanoparticles cannot be used directly neither for biocompatibility tests nor for magnetic investigations because of their deposition onto 0.7 mm x 0.7 mm (0.3 mm thickness) graphite substrate and their ferromagnetism behaviour due to the presence of agglomerated particles. Furthermore, the concentration of PdCo NPs is very low resulting in difficulties for studying the crystalline structure using XRD analysis.

The toxicity of untreated/treated Pd₆₅Co₃₅ NPs must be evaluated in vitro to investigate the toxicity potential of these NPs for medical applications. Colorimetry assay (such as MTT assay) can be done in order to investigate the cell viability in the presence of untreated/treated Pd₆₅Co₃₅ NPs. In fact, viable cells with active metabolism convert MTT into a purple colored formazan product via reducing molecules (e.g. NADH). However, died cells lose the ability to convert MTT into formazan and thus the color formation serves as a useful marker of only the viable cells.

Also, flow cytometry can be used to assess ROS levels by using fluorescent probes such as dichlorodihydrofluorescein and its derivatives, or to distinguish cells in different phases of the cell cycle by treating cells with a fluorescent dye (e.g. propidium iodide) that stains DNA quantitatively, in order to study the genotoxic effect of NPs.

Since the toxicity of NPs is affected by the level of induced ROS generated by leached metallic ions and corrosion tests done over untreated/treated Pd₆₅Co₃₅ NPs showed a high corrosion resistance, low ROS levels and high cells viability are expected during toxicity tests over Pd₆₅Co₃₅

NPs. Therefore, it will be very interesting to study the biocompatibility of untreated/treated Pd₆₅Co₃₅ NPs and determine their ability to perform without having toxic effects on biological systems

6.2 Recommendations

After discussing the original contribution of this work to the advancement of the knowledge and the corresponding limitations, the following list of recommendations for future works are proposed:

- Development of new strategies to improve the deposited mass of PdCo NPs onto graphite substrate, essential for high magnetizations and heating efficiencies.

Magnetic tests showed that untreated PdCo NPs display low maximum magnetic moment ($m = 0.55$ memu) and consequently low saturation magnetization ($M_s = 233.54$ memu/g) as result of low deposited mass of particles (about 2.355 mg). Therefore, new strategies to improve the deposited mass of PdCo NPs must be developed to increase the saturation magnetization and therefore the heating efficiency and the reliability of the magnetization.

The deposited mass can be improved in several ways, such as:

- a) Increasing the surface area of the working electrode: the enhancement of the graphite electrode's surface aims to broaden the electrode-electrolytes interface and thus enhance the electron transfer required for the reduction of Pd and Co salts into metallic PdCo alloy.
 - b) Increasing the concentration of the electrolytes: in a concentrated Pd(II) and Co(II) solution, there are more precursor ions that can be reduced to Pd(0) and Co(0). Therefore, in higher concentrated electrolytes there are more deposited Pd and Co atoms and consequently higher deposited mass of PdCo NPs.
 - c) Heating the electrolytic bath: the increased temperature of the electrolytic bath will increase the diffusion of the Pd(II) and Co(II) ions towards the working electrode. So, heating the bath solution will lower the value of the mass transport overpotential and subsequently increase the deposited mass.
- Optimization of sonication and filtration techniques, in order to study the biocompatibility and superparamagnetism of PdCo NPs.

The PdCo NPs investigated in this project are deposited onto graphite substrate and exhibit a ferromagnetism behavior as result of agglomerated particles. Thus, these NPs cannot be used directly neither for biocompatibility tests nor for magnetic investigations. To solve this problem and obtain superparamagnetic behavior, NPs must be transferred to a solution and then the solution of dispersed NPs is filtered to eliminate the big and very small particles. We tested the feasibility of separating the NPs from the graphite using ultrasonic bath. According to ultrasonic bath tests, it is possible to obtain a solution of dispersed PdCo NPs using a sonicator. Also, these tests showed that the separation of PdCo NPs from the graphite surface is time and temperature dependent. Hence the need to optimize the techniques of sonication and filtration to produce superparamagnetic NPs, dispersed in culture medium, in order to perform biocompatibility tests and study their superparamagnetism behavior.

- Investigation on the effect of length and composition of alkanethiol monomers on the corrosion resistance of PdCo NPs.

The corrosion passivation of PdCo NPs using an electrically insulating layer of self-assembled alkanethiol monomers showed to enhance their corrosion resistance compared to untreated PdCo NPs. The effectiveness of these monomers in corrosion resistance is due to their ability to resist to electron transfer at the metal-solution surface, as result of their hydrophobic alkyl chain. Moreover, the length and the composition of these monomers also determine the behavior of the NPs towards corrosion. Thus, it is very important to study the effect of length and composition of self-assembled alkanethiol monomers on the corrosion behavior of PdCo NPs.

BIBLIOGRAPHY

- [1] R. Freynman, "There's Plenty of Room at the Bottom," vol. 23, no. 5, pp. 22-36, 1960.
- [2] L. A. Austin, M. A. Mackey, M. A. El-Sayed, E. C. Dreaden "Size matters: gold nanoparticles in targeted cancer drug delivery," *Therapeutic delivery*, vol. 3, no. 4, pp. 457-478, 2012.
- [3] M. C. Roco, J. Son, S. Jiang, C. Larson and Q. Gao. H. Chen, "Global nanotechnology development from 1991 to 2012: patents, scientific publications, and effect of NSF funding," *Journal of Nanoparticle Research*, 2013.
- [4] M. C. Roco, "The long view of nanotechnology development: the National Nanotechnology Initiative at 10 years," *Journal of Nanoparticle Research*, vol. 13, pp. 427-445, 2011.
- [5] B. Walker and C. P. Mouton, "Nanotechnology and Nanomedicine," *Journal of the National Medical Association*, vol. 98, no. 12, pp. 1985-1988, 2006.
- [6] J. H. Thrall, "Nanotechnology and medicine," *Radiology*, vol. 230, no. 2, pp. 315-318, 2004.
- [7] M. E. Gaguski, "Nanotechnology Treats Cancer at the Atomic Level," vol. 23, no. 7, p. 23, 2008.
- [8] E. S. Kawasaki and A. Player, "Nanotechnology, nanomedicine, and the development of new, effective therapies for cancer," *Nanomedicine: Nanotechnology, Biology, and Medicine*, vol. 1, no. 2, pp. 101-109, 2005.
- [9] J. W. Rhee, J. P. Richie, R. Langer and O. C. Farokhzad F. Alexis, "New frontiers in nanotechnology for cancer treatment," *Urologic Oncology*, vol. 26, no. 1, pp. 74-85, 2008.

- [10] S. Venkatraman, R. V. Ramanujan K. L. Ang, "Magnetic PNIPA hydrogels for hyperthermia applications in cancer therapy," *Materials Science and Engineering*, vol. 27, pp. 347-351, 2007.
- [11] A. Januszewski and J. Stebbing, "Hyperthermia in cancer: is it coming of age?," *Lancet Oncology*, vol. 15, no. 6, pp. 565-566, 2014.
- [12] P. Wust, O. Ahlers, A. Dieing, G. Sreenivasa, T. Kerner, R. Felix and H. Riess B. Hildebrandt, "The cellular and molecular basis of hyperthermia.," *Critical Reviews in Oncology/Hematology*, vol. 43, no. 1, pp. 33-56, 2002.
- [13] R. J. Griffin, R. P.M. Dings, A. Jamshidi-Parsian , "Mild temperature hyperthermia and radiation therapy: role of tumor vascular thermotolerance and relevant physiological factors," *International Journal of Hyperthermia*, vol. 3, no. 26, pp. 256–263, 2010.
- [14] C. W. Song, H. Park, R. J. Griffin , "Improvement of tumor oxygenation by mild hyperthermia," *Radiation Research*, vol. 4, no. 155, pp. 515-28, 2001.
- [15] S. J. Kim, C. K. Lee, Y. M. Lee and S. I. Kim , "Thermal characterizations of semi-interpenetrating polymer networks composed of poly(ethylene oxide) and poly(N-isopropylacrylamide)," *Journal of Applied Polymer Science*, vol. 90, p. 3032, 2003.
- [16] G. Loo, X. Sealens, M. Gurp, M. MacFarlane, "The role of mitochondrial factors in apoptosis: a Russian roulette with more than one bullet," *Cell Death and Differentiation*, vol. 10, no. 9, pp. 1031-1042, 2002.
- [17] C. W. Song , "Effect of local hyperthermia on blood flow and microenvironment: a review," *Cancer Research*, vol. 44, pp. 4721s-4730s, 1984.

- [18] O. Ahlers, B. Hildebrandt, T. Kerner, I. Tamm, K. Possinger and P. Wust A. Dieing, "The effect of induced hyperthermia on the immune system," *Progress in Brain Research*, vol. 162, pp. 137-152, 2007.
- [19] R.N. Shen, N. B. Hornback, H. Shidnia, R. E. Shupe, "Whole-body hyperthermia decreases lung metastases in lung tumor-bearing mice, possibly via a mechanism involving natural killer cells," *Journal of Clinical Immunology*, vol. 7, no. 3, pp. 246-253, 1987.
- [20] R. B. Herberman, *Natural killer (NK) cells and their possible roles in resistance against disease*, vol. 1, no. 1, pp. 1-65, 1981.
- [21] A. Singh and B. Wesley V. V. Mody, "Basics of magnetic nanoparticles for their application in the field of magnetic fluid hyperthermia," *European Journal of Nanomedicine*, vol. 5, no. 1, pp. 11-21, 2013.
- [22] M. Bettge, Y. Haik and C. J. Chen. J. Chatterjee, "Synthesis and characterization of polymer encapsulated Cu-Ni magnetic nanoparticles for hyperthermia applications," *Journal of Magnetism and Magnetic Materials*, vol. 293, no. 1, pp. 303-309, 2005.
- [23] N. A. Brusentsov, V. D. Kuznetsova and V.N. Nikiforov T. N. Brusentsova, "Synthesis and investigation of magnetic properties of Gd- substituted Mn-Zn ferrite nanoparticles as a potential low-TC agent for magnetic fluid hyperthermia," *Journal of Magnetism and Magnetic Materials*, vol. 293, pp. 298-302, 2005.
- [24] D. E. Nikles and C. S. Brazel D. H. Kim, "Heat generation of aqueously dispersed CoFe₂O₄ nanoparticles as heating agents formagnetically-activated drug delivery and hyperthermia," *Journal of Magnetism and Magnetic Materials*, vol. 320, pp. 2390-2396, 2008.
- [25] K. S. Suslick, G. D. Stucky and Y. H. Suh W. H. Suh, "Nanotechnology, nanotoxicology, and neuroscience," *Progress in Neurobiology*, vol. 87, no. 3, pp. 133-170, 2009.

- [26] S. Dutz, R. Müller, R. Hergt, N. Matoussevitch and H. Bönemann M. Zeisberger, "Metallic cobalt nanoparticles for heating applications," *Journal of Magnetism and Magnetic Materials*, vol. 311, pp. 224-227, 2007.
- [27] S. Hashimoto, T. Kayano, M. Minagawa, H. Yanagihara, et al. E. Kita, "Heating characteristics of ferromagnetic iron oxide nanoparticles for magnetic hyperthermia," *Journal of Applied Physics*, vol. 107, no. 09, p. 321, 2010.
- [28] R. E. Rosensweig, "Heating magnetic fluid with alternating magnetic field," *Journal of Magnetism and Magnetic Materials*, vol. 252, p. 370, 2002.
- [29] S. Barua, G. Sharma, S. K. Dey and K. Rege H. C. Huang, "Inorganic nanoparticles for cancer imaging and therapy," *Journal of Controlled Release*, vol. 155, pp. 344-357, 2011.
- [30] O. Savadogo, S. Martel, V. Segura and J. C. Leroux P. Pouponneau, "Annealing of magnetic nanoparticles for their encapsulation into microcarriers guided by vascular magnetic resonance navigation," *Journal of Nanoparticle Research*, vol. 14, p. 1307, 2012.
- [31] A. H. Lu, E. L. Salabas, F. Schüth, "Magnetic Nanoparticles: Synthesis, Protection, Functionalization, and Application," *Angewandte Chemie International Edition*, vol. 46, no. 8, pp. 1222-1244, 2007.
- [32] D. Horák, K. Piksová, T. Q. Trung and Skereň, T. A. Fojtik, "Magnetic and Metallic Nanoparticles for Biomedical Application," in *Nanoconference*, Roznov pod Radhostem, 2009.
- [33] D. F. Williams, "On the mechanisms of biocompatibility," *Biomaterials*, vol. 29, no. 20, pp. 2941-2953, 2008.

- [34] H. Iida, S. Tominaka and T. Hachisu T. Osaka, "New Trends in Nanoparticles: Syntheses and Their Applications to Fuel Cells, Health Care, and Magnetic Storage," *Israel Journal of Chemistry*, vol. 48, pp. 333-347, 2008.
- [35] N. Barelli, R. F. C. Marques, P. T. A. Sumodjo and A. V. Benedetti R. D. Noce, "The influence of residual stress and crystallite size on the magnetic properties of electrodeposited nanocrystalline Pd–Co alloys," *Surface and Coatings Technology*, vol. 202, no. 1, pp. 107-113, 2007.
- [36] G. F. Breck, H. K. Straschil and I. Bogustavsky J. A. Abys, "The electrodeposition and material properties of palladium-cobalt," *Plating and Surface Finishing*, vol. 86, no. 1, pp. 108-115, 1999.
- [37] J. Carrey, S. Lachaize, B. Chaudret and M. Respaud L. M. Lacroix, in *International conference on magnetism*, Karlsruhe, 2009, pp. 26-31.
- [38] D. M. S. Bagguley, W. A. Crossley, J. Liesegang, "PRINTED IN GREAT BRITAIN Ferromagnetic resonance in a series of alloys 11. Binary alloys of cobalt with platinum and palladium, and one iron-palladium alloy," *Proceedings of the Physical Society*, vol. 90, pp. 1047-1058, 1967.
- [39] V Melini, D. Contreras, Y. Moreno, H. D. Mansilla P. Salgado, "Fenton reaction driven by iron ligands," *Journal of the Chilean Chemical Society* , vol. 58, no. 4, pp. 0717-9707, 2013.
- [40] H. C. Hsieh, C. M. Chen, W. Y. Hsieh, C. Y. Chen, "ROS-induced toxicity: exposure of 3T3, RAW264.7, and MCF7 cells to superparamagnetic iron oxide nanoparticles results in cell death by mitochondria dependent apoptosis," *Journal of Nanoparticle Research*, vol. 17, p. 71, 2015.
- [41] F. Marano, S. Hussain, F. Rodrigues-Lima, A. Baeza, "Nanoparticles: molecular targets and cell signalling," *Archives of Toxicology*, vol. 85, pp. 733–741, 2011.

- [42] T. T. D. Tran, T. V. Vo and B. J. Lee P. H. L. Tran, "Promising Iron Oxide-based Magnetic Nanoparticles in Biomedical Engineering," *Archives of Pharmacal Research*, vol. 12, no. 35, pp. 2045-2061, 2012.
- [43] X. Saelens, M. V. Gurp, M. MacFarlane, S. J. Martin and P. Vandenabeele G. V. Loo, "The role of mitochondrial factors in apoptosis: a Russian roulette with more than one bullet," *Cell Death and Differentiation*, no. 9, pp. 1031-1042, 2002.
- [44] D. R. Green, "Apoptotic pathways: The roads to ruin," *Cell*, vol. 94, pp. 695–698, 1998.
- [45] G. H. Wong, D. V. Goeddel, "Fas antigen and 55-kD TNF receptor signal apoptosis through distinct pathways," *The Journal of Immunology*, vol. 152, pp. 1751–1755, 1994.
- [46] Y. Deng, Y. Lin, X. Wu, "TRAIL-induced apoptosis requires Bax-dependent mitochondrial release of Smac/DIABLO," *Genes & Development*, vol. 16, pp. 33-45, 2002.
- [47] M. Insausti, I. Gil de Muro, T. Rojo, D. Carolina Arias-Duque, J. C. Hernandez-Garrido, L. Lezama I. Castellanos-Rubio, "The impact of the chemical synthesis on the magnetic properties of intermetallic PdFe nanoparticles," *Journal of nanoparticle research*, no. 17, p. 229, 2015.
- [48] S. Dutz, U. O. Häfeli, M. Mahmoudi S. Laurent, "Magnetic fluid hyperthermia: Focus on superparamagnetic iron oxide nanoparticles," *Advances in Colloid and Interface Science*, no. 166, pp. 8-23, 2011.
- [49] A. Singh and B. Wesley V. V. Mody, "Basics of magnetic nanoparticles for their application in the field of magnetic fluid hyperthermia," *VEuropean Journal of Nanomedicine*, vol. 1, no. 5, pp. 11-21, 2013.
- [50] N. A. Spaldin, *Magnetic Materials: Fundamentals and Applications*, 2nd ed. New York: Cambridge University Press, 2011.

- [51] R. Skomski, "Nanomagnetics," *Journal of physics: condensed matter*, no. 15, pp. R841–R896, 2003.
- [52] E. P. Wohlfarth and E. C. Stoner, "A Mechanism of Magnetic Hysteresis in Heterogenous Alloys," *Philosophical Transactions of the Royal Society*, pp. 599-642, 1948.
- [53] K. M. Krishnan, "Biomedical nanomagnetics: a spin through possibilities in imaging, diagnostics, and therapy," *IEEE Transaction Magnetism*, vol. 7, no. 46, pp. 2523-2558, 2010.
- [54] S. Martel, "Magnetic nanoparticles in medical nanorobotics," *Journal of Nanoparticle Research*, no. 7, p. 75, 2015.
- [55] A. C. Jamison, D. Litvinov, R. C. Willson, T. Randall Lee A. G. Kolhatkar, "Tuning the Magnetic Properties of Nanoparticles," *International Journal of Molecular Sciences*, vol. 8, no. 14, pp. 15997-16009, 2013.
- [56] J. W. Seo, J. Cheon Y. W. Jun, "Nanoscaling laws of magnetic nanoparticles and their applicabilities in biomedical sciences," *Accounts of Chemical Research*, no. 41, pp. 179-189, 2008.
- [57] A. M. Pereira, C. Fernandes, M. Rocha, R. Mendes, M. Fernandez-Garcia, A. Guedes, P. B. Tavares, J. M. Greneche, J. P. Araujo, C. Freire C. Pereira, "Superparamagnetic MFe₂O₄ (M = Fe, Co, Mn) nanoparticles: Tuning the particles size and magnetic properties through a novel one-step coprecipitation route," *Chemistry of Materials*, no. 24, pp. 1496-1504, 2012.
- [58] H. Shi X. He, "Size and shape effects on magnetic nanoparticles," *Particuology*, vol. 10, pp. 497-502, 2012.

- [59] B. Batlle-Brugal, A. Roca, O. Iglesias, M. Morales, C. J. Serna, A. Labarta and X. Batlle P. Guardia, "Surfactant effects in monodisperse magnetite nanoparticles of controlled size," *Journal of Magnetism and Magnetic Materials*, no. 316, pp. 756-758, 2007.
- [60] R. E. Rosensweig, "Heating magnetic fluid with alternating magnetic field," *Journal of Magnetism and Magnetic Materials*, no. 252, pp. 370-374, 2002.
- [61] G. Richardson A. D. Grief, "Mathematical modelling of magnetically targeted drug delivery," *Journal of Magnetism and Magnetic Materials*, no. 293, pp. 455-463, 2005.
- [62] V. I. Stepanov M. I. Shliomis, "Magnetization relaxation in ferrofluid," *IEEE Conference Publications*, 1990.
- [63] S. W. Charles P. C. Fannin, "Measurement of the Neel relaxation of magnetic particles in the frequency range 1 kHz to 160MHz," *Journal of Physics D : Applied physics*, vol. 1, no. 24, pp. 76-77, 1991.
- [64] B. K. P. Skaife, S. W. Charles P. C. Fannin, "Relaxation and resonance in ferrofluids," *Journal of Magnetism and Magnetic Materials*, no. 122, pp. 159-163, 1993.
- [65] M. R. Ferguson, J. A. Simon, K. M. Krishnan A. P. Khandhar, "Tailored magnetic nanoparticles for optimizing magnetic fluid hyperthermia," *Journal of Biomedical Materials Research A* , pp. 728-737, 2011.
- [66] T. Tran, T. Vo, B. J. Lee P. Tran, "Promising Iron Oxide-based Magnetic Nanoparticles in Biomedical Engineering," *Archives of Pharmacal Research*, vol. 12, no. 35, pp. 2045-2061, 2012.
- [67] C. H. Sua, Y. S. Yanga, C. S. Yeha, C. Y. Tsaib, C. L. Wub, M. T. Wuc, D. B. Shieh F. Y. Chenga, "Characterization of aqueous dispersions of Fe₃O₄ nanoparticles and their biomedical applications," *Biomaterials*, no. 26, pp. 729-738, 2005.

- [68] M. Geppert, R. Dringen M. C. Hohnholt, "Treatment with iron oxide nanoparticles induces ferritin synthesis but not oxidative stress in oligodendroglial cells," *Acta Biomaterialia*, vol. 11, no. 7, pp. 3946-3954, 2011.
- [69] Z. Wu, T. Yu, C. Jiang, W. S. Kim W. Wu, "Recent progress on magnetic iron oxide nanoparticles: synthesis, surface functional strategies and biomedical applications," *Science and technology of advanced materials*, no. 16, p. 023501, 2015.
- [70] S. Sun, J. Li, Z. L. Wang, J. P. Liu H. Zenga, "Tailoring magnetic properties of core/shell nanoparticles," *Applied Physics Letters*, vol. 85, no. 5, pp. 792-794, 2004.
- [71] J. Antony, A. Sharma, J. Nutting, D. Sikes, D. Meyer. D. Y. Qiang, "Iron/iron oxide core-shell nanoclusters for biomedical applications," *Journal of nanoparticle research* , no. 8, pp. 489-496, 2006.
- [72] B. Singhana, W. W. Bryan, S. Sarangi, A. C. Jamison, A. Brazdeikis, T. R. Lee S. Rittikulsittichai, "Preparation, characterization, and utilization of multifunctional magnetic-fluorescent composites for bio-imaging and magnetic hyperthermia therapy," *RSC Advances*, no. 3, pp. 7838-7849, 2013.
- [73] C. Gomez-Polo, J. Perez-Landazabal, J. M. J. Pastor S. Larumbe, "Effect of SiO₂ coating on the magnetic properties of Fe₃O₄ nanoparticles," *Journal of Physics Condensed Materials* , no. 24, pp. 1-6, 2012.
- [74] M. Korkmaz, T. Fırat, G. H. Jaffari and S. I. Shah M. Coşkun, "Synthesis of SiO₂ coated NiFe₂O₄ nanoparticles and the effect of SiO₂ shell thickness on the magnetic properties," *Journal of applied physics*, vol. 9, no. 107, p. 09B523, 2010.
- [75] A. E. Berkowitz, E. J. McNiff, S. Foner R. H. Kodama, "Surface Spin Disorder in NiFe₂O₄ Nanoparticle," *Physical review letters*, vol. 2, no. 77, pp. 394-397, 1996.

- [76] J. Hong, J. P. Ahn K. Woo, "Synthesis and surface modification of hydrophobic magnetite to processible magnetite@silica-propylamine," *Journal of Magnetism and Magnetic Materials* , no. 293, pp. 177-181, 2005.
- [77] R.L. Camilo, L.C. Sampaio, M.A. Macedo, M. Nakamura, H.E. Toma M. Yamaura, "Preparation and characterization of (3-aminopropyl)triethoxysilane-coated magnetite nanoparticles," *Journal of Magnetism and Magnetic Materials* , no. 279, pp. 210-217, 2004.
- [78] F. Bartolome, F. Petroff, J. Bartolome, L. M. Garcia, C. Deranlot, H. Jaffres, M. J. Martinez, P. Bencok, F. Wilhelm, A. Rogalev, N. B. Brookes F. Luis, "Tuning the magnetic anisotropy of Co nanoparticles by metal capping," *Europhysics letters* , vol. 1, no. 76, pp. 142-148, 2006.
- [79] J. T. Jang, J. S. Choi, S. H. Moon, S. H. Noh, J. W. Kim, J. G. Kim, I. S. Kim, K. I. Park, J. Cheon J. H. Lee, "Exchange-coupled magnetic nanoparticles for efficient heat induction," *Nature Nanotechnology* , no. 6, pp. 418-422, 2011.
- [80] W. Na, J. T. Jang, J. H. Lee, E. J. Lee, S. H. Moon, Y. Lim, J. S. Shin, J. Cheon S. H. Noh, "Nanoscale magnetism control via surface and exchange anisotropy for optimized ferromagnetic hysteresis," *Nano Letter* , no. 12, pp. 3716-3721, 2012.
- [81] C. L. Zhu, S. Neeleshwar, C. L. Chen, Y. Y. Chen, C. C. Chen S. W. Chou, "Controlled Growth and Magnetic Property of FePt Nanostructure: Cuboctahedron, Octapod, Truncated Cube, and Cube," *Chemistry of materials* , no. 21, pp. 4955-4961, 2009.
- [82] D. V. Talapin, H. Schnablegger, A. Kornowski, O. Festin, P. Svedlindh, M. Haase, H. Weller E. V. Shevchenko, "Study of Nucleation and Growth in the Organometallic Synthesis of Magnetic Alloy Nanocrystals: The Role of Nucleation Rate in Size Control of CoPt₃ Nanocrystals," *Journal of the American Chemical Society*, vol. 30, no. 125, pp. 9090-9101, 2003.

- [83] B. W. Muir, B. A. Moffat, P. Harbour, K. S. Murray, B. Moubaraki, K. Suzuki, I. Madsen, N. Agron-Olshina, L. Waddington, L. G. Zhen and et al., "Comparative study of magnetic behavior of spherical and cubic superparamagnetic iron oxide nanoparticles," *Journal Physical Chemistry C* , no. 115, pp. 327-334, 2011.
- [84] L. Hu, I. Milosevic, V. Russier, D. Bonnin, L. Motte, A. Brioude, Y. Lalatonne C. Montferrand, "Iron oxide nanoparticles with sizes, shapes and compositions resulting in different magnetization signatures as potential labels for multiparametric detection," *Acta Biomaterials* , no. 9, pp. 6150-6157, 2013.
- [85] Y. M. Huh, Y. W. Jun, J. W. Seo, J. T. Jang, H. T. Song, S. Kim, E. J. Cho, H. G. Yoon, J. S. Suh and J. Cheon J. H. Lee, "Artificially engineered magnetic nanoparticles for ultra-sensitive molecular imaging," *Nature Medicine*, no. 13, pp. 95-99, 2006.
- [86] G. Campo, D. Carta, A. Corrias, C. Fernandez, D. Gatteschi, C. Innocenti, F. Pineider, F. Ruggi, C. Sangregorio E. Fantechi, "Exploring the effect of Co doping in fine maghemite nanoparticles," *Journal of Physical Chemistry C* , no. 116, pp. 8261-8270, 2012.
- [87] C. Gómez-Polo, J. I. Pérez-Landazábal, A. García-Prieto, J. Alonso, M. L. Fdez-Gubieda, D. Cordero, J. Gómez S. Larumbe, "Ni doped Fe₃O₄ magnetic nanoparticles," *Journal of nanoscience and nanotechnology*, no. 12, pp. 1-9, 2012.
- [88] M.H. Enayatia, P. Kamelib, F. Karimzadeh M. Jalalya, "Effect of composition on structural and magnetic properties of nanocrystalline ball milled Ni(1-x)Zn(x)Fe₂O₄ ferrite," *Physica B: Condensed Matter* 4, vol. 2, no. 405, pp. 507-512, 2010.
- [89] C. Barcena, N. Poudyal, C. Rong, J. Gao, S. Sun, J. P. Liu G. S. Chaubey, "Synthesis and Stabilization of FeCo Nanoparticles," *Journal of American Chemical Society*, no. 129, pp. 7214-7215, 2007.

- [90] O. Amponsah, M. Arslan, T. Holloway, W. Cao, A. K. Pradhan K. Zhang, "Co-ferrite spinel and FeCo alloy core shell nanocomposites and mesoporous systems for multifunctional applications," *Journal of applied physics* , no. 111, p. 07B525, 2012.
- [91] W. R. Scott J. Crangle, "Dilute Ferromagnetic Alloys," *Journal of applied physics* , no. 36, p. 921, 1965.
- [92] P. J. W. Weijs, J. C. Fuggle, K. Horn, H. Haak, K. H. J. Buschow J. F. van Acker, "Photoemission investigation of the electronic structure of Fe-Pd and Fe-Pt alloys," *Physical Review B*, vol. 11, no. 43, p. 8903, 1991.
- [93] R. D. Tucker J. A. Paulus, "Cobalt palladium seeds for thermal treatment of tumors," 5,429,583, 1995.
- [94] D. Boehmer, I. Türk, J. Roigas, V. Budach, S. A. Loening S. Deger, "Interstitial Hyperthermia using Self-Regulating Thermoseeds Combined with Conformal Radiation Therapy," *European Urology* , vol. 2, no. 42, pp. 147-153, 2002.
- [95] R. F. Meredith I. A. Brezovich, "Practical aspects of ferromagnetic thermoseed hyperthermia," *Radiologic Clinics of North America*, vol. 27, no. 3, pp. 589-602, 1989.
- [96] M. Mekawy, A. A. El-Gendy, N.I. El-Sayed, A. A. Aly A. H. El-Sayed, "Magnetization Measurements of PdNi, PdCo and CuNi Ferromagnetic Thermoseeds," *International Journal of Pure and Applied Physics* , vol. 3, no. 2, pp. 155-162, 2007.
- [97] R. G. Craig, C. T. Hanks J. C. Wataha, "The release of elements of dental casting alloys into cell-culture medium," *Journal of Dental Research* , vol. 70, pp. 1014-1018, 1991.
- [98] L. B. Wilson, P. Ashari, E. K. Jordan, B. K. Lewis, J. A. Frank A. S. Arbab, "A model of lysosomal metabolism of dextran coated superparamagnetic iron oxide (SPIO)

- nanoparticles: implications for cellular magnetic resonance imaging," *NMR in Biomedicine*, vol. 18, no. 6, pp. 383-389, 2005.
- [99] I. Lynch, M. Foy, T. Berggård, S. C. Donnelly, G. Cagney, S. Linse, K. A. Dawson T. Cedervall, "Detailed Identification of Plasma Proteins Adsorbed on Copolymer Nanoparticles," *Angewandte Chemie International Edition*, vol. 46, pp. 5754-5756, 2007.
- [100] J. Buijs V. Hlady, "Protein adsorption on solid surfaces," *Current Opinion in Biotechnology*, vol. 7, no. 1, pp. 72-77, 1996.
- [101] D. R. McKenzie, N. J. Nosworthy, J. A. Denman, O. U. Sezerman, M. M. M. Bilek S. L. Hirsh, "The Vroman effect: Competitive protein exchange with dynamic multilayer protein aggregates," *Colloids and Surfaces B: Biointerfaces*, vol. 103, pp. 395-404, 2013.
- [102] A. E. Friedman, J. N. Finkelstein, G. Oberdörster, J. L. McGrath M. S. Ehrenberg, "The influence of protein adsorption on nanoparticle association with cultured endothelial cells," *Biomaterials*, vol. 30, no. 4, pp. 603-610, 2009.
- [103] M. Braide, C. Karlsson H. Nygren, "Protein–platelet and platelet–leukocyte interaction at materials in contact with human blood.," *Journal of Vacuum Science & Technology A*, vol. 13, p. 2613, 1995.
- [104] H. Nygren J. H. Elam, "Adsorption of coagulation proteins from whole blood on to polymer materials: relation to platelet activation," *Biomaterials*, vol. 13, no. 1, pp. 3-8, 1992.
- [105] S. Rammelt, D. Scharnweber, J. C. Simon S. Franz, "Immune responses to implants - A review of the implications for the design of immunomodulatory biomaterials," *Biomaterials*, vol. 32, pp. 6692-6709, 2011.
- [106] L. Öhman, H. Elwing, J. Wetterö, T. Bengtsson G. Nimeri, "The influence of plasma proteins and platelets on oxygen radical production and F-actin distribution in neutrophils adhering to polymer surfaces. ," *Biomaterials*, vol. 23, no. 8, pp. 1785-1795, 2002.

- [107] H. Marcal, S. M. Mahler, J. P. Santerre, R. S. Labow D. L. Dinnes, "Material surfaces affect the protein expression patterns of human macrophages: a proteomics approach," *Journal Biomedical Materials Research A* , vol. 80, pp. 895-908, 2007.
- [108] M. Papisov V. P. Torchilin, "Why do Polyethylene Glycol-Coated Liposomes Circulate So Long?: Molecular Mechanism of Liposome Steric Protection with Polyethylene Glycol: Role of Polymer Chain Flexibility," *Journal of Liposome Research* , vol. 4, no. 1, pp. 725-739, 1994.
- [109] D. Lee W. J. Kao, "In vivo modulation of host response and macrophage behavior by polymer networks grafted with fibronectin-derived biomimetic oligopeptides: the role of RGD and PHSRN domains," *Biomaterials* , vol. 22, pp. 2901-2909, 2001.
- [110] T. Kino, J. Galon, G. U. Meduri, G. Chrousos D. Franchimont, "Glucocorticoids and inflammation revisited: the state of the art. NIH clinical staff conference," *Neuroimmunomodulation* , vol. 10, pp. 247-260, 2002.
- [111] O. Stojadinovic, M. S. Golinko, H. Brem, M. Tomic-Canic S. Barrientos, "Growth factors and cytokines in wound healing," *Wound Repair and Regeneration* , vol. 16, pp. 585-601, 2008.
- [112] J. F. Gibson, T. J. Peters M. P. Weir, "Haemosiderin and tissue damage," *Cell Biochemistry and Function* , vol. 2, no. 4, pp. 186-194, 1984.
- [113] Z. Claus, G. Cindy, J. Manuela, M. Franziska, J. Tobias, P. Herbert, G. Tilman S. Albrecht, "Iron oxide particles for molecular magnetic resonance imaging cause transient oxidative stress in rat macrophages," *Free Radical Biology and Medicine* , vol. 36, no. 8, pp. 976-984, 2004.

- [114] E. Perez, R. Liu, L. J. Yan, R. T. Mallet, S. H. Yang X. Wang, "Pyruvate protects mitochondria from oxidative stress in human neuroblastoma SK-N-SH cells," *Brain Research* , vol. 1132, no. 1, pp. 1-9, 2007.
- [115] E. McCafferty, *Thermodynamics of Corrosion: Pourbaix Diagrams. Introduction to Corrosion Science*. New York, USA: Springer, 2010.
- [116] M. G. Garnica-Romo, J. F. Pérez-Robles, J. A. Cortes M. Villicaña, "A new process to obtain palladium as metal powders from salts: thermodynamic and kinetic study," *Latin American applied research* , vol. 37, no. 2, pp. 0327-0793, 2007.
- [117] J. Holman G. Hill, *Chemistry in Context*, 5th ed. Cheltenham, USA: Nelson Thornes, 2000.
- [118] J. D. Blackwe, V. I. Shubayev, R. R. Fiñones, S. Jin T. R. Pisanic, "Nanotoxicity of iron oxide nanoparticle internalization in growing neurons," *Biomaterials* , vol. 28, no. 16, pp. 2572-2581, 2007.
- [119] S. Fruhauf, W. Linss, R. Hiergeist, W. Andra, R. Hergt, et al. I. Hilger, "Cytotoxicity of selected magnetic fluids on human adenocarcinoma cells," *Journal of Magnetism and Magnetic Materials*, vol. 261, pp. 7-12, 2003.
- [120] W. A. Pryor, *The role of free radical reactions in biological systems, in Free Radicals in Biology*. San Diego, USA: Academic Press, 1976.
- [121] D. Bagchi S. J. Stohs, "Oxidative mechanisms in the toxicity of metal ions," *Free Radical Biology and Medicine* , vol. 18, no. 2, pp. 321-336, 1995.
- [122] C. V. Smith. M. T. Moslen, *Free Radical Mechanisms of Tissue Injury*. Florida, USA: CRC Press, 1992.

- [123] M. Shiota, H. Tsutsui, Y. Yoshida, H. Sasaki, Y. Kinouchi Y. Kawata, "Cytotoxicity of PdCo Dental Casting Ferromagnetic Alloys," *Journal of dental research* , vol. 60, no. 8, pp. 1403-1409, 1981.
- [124] M. Marek V. Goehlich, "Corrosion behavior of Pd-Cu and PdCo alloys in synthetic saliva," *Dental Materials* , vol. 6, no. 2, pp. 103-110, 1990.
- [125] C. T. Hanks J. C. Wataha, "Biological effects of palladium and risk of using palladium in dental casting alloys," *Journal of Oral Rehabilitation* , vol. 23, no. 5, pp. 309-20, 1996.
- [126] D. Beyersmann J. D. Donaldsaon, *Cobalt and Cobalt Compounds*. Wheinheim: Wiley VCH, 2005.
- [127] C. Melber, D. Keller, I. Mangelsdorf J. Kielhorn, "Palladium- A review of exposure and effects to human health," *International Journal of Hygiene and Environmental Health* , vol. 205, pp. 417-432, 2002.
- [128] B. A. Fowler, M. Nordberg G. F. Nordberg, *Handbook on the Toxicology of Metals*, 4th ed. San Diego, USA, 2014.
- [129] G.R. Parida, R.D. Tucker, J.B. Park J. A. Paulus, "Corrosion analysis of NiCu and PdCo thermal seed alloys used as interstitial hyperthermia implants.," *Biomaterials*, vol. 18, pp. 1690-1614, 1997.
- [130] C. Wagner H. W. Pickering, "Electrolytic Dissolution of Binary Alloys Containing a Noble Metal," *Electrochemical Society* , vol. 114, pp. 698-706, 1967.
- [131] P. Chartrand, S. A. Degterov, G. Eriksson, K. Hack, R. Ben Mahfoud, J. Melançon, A. D. Pelton and S. Petersen C. W. Bale, "FactSage thermochemical software and databases," *Calphad- Computer Coupling of Phase Diagrams and Thermochemistry*, vol. 26, no. 2, pp. 189-228, 2002.

- [132] M. Auffan, L. Decome, J. Rose, T. Orsiere, "In vitro interactions between DMSA-coated maghemite nanoparticles and human fibroblasts: A physicochemical and cyto-genotoxic study," *Environmental Science & Technology*, vol. 40, no. 14, pp. 4367-73, 2006.
- [133] S. Barua, K. Rege , "Cancer-cell-phenotype-dependent differential intracellular trafficking of unconjugated quantum dots," *Small*, vol. 5, no. 3, pp. 370-6, 2009.
- [134] X. Zhu, S. Tian S, Z. Cai , "Toxicity assessment of iron oxide nanoparticles in zebrafish (*Danio rerio*) early life stages," *PLoS One*, vol. 7, no. 9, p. e46286, 2012.
- [135] R. Schäfer, R. Kehlbach, J. Wiskirchen, R. Bantleon, "Transferrin receptor upregulation: in vitro labeling of rat mesenchymal stem cells with superparamagnetic iron oxide," *Radiology*, vol. 244, no. 2, pp. 514-23, 2007.
- [136] D. Huang, J. Hsiao, Y. Chen, L. Chien, M. Yao, "The promotion of human mesenchymal stem cell proliferation by superparamagnetic iron oxide nanoparticles," *Biomaterials*, vol. 30, no. 22, pp. 3645-51, 2009.
- [137] T. R. Pisanic, J.D Blackwell, V. I. Shubayev, "Nanotoxicity of iron oxide nanoparticle internalization in growing neurons," *Biomaterials*, vol. 28, no. 16, pp. 2572-81, 2007.
- [138] P. Koedrith, R. Boonprasert, J. Y. Kwon, I. Kim, "Recent toxicological investigations of metal or metal oxide nanoparticles in mammalian models in vitro and in vivo: DNA damaging potential, and relevant physicochemical characteristics," *Journal of Biochemical and Molecular Toxicology*, vol. 10, pp. 107-126, 2014.
- [139] S. Toyokuni , "Iron-induced carcinogenesis: the role of redox regulation," *Free Radical Biology and Medicine*, vol. 20, no. 4, pp. 553-66, 1996.

- [140] K. Buyukhatipoglu, A. M. Clyne, "Superparamagnetic iron oxide nanoparticles change endothelial cell morphology and mechanics via reactive oxygen species formation," *Journal of Biomedical Materials Research Part A*, vol. 96, no. 1, pp. 186-95, 2011.
- [141] M. P. Weir, J. F. Gibson, T. J. Peters, "Haemosiderin and tissue damage," *Cell Biochemistry and Function*, pp. 186-194, 1984.
- [142] Z. Claus, G. Cindy, J. Manuela, M. Franziska, J. Tobias, P. Herbert and G. Tilman S. Albrecht, "Iron oxide particles for molecular magnetic resonance imaging cause transient oxidative stress in rat macrophages," *Free Radical Biology and Medicine*, vol. 36, no. 8, pp. 976-984, 2004, P. Herbert, G. Tilman. I.. 976–984.
- [143] E. Perez, R. Liu, L. J. Yan, R. T. Mallet and S. H. Yang, X. Wang, "Pyruvate protects mitochondria from oxidative stress in human neuroblastoma SK-N-SH cells," *Brain Research*, vol. 1132, no. 1, pp. 1-9, 2007.
- [144] V. Geohlich and M. Marek, "Corrosion behavior of Pd-Cu and Pd-Co alloys in synthetic saliva.," *Journal of dental materials*, vol. 6, pp. 103-110, 1990.
- [145] D. Boehmer, I. Turk, J. Roigas, V. Budach and S. A. Loening S. Deger, "Interstitial Hyperthermia using Self-Regulating Thermoseeds Combined with Conformal Radiation Therapy.," *European Urology*, vol. 42, no. 2, pp. 147-153, 2002.
- [146] I. M. Dharmadasaz and J. Haigh, "Strengths and Advantages of Electrodeposition as a Semiconductor Growth Technique for Applications in Macroelectronic Devices," *Journal of Electrochemical Society*, vol. 153, no. 1, pp. G46-G52, 2006.
- [147] J. Colomer-Farrarons and P. L. Miribel J. P. Villagrasa, "Bioelectronics for Amperometric Biosensors," in *State of the Art in Biosensors - General Aspects.*: InTech, 2013.

- [148] C. N. Eliasa, Y. Oshidab, J. H. C. Limad, "Relationship between surface properties (roughness, wettability and morphology) of titanium and dental implant removal torque," *Journal of the mechanical behavior of biomedical materials*, pp. 234–242, 2008.
- [149] A. Singh, and B. Wesley V. V. Mody, "Basics of magnetic nanoparticles for their application in the field of magnetic fluid hyperthermia," *European Journal of Nanomedicine*, vol. 5, no. 1, pp. 11-21, 2013.
- [150] S. Hamdan and A. Elengoe , "Heat sensitivity between human normal liver (WRL-68) and breast cancer (MCF-7) cell lines," *Journal of Biotechnology Letters*, vol. 4, no. 1, pp. 45-50, 2013.
- [151] D. L. Huber, "Synthesis, properties, and applications of iron nanoparticles," *Small*, vol. 1, no. 5, pp. 482-501, 2005.
- [152] C. C. Berry and A. S. G. Curtis, "Functionalisation of magnetic nanoparticles for applications in biomedicine," *Journal of Physics D: Applied Physics*, vol. 36, no. 13, pp. 198-206, 2003.
- [153] T. T. Tran, T. V. Vo, and B. Lee P. H. Tran, "Promising iron oxide-based magnetic nanoparticles in biomedical engineering," *Archives of Pharmacal Research*, vol. 35, no. 12, pp. 2045-2061, 2012.
- [154] A. V. Tarasevych, V. P. Kukhar, R. Bokherroub, and S. Szunerits K. Turcheniuk, "Recent advances in surface chemistry strategies for the fabrication of functional iron oxide based magnetic nanoparticles," *Nanoscale*, vol. 5, pp. 10729-10752, 2013.
- [155] K. Piksova, T. Q. Trung and T. Skeren D. Horak, "Magnetic and metallic nanoparticles for biomedical application," *International Conference en Nanomaterials*, vol. 10, pp. 20-22, 2009.

- [156] G. R. Parida, R.D. Tucker and J. B. Park A. Paulus, "JCorrosion analysis of NiCu and PdCo thermal seeds alloys used as interstitial hyperthermia implant," *Biomaterials*, vol. 18, no. 24, pp. 1609-1614, 1997.
- [157] S. Hashimoto, T. Kayano, and I. Nagano E. Kita, "Heating characteristics of ferromagnetic iron oxide nanoparticles for magnetic hyperthermia," *Journal of Applied Physics*, vol. 107, no. 9, p. 09B321, 2010.
- [158] Y. Su, F. Cheng, J. Chen J. Zhu, "Improving the performance of PtRu/C catalysts for methanol oxidation by sensitization and activation treatment," *Journal of Power Sources*, vol. 166, no. 2, pp. 331-336, 2007.
- [159] R. L. McCreery and K. R. Kneten, "Effects of redox system structure on electron-transfer kinetics at ordered graphite and glassy carbon electrodes," *Analytical Chemistry*, vol. 64, no. 21, pp. 2518-2524, 1992.
- [160] P. T. A. Sumodjo and F. M. Takata , "Electrodeposition of magnetic CoPd thin films: Influence of plating condition," *Electrochimica Acta*, vol. 52, no. 20, pp. 6089-6096, 2007.
- [161] J. Na'aliya and H. N. Aliyu , "Stability constant of the trisglycinato metal complexes," *Journal of Pure and Applied Sciences*, vol. 3, no. 2, pp. 52-55, 2010.
- [162] N. V. Myung and K. Nobe M. Schawtrz, "Electrodeposition of iron group-rare earth alloys from aqueous media," *Journal of The Electrochemical Society*, vol. 151, no. 7, pp. 468-477, 2004.
- [163] H. Iida, S. Tominaka and T. Hachisu T. Osaka, "New Trends in Nanoparticles: Syntheses and Their Applications to Fuel Cells, Health Care, and Magnetic Storage," *Israel Journal of Chemistry*, vol. 48, pp. 333-347, 2008.

- [164] C. J. Goodacre, "Palladium-silver alloys: A review of the literature," *The Journal of Prosthetic Dentistry*, vol. 62, pp. 34-37, 1989.
- [165] J. Wirz, "Clinical testing of alloys," *Quintessenz*, vol. 41, pp. 2039-2044, 1990.
- [166] M. Augthunt A. Brammertz, "Intratracheal experiment on rats concerning the fibrogenic effect of respirable dental laboratory dust containing palladium," *Annals of Occupational Hygiene*, vol. 41, pp. 615-620, 1997.
- [167] C. J. Kirkpatrick, S. Schyma M. Augthun, "Studies on the pneumoconiosis risk of dental laboratory technicians due to palladium particles in dust," *Dtsch Zahnärztl Z*, vol. 46, pp. 519-522, 1991.
- [168] C.T. Hanks J. C. Wataha, "Biological effects of palladium and risk of using palladium in dental casting alloys," *Journal of Oral Rehabilitation*, vol. 23, pp. 309-320, 1996.
- [169] R. D. Tucker J. A. Paulus, "Cobalt palladium seeds for thermal treatment of tumors," 5,429,583, July 4, 1995.
- [170] J. C. Wataha, "Alloys for prosthodontic restorations," *Journal of Prosthetic Dentistry*, vol. 87, pp. 351-363, 2002.
- [171] P. Chartrand, S. A. Degterov, G. Eriksson, K. Hack, R. Ben Mahfoud, J. Melançon, A. D. Pelton and S. Petersen C. W. Bale, "FactSage thermochemical software and databases," *Calphad- Computer Coupling of Phase Diagrams and Thermochemistry*, vol. 26, pp. 189-228, 2002.
- [172] M. Marek V. Geohlich, "Corrosion behavior of Pd-Cu and PdCo alloys in synthetic saliva," *Journal of dental materials*, vol. 6, pp. 103-110, 1990.
- [173] H. Kaiser, *Alloy dissolution. Corrosion mechanism*. New York: Marcel Dekker, 1987.

- [174] k.s. Shi, B. Penugonda, J. Vaidyanathan T. K. Vaidyanathan, "Active-passive polarization behavior of Pd-based binary alloys," *Canadian Metallurgical Quarterly* , vol. 25, pp. 123-129, 1986.
- [175] H. Terryn, J. H. W. De Wit F. Andreatta, "Corrosion behaviour of different tempers of AA7075 aluminium alloy," *Electrochimica Acta* , vol. 49, pp. 2851-2862, 2004.
- [176] K. Lee, K. Oishi, S. Mitsushima, N. Kamiya, K. I. Ota O. Savadogo, "New Palladium Alloys Catalyst for the Oxygen Reduction Reaction in an Acid Medium," *Electrochemistry Communications*, vol. 6, pp. 105-109, 2004.
- [177] O. Savadogo K. Oishi, "Electrochemical investigation of PdCo thin films binary alloy for the oxygen reduction reaction in acid medium," *Journal of Electroanalytical Chemistry*, vol. 703, pp. 108-116, 2013.
- [178] R. M. Crooks F. P. Zamborini, "Corrosion Passivation of Gold by n-Alkanethiol Self-Assembled Monolayers: Effect of Chain Length and End Group," *Langmuir* , vol. 14, pp. 3279-3286, 1998.
- [179] R. Rego, O. Savadogo L. Kafrouni, "Electrodeposition of PdCo nanoparticles onto Pd-modified graphite electrode for future medical nanodevices ," *Journal of Electroanalytical Chemistry (Submitted)* , February 2016.
- [180] Z. Chen, "The open-circuit potential of a polarizable and reactive electrode.," *Electrochemical Society Transactions*, vol. 6, pp. 1-15, 2008.
- [181] H. Schönherr, A. Tobias, A. Jenkins R. Förch, *Surface design: applications in bioscience and nanotechnology.*: Wiley-VCH, 2009.
- [182] J. F. Moulder et al. , *Handbook of X-ray photoelectron spectroscopy*. Eden Prairie: Physical Electronics Division, 1992.

- [183] G. R. Parida, R. D. Tucker, J.B. Park J. A. Paulus, "Corrosion analysis of NiCu and PdCo thermal seed alloys used as interstitial hyperthermia implants," *Biomaterials* , vol. 18, pp. 1609-1614, 1997.
- [184] M. Pezzoli, F. Zucchi. C E. Angelini, "Corrosion under static and dynamic conditions of alloys used for magnetic retention in dentistry," *The Journal of Prosthetic Dentistry*, vol. 65, pp. 848-853, 1991.
- [185] T. Ushita, H. Tsutsui, Y. Y. Shida, H. Sasaki, and T. Miyazaki Y. Kinouchi, "PdCo Dental Casting Ferromagnetic Alloys," *Journal of Dental Restauration* , vol. 60, pp. 50-58, 1981.
- [186] F. W. Constant, "The magnetic properties of certain Pt-Co and Pd-Co alloys," *Physical review*, vol. 36, pp. 1654-1660, 1930.
- [187] J. C. Wattaha, K. Shor, "Palladium alloys for biomedical devices," *Expert Review of Medical Devices*, vol. 7, no. 4, pp. 489–501, 2010.
- [188] M. Latorre, C. Rinaldi, "Applications of Magnetic Nanoparticles in Medicine: Magnetic Fluid Hyperthermia," *Puerto Rico health sciences journal*, vol. 28, no. 3, pp. 227-38, 2009.
- [189] M. Schwartz, *Encyclopedia of Materials, Parts and Finishes*, 2nd ed.: CRC press, 2002.
- [190] A. K. N. Reddy, M. Gamboa-Aldeco J. Bockris, *Modern Electrochemistry*, 2nd ed.: Kluwer Academic/Plenum, 2000, vol. 2A.
- [191] B. Ershler and A. Frumkin P. Dolin, *Acta Physicochimica URSS*, vol. 13, p. 779, 1940.
- [192] G. Hodes, *Electrochemistry of Nanomaterials*, Wiley–VCH, Ed. Weinheim, 2001.
- [193] X. Sealens, M. V. Gurp, M. MacFarlane, S. J. Martin and P. Vandenabeele G. V. Loo, "The role of mitochondrial factors in apoptosis: a Russian roulette with more than one bullet," *Cell Death and Differentiation*, vol. 9, no. 10, pp. 1031-1042, 2002.

- [194] J. Colomer-Farrarons and J. L. Miribel J. P. Villagrasa, *state of the art in biosensors general aspects/bioelectronics for amperometric biosensors*, Toonika Rinken, Ed., 2013.
- [195] J. F. Gibson and T. J. Peters M. P. Weir, "Haemosiderin and tissue damage," *Cell Biochemistry and Function*, pp. 186-194, 1984.
- [196] G. Zangari and Y. D. Gamburg , *Theory and Practice of Metal Electrodeposition.*: Springer, 2011.
- [197] L.-P. Carignan, D. Ménard and A. Yelon F. Béron, "Extracting Individual Properties from Global Behaviour: First-order Reversal Curve Method Applied to Magnetic Nanowire Arrays," in *Electrodeposited Nanowires and their Applications*, Nicoleta Lupu, Ed.: InTech, 2010.
- [198] V. Melini, D. Contreras, Y. Moreno, H.D. Mansilla , "Fenton reaction driven by iron ligands," *Journal of the Chilean Chemical Society*, vol. 58, no. 4, pp. 0717-9707, 2013.
- [199] R. F. Service, "Nanotoxicology. Nanotechnology grows up," *Science*, vol. 304, no. 5678, pp. 1732-4, 2004.
- [200] N. M. Dissanayake, K. M. Current KM2, S. O. Obare, "Mutagenic Effects of Iron Oxide Nanoparticles on Biological Cells," *International Journal of Molecular Sciences*, vol. 16, no. 10, pp. 3482-516, 2015.